A15

REPORT NO. FHWA/CA/TL-80/31

BACKGROUND AND DEVELOPMENT OF THE CALINE3 LINE SOURCE DISPERSION MODEL

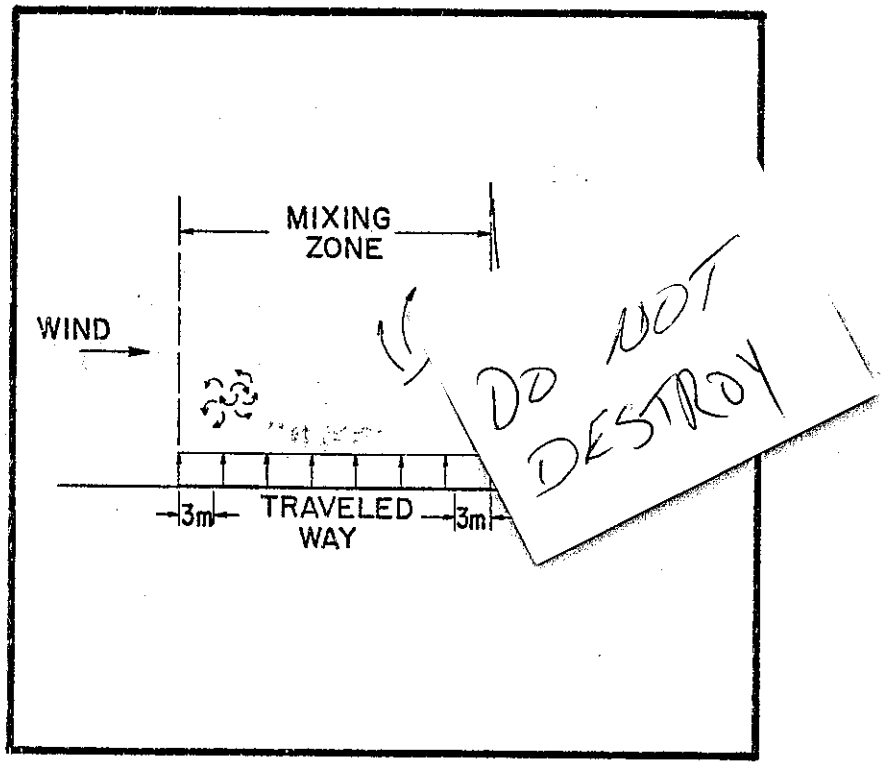

INTERIM REPORT

NOV. 1980

STATE OF CALIFORNIA
DEPARTMENT OF TRANSPORTATION
DIVISION OF CONSTRUCTION
OFFICE OF TRANSPORTATION LABORATORY

BACKGROUND AND DEVELOPMENT OF THE CALINE3 LINE SOURCE DISPERSION MODEL

Study Supervised by ..... Earl C. Shirley, P.E.
& Roy W. Bushey, P.E.

Principal Investigator ..... Paul E. Benson, P.E.

Report Prepared by ..... Paul E. Benson

ROBERT O. WATKINS, P.E.
Chief, Office of Transportation Laboratory

TECHNICAL REPORT STANDARD TITLE PAGE

1. REPORT NO. FHWA/CA/TL-80/31	2. GOVERNMENT ACCESSION NO.	3. RECIPIENT'S CATALOG NO.
4. TITLE AND SUBTITLE BACKGROUND AND DEVELOPMENT OF THE CALINE3 LINE SOURCE DISPERSION MODEL		5. REPORT DATE November, 1980
		6. PERFORMING ORGANIZATION CODE
7. AUTHOR(S) Paul E. Benson		8. PERFORMING ORGANIZATION REPORT NO. 19701-604167
9. PERFORMING ORGANIZATION NAME AND ADDRESS Office of Transportation Laboratory California Department of Transportation Sacramento, California 95819		10. WORK UNIT NO. E78TL06
		11. CONTRACT OR GRANT NO. 1-D-27
12. SPONSORING AGENCY NAME AND ADDRESS California Department of Transportation Sacramento, California 95807		13. TYPE OF REPORT & PERIOD COVERED Interim
		14. SPONSORING AGENCY CODE

15. SUPPLEMENTARY NOTES

This study was conducted in cooperation with the U.S. Department of Transportation, Federal Highway Administration. This study was entitled: "Distribution of Air Pollutants Within the Freeway Corridor".

16. ABSTRACT

A brief description of the theoretical considerations and limitations behind the Gaussian line source dispersion model, CALINE3, is given. A history of the development of the Gaussian method is discussed along with a review of current literature on the subject with particular reference to near-roadway applications. Descriptions of the experimental studies which provided the basis for development of CALINE3 are also given. Analyses of the results from these studies are presented in two sections, one dealing with meteorological effects, and the other with characterization of Gaussian dispersion parameters near roadways. The findings indicate that the vertical distribution of vehicular emissions at the roadway edge can be adequately described by a Gaussian distribution, and that the height of this initial vertical spread is positively correlated with emissions residence time over the roadway. The effects of vehicle induced turbulence are studied in terms of upwind and downwind measures of several micrometeorological parameters. The conclusion that vehicle induced turbulence is a significant effect for cases of neutral to stable atmospheric conditions is reached.

17. KEY WORDS Air pollution, air quality, theory, highways, transportation, Gaussian model, dispersion, carbon monoxide, line source.		18. DISTRIBUTION STATEMENT No restrictions. This document is available to the public through the National Technical Information Service, Springfield, VA 22161.	
19. SECURITY CLASSIF. (OF THIS REPORT) Unclassified	20. SECURITY CLASSIF. (OF THIS PAGE) Unclassified	21. NO. OF PAGES 193	22. PRICE

DS-TL-1242 (Rev.6/76)

CONVERSION FACTORS

English to Metric System (SI) of Measurement

Quantity	English unit	Multiply by	To get metric equivalent
Length	inches (in)or(")	25.40	millimetres (mmm)
		.02540	metres (m)
	feet (ft)or(')	.3048	metres (m)
	miles (mi)	1.609	kilometres (km)
Area	square inches (in^2)	6.432×10^{-4}	square metres (m^2)
	square feet (ft^2)	.09290	square metres (m^2)
	acres	.4047	hectares (ha)
Volume	gallons (gal)	3.785	litres (l)
	cubic feet (ft^3)	.02832	cubic metres (m^3)
	cubic yards (yd^3)	.7646	cubic metres (m^3)
Volume/Time (Flow)	cubic feet per second (ft^3/s)	28.317	litres per second (l/s)
	gallons per minute (gal/min)	.06309	litres per second (l/s)
Mass	pounds (lb)	.4536	kilograms (kg)
Velocity	miles per hour (mph)	.4470	metres per second (m/s)
	feet per second (fps)	.3048	metres per second (m/s)
Acceleration	feet per second squared (ft/s^2)	.3048	metres per second squared (m/s^2)
	acceleration due to force of gravity (G)	9.807	metres per second squared (m/s^2)
Weight Density	pounds per cubic (lb/ft^3)	16.02	kilograms per cubic metre (kg/m^3)
Force	pounds (lbs)	4.448	newtons (N)
	kips (1000 lbs)	4448	newtons (N)
Thermal Energy	British thermal unit (BTU)	1055	joules (J)
Mechanical Energy	foot-pounds (ft-lb)	1.356	joules (J)
	foot-kips (ft-k)	1356	joules (J)
Bending Moment or Torque	inch-pounds (ft-lbs)	.1130	newton-metres (Nm)
	foot-pounds (ft-lbs)	1.356	newton-metres (Nm)
Pressure	pounds per square inch (psi)	6895	pascals (Pa)
	pounds per square foot (psf)	47.88	pascals (Pa)
Stress Intensity	kips per square inch square root inch (ksi $\sqrt{in}$)	1.0988	mega pascals $\sqrt{metre}$ (MPa $\sqrt{m}$)
	pounds per square inch square root inch (psi $\sqrt{in}$)	1.0988	kilo pascals $\sqrt{metre}$ (KPa $\sqrt{m}$)
Plane Angle	degrees (°)	0.0175	radians (rad)
Temperature	degrees fahrenheit (F)	$\frac{tF - 32}{1.8} = tC$	degrees celsius (°C)

ACKNOWLEDGMENTS

The author is indebted to Drs. Leonard Myrup, Daniel Chang, and Gerald Orlob of the University of California at Davis and Messrs. Earl Shirley and Roy Bushey of the Transportation Laboratory for their constructive review of this document. Special credit is due Drs. Myrup and Chang and Mr. Shirley for providing training and guidance to the author in the early stages of the development of CALINE3. Credit is also due Mrs. Marion Ivestor and Mr. William Taylor for the excellent graphics contained in the report, and Ms. Helen Gayther for the neatly typed manuscript.

TABLE OF CONTENTS

		Page
1.	INTRODUCTION	1
2.	THEORETICAL BACKGROUND	6
	2.1 Definitions of Statistical Parameters Used to Describe Turbulence	6
	2.2 The Gaussian Model	12
	2.3 Dispersion Parameters, σ_y and σ_z	20
3.	LITERATURE REVIEW	24
	3.1 Generalized Dispersion Parameters	24
	3.2 Traffic Induced Turbulence	35
	3.3 Wind Speed Effect	43
4.	FIELD MONITORING PROGRAMS	47
	4.1 General Motors Sulfate Dispersion Experiment	47
	4.2 Stanford Research Institute Bayshore Freeway Study	50
	4.3 New York State Long Island Expressway Tracer Study	52
	4.4 Caltrans Los Angeles Freeway Study	55
	4.5 Caltrans Sacramento Intersection Study	58
5.	METEOROLOGICAL ANALYSIS	65
	5.1 Methodology	65
	5.2 Results	74
	5.3 Discussion	81

TABLE OF CONTENTS (Cont'd)

		Page
6.	DISPERSION PARAMETER ANALYSIS	89
	6.1 Methodology	89
	6.2 Results	93
	6.3 Discussion	106
7.	SUMMARY OF FINDINGS AND CONCLUSIONS	129
8.	MODEL DEVELOPMENT AND DESCRIPTION	132
	8.1 Improvements of CALINE3 Over CALINE2	132
	8.2 Equivalent Finite Line Source Formulation	136
	8.3 Mixing Zone Model	152
	8.4 Vertical Dispersion Curves	156
	8.5 Horizontal Dispersion Curves	166
	8.6 Site Geometry	168
	8.7 Deposition and Settling Velocity	176
REFERENCES		178

1. INTRODUCTION

Passage of the National Environmental Policy Act of 1969 (NEPA), and specifically the requirement for filing environmental impact statements (Public Law 91-190, Title 1, Sec. 102), has led to increased activity in air quality dispersion modeling over the past decade. The resulting mathematical models, characterizing transport and dispersion of gaseous and particulate emissions within the planetary boundary layer, attempt to predict temporally and spatially resolved pollutant concentrations arising from proposed power plants, transportation facilities or other large scale human endeavors. These predictions are used to judge compliance of proposed projects with the National Ambient Air Quality Standards or as a means for comparing alternative Air Quality Management Plan control measures.

The prime thrust of research in this area has been to parameterize meteorological phenomena so as to better predict the dynamics of transport and dispersion processes within the atmosphere. Specific processes that are of most interest to the air quality modeler are those which affect wind direction, speed and turbulence. The complexity of these processes has led to many empirical and quasi-empirical descriptions of their behavior.

Prior to the passage of NEPA, research on atmospheric transport and dispersion during the fifties and sixties centered on problems associated with large stationary sources such as coal-fired power plants and emergency or accidental releases of airborne radioactive substances from nuclear facilities. By making certain simplifying assumptions, it was hypothesized that pollutant concentration profiles downwind from these type of sources could be described by a Gaussian or normal distribution function. The spread of this distribution function, as described by its standard deviation, was characterized as increasing with distance from the source and with level of atmospheric turbulence. These relationships were quantified empirically by a series of independent experiments resulting in families of dispersion curves for both vertical and horizontal plume spread.

It soon became apparent that the nature of the source was also an important determining factor in construction of these dispersion curves. Different sets of curves were needed for ground level and elevated releases. Plume rise adjustments were needed for hot, buoyant effluents released from power plants. Puff models were needed to simulate noncontinuous, accidental releases from nuclear facilities. Each of these source related effects tended to be most

significant near the point of release in what is termed the microscale region by air quality modelers.

Passage of NEPA meant that air quality impacts within the microscale region surrounding proposed highways and arterial streets would have to be assessed. Many modelers chose to use the existing Gaussian methodology to do this. Sophisticated numerical models tended to require more input data than was usually available, were more difficult to implement because of their complexity, and were not yet fully developed or proven. Gaussian models, on the other hand, required minimal input data, were relatively easy to implement and use, and had been proven to work well for sites where their somewhat restrictive assumptions were at least marginally satisfied. However, the physics of emissions release for moving vehicles was, in several respects, significantly different than that for the stationary sources which had been used for developing previous Gaussian dispersion curves. The source geometry changed from a point to a semi-infinite line source. Instead of a single source, there were numerous contributing line sources following along a path of finite width. Emissions were released into a region of augmented turbulence caused by the passage of the emitting vehicle itself, and by other vehicles immediately preceding or following it.

The objective of this research has been to investigate the validity of existing Gaussian dispersion curves for use near roadways and recommend necessary changes. The results of this work have already been implemented in the Gaussian line source model, CALINE3, developed by the author (Benson, 1979), and described later in this report. As with previous work on Gaussian dispersion parameters, the results are empirically derived from field observations and apply only to conservative pollutant species such as carbon monoxide.

This report is intended to serve as a support document for the CALINE3 model. It begins with a brief description of the theoretical considerations and limitations inherent in the Gaussian dispersion methodology upon which CALINE3 is based. A history of the development of the Gaussian method is then discussed along with a review of current literature on the subject with particular reference to near-roadway applications. A description of the experimental studies which provided the basis for development of CALINE3 follows. Analyses of the results from these studies are presented in two sections, one dealing with meteorological effects, and the other with characterization of Gaussian dispersion parameters near roadways. These analyses provided most of the rationale for the differences between

CALINE3 and its predecessor, CALINE2. In the final section of this report these differences are discussed, and a complete description of the CALINE3 model is given.

2. THEORETICAL BACKGROUND

2.1 Definitions of Statistical Parameters Used To Describe Turbulence

This section is intended to give the reader an introduction to some of the more basic statistical parameters used to describe turbulence. An understanding of these definitions will be helpful in following later discussions in this paper.

Statistical methods are extremely useful in describing transport and diffusion of materials and properties in turbulent flows because of the inherent randomness of turbulence. The classical approach devised by Reynolds (1895) involves separation of fluid motions into mean and randomly fluctuating parts such that

$$u = \overline{u} + u' \tag{2-1}$$

The mean value, $\overline{u}$, is determined by averaging motions over a time period long enough to attain a relatively stable value representative of the mean flow of the fluid in a particular direction. The fluctuating part, u', can be thought of as a continuous, quasi-random deviation from

the mean flow caused by the turbulent eddies contained in the flow. The mean square and root mean square (rms) values of a series of discrete observations of u' are defined in statistics as the variance, σ^2, and standard deviation, σ, respectively so that,

$$\sigma_u^2 = \overline{u'^2}, \quad \sigma_u = (\overline{u'^2})^{1/2} \tag{2-2}$$

Assuming that the deviations about $\bar{u}$ are generated by a quasi-random process, the frequency distribution of u can be characterized reasonably well by a Gaussian or normal distribution. In this case, $\bar{u}$ and σ_u can be used to precisely define the position and shape of the distribution. Departures from normality are commonly quantified by the following measures:

$$\gamma_1 = \overline{u'^3}/\sigma_u^3 \tag{2-3}$$

$$\gamma_2 = \overline{u'^4}/\sigma_u^4 \tag{2-4}$$

where γ_1 is the skewness, and γ_2 the kurtosis of the distribution. Significant values for γ_1 indicate that the distribution is not symmetrical about $\bar{u}$, implying a

systematic or biased component to u'. A significant γ_2 measure indicates a tendency of u' to be, on the average, either smaller or larger than would be described by a normal distribution.

Relative intensities of turbulence in the x, y, z directions are defined as:

$$I_x \equiv (\overline{u'^2})^{1/2} / \overline{u} \tag{2-5}$$

$$I_y \equiv (\overline{v'^2})^{1/2} / \overline{u} \tag{2-6}$$

$$I_z \equiv (\overline{w'^2})^{1/2} / \overline{u} \tag{2-7}$$

where,

u = Horizontal wind velocity in the direction of mean flow (x-axis),

v = Horizontal wind velocity perpendicular to the mean flow (y-axis),

w = Vertical wind velocity (z-axis).

The overall relative intensity of turbulence is given as:

$$I \equiv \frac{1}{\overline{u}} \left[\frac{\overline{u'^2} + \overline{v'^2} + \overline{w'^2}}{3} \right]^{1/2} \tag{2-8}$$

Correlations between wind velocity components and other measurable properties such as air temperature (T) can be used to estimate vertical fluxes of momentum and heat in the atmosphere. For instance, the instantaneous vertical flux of momentum can be written as $-\rho uw'$ where ρ represents the mass density of air and the negative sign accounts for the positive downward definition of momentum flux versus the positive upward definition of w. Thus, the average momentum flux, τ, is given as,

$$\tau = -\overline{\rho uw'} \tag{2-9}$$

Assuming that the fluctuating component of ρ, ρ', is negligibly small (Munn, 1966), Equation 2-9 can be rewritten as,

$$\begin{aligned} \tau &= -\rho\overline{(\overline{u} + u')w'} \\ &= -\rho(\overline{\overline{u}w'} + \overline{u'w'}) \end{aligned} \tag{2-10}$$

By definition, $\overline{w'} = 0$ so that $\overline{\bar{u}\, w'} = \bar{u}\, \overline{w'} = 0$ and

$$\tau = -\rho\overline{u'w'} \tag{2-11}$$

A similar argument can be made for the average vertical heat flux, H, yielding

$$H = \rho C_p \overline{T'w'} \tag{2-12}$$

where C_p is the specific heat of air at constant pressure. Over sufficiently long sampling times, and barring regions of convergence or divergence, $\bar{w} = 0$. This leads to $\overline{uw} = \overline{uw'} = \overline{u'w'}$ as follows:

$$\begin{aligned} \overline{uw} &= \overline{(\bar{u} + u')(\bar{w} + w')} \\ &= \overline{\bar{u}\bar{w} + \bar{u}w' + u'\bar{w} + u'w'} \\ &= \overline{u'w'} \end{aligned} \tag{2-13}$$

Thus, the more readily computed covariances of $\overline{uw}$ and $\overline{Tw}$ can be used to determine τ and H.

The value τ can also be thought of as a shear stress exerted parallel to the mean flow. In the atmosphere, τ arises from the frictional drag exerted by the Earth's surface. The surface shear stress, τ_o, is customarily expressed in terms of the friction velocity, u_*, where

$$u_* \equiv (\tau_o/\rho)^{1/2} \tag{2-14}$$

The autocorrelation coefficient is another useful statistic for analyzing turbulence. It is defined as follows:

$$R(t) = \frac{\overline{u'(t_o)u'(t_o + t)}}{(\overline{u'^2(t_o)})^{1/2}(\overline{u'^2(t_o + t)})^{1/2}} \tag{2-15}$$

For stationary turbulence $\overline{u'^2(t_o)} = \overline{u'^2\ (t_o+t)} = \overline{u'^2}$, so that,

$$R(t) = \frac{\overline{u'(t_o)u'(t_o + t)}}{\overline{u'^2}} \tag{2-16}$$

As t increases, R(t) decreases from a maximum absolute value of one toward zero. The mean time required for R(t) to reach zero is a gross measure of the scale of turbulence. This is because autocorrelation is generated by the

correlated movements found within turbulent eddies. Given a flow made up of predominantly small scale turbulence, the reference point at which R(t) is being measured will more rapidly fall out of the influence of each single eddy than it would for a flow containing larger scales of turbulence.

The autocorrelation coefficient can be measured in either an Eulerian (fixed) or Lagrangian (moving) reference frame. In practice, measurements of the Eulerian autocorrelation, $R_E(t)$, are more easily made than the Lagrangian value, $R_L(\xi)$. Because $R_L(\xi)$ is measured at a point which follows the mean flow, the influence of individual eddies also carried along by the flow are felt for a longer period of time than when fixed measurements are made. Thus, $R_L(\xi)$ has a characteristically slower rate of decay with respect to time than $R_E(t)$.

2.2 The Gaussian Dispersion Model

The Gaussian dispersion model can best be described as a simplified solution to a three-dimensional, first order gradient transport description of turbulent mixing. The simplifying assumptions used to develop the model limit application to neutral to stably stratified surface layer flows with wind speeds of at least 1 m/s. The model is

quasi-empirical in nature. A pollutant or tracer release is assumed to be dispersed in a manner which results in a Gaussian or normal distribution of the material about the principle axis of flow. The spread of this distribution as a function of distance downwind from the source and intensity of turbulence is determined experimentally.

The model can be derived independently from two separate mathematical descriptions of turbulent diffusion. The first to be discussed here is the mixing length approach developed by Prandtl (1934) in which the rate of turbulent diffusion is proportional to the intensity of the turbulence and to a length measure characteristic of the scale of the dominant turbulence in the flow. Later, the statistical method advanced by Taylor (1921) and applied by Sutton (1932) will be shown to yield similar results.

The mixing length model was developed primarily for boundary layer flows in pipes and similar engineering applications. A basic assumption of the model is that a fluid parcel retains its identity when transported over distances equivalent to the characteristic mixing length of the turbulent flow. Clearly, large-scale convective turbulence and synoptic flows common in the planetary boundary layer do not meet this assumption. Modeling of such phenomena

are better handled by dynamical similarity methods or second order closure solutions to the Navier-Stokes equations of fluid motion. For surface layer applications in neutrally buoyant or stable turbulent flows, the mixing length model may be considered appropriate for use.

By way of analogy to molecular or Fickian diffusion, the rate of transfer of a substance or property across a boundary within a turbulent flow is said by mixing length theory to be directly proportional to the gradient of the substance or property at the boundary. In a turbulent regime, the dominant process causing exchange across the boundary is the random motion of parcels of fluid attributable to a field of various size turbulent eddies, rather than the random motion of individual molecules. The constant of proportionality between the rate of transfer and gradient in a particular direction x is called the mass diffusivity coefficient, D_x. In molecular diffusion, the analogous molecular diffusivity is related to the average kinetic energy of the molecules and their mean free path. Similarly, D_x is related to the intensity of turbulence in the x-direction and the average size of the eddies constituting the turbulent flow. Thus, the mixing length, and, in part, the rate of turbulent diffusion, is determined by the scale of the turbulence.

In order to apply the mixing length model to pollutant dispersion problems, a mass balance is customarily performed on a control volume of size dx, dy, dz fixed in an Eulerian frame of reference. The net rate of change of mass within the control volume due to turbulent transfer in the x-direction can then be written as

$$\frac{\partial M_x^{TURB}}{\partial t} = \frac{\partial}{\partial x}\left(\frac{\partial (D_x C)}{\partial x}\right) dx\ dy\ dz \qquad (2\text{-}17)$$

where C is the mass concentration at the centroid of the control volume. Similar equations can be written for turbulent transfer in the y and z directions. If we align the x-axis in the direction of mean flow of velocity u, we can add the following advective transfer term,

$$\frac{\partial M_x^{ADVEC}}{\partial t} = -\frac{\partial (C\bar{u})}{\partial x}\ dx\ dy\ dz \qquad (2\text{-}18)$$

where $\partial M_x^{ADVEC}/\partial t$ is the net rate of change of mass within the control volume due to advective transport.

Assuming there are no sources or sinks occurring within the control volume (i.e., the pollutant is not undergoing any significant chemical transformations), the total rate of

change of mass within the volume is described by

$$\frac{\partial C}{\partial t}\,dV = -\frac{\partial(C\bar{u})}{\partial x}\,dV + \frac{\partial}{\partial x}\left(\frac{\partial(D_x C)}{\partial x}\right)dV$$

$$+ \frac{\partial}{\partial y}\left(\frac{\partial(D_y C)}{\partial y}\right)dV + \frac{\partial}{\partial z}\left(\frac{\partial(D_z C)}{\partial z}\right)dV \qquad (2\text{-}19)$$

where $dV=dxdydz$ and $CdV=M^{TOTAL}$. By assuming that the intensity of the turbulent flow is homogenous so that the mass diffusivity terms are independent of position, and by cancelling the dV terms, Equation 2-19 can be rewritten as

$$\frac{\partial C}{\partial t} = \frac{-\partial(C\bar{u})}{\partial x} + D_x\left(\frac{\partial^2 C}{\partial x^2}\right) + D_y\left(\frac{\partial^2 C}{\partial y^2}\right) + D_z\left(\frac{\partial^2 C}{\partial z^2}\right) \qquad (2\text{-}20)$$

Now a series of additional simplifying assumptions are made to facilitate solution of this differential equation:

1. Wind speed u is invariant with height and horizontal position,
2. Turbulent diffusion in the x-direction is negligible when compared to the advective transport term, and can therefore be ignored,
3. A steady-state condition exists so that $\partial C/\partial t=0$.

These assumptions lead to

$$\bar{u}\left(\frac{\partial C}{\partial x}\right) = D_y\left(\frac{\partial^2 C}{\partial y^2}\right) + D_z\left(\frac{\partial^2 C}{\partial z^2}\right) \qquad (2\text{-}21)$$

The following boundary conditions are applied to solve Equation 2-21 for a ground level source:

1. $C \to \infty$ as $x \to 0$,
2. $C \to 0$ as $x, y, z \to \infty$,
3. $D_z\left(\frac{\partial C}{\partial z}\right) \to 0$ as $z \to 0$ (perfect reflection at the ground surface),
4. $\int_0^{\infty}\int_{-\infty}^{\infty} \bar{u}C(x,y,z)\,dy\,dz = Q$ (for all $x>0$, Q can be either the mass or volume rate of pollutant release at the source).

The resulting solution is

$$C = \frac{Q}{2\pi x(D_y D_z)^{1/2}} \exp\left\{-\left[\left(\frac{y^2}{D_y}\right) + \left(\frac{z^2}{D_z}\right)\right]\cdot\frac{\bar{u}}{4x}\right\} \qquad (2\text{-}22)$$

By substituting $D_y = \sigma_y^2\bar{u}/2x$ and $D_z = \sigma_z^2\bar{u}/2x$ into Equation 2-22, we obtain an equation for which the factors f_1 and f_2 represent ordinates of the normalized Gaussian distribution

function at distances y and z, respectively, from the plume centerline:

$$C(x,y,z) = \frac{Q}{\bar{u}} \cdot \underbrace{\frac{1}{\sigma_y\sqrt{2\pi}} \exp\left(\frac{-y^2}{2\sigma_y^2}\right)}_{f_1} \cdot \underbrace{\frac{1}{\sigma_z\sqrt{2\pi}} \exp\left(\frac{-z^2}{2\sigma_z^2}\right)}_{f_2} \qquad (2\text{-}23)$$

This equation results in a binormal distribution of pollutant concentration about the plume centerline. The variables σ_y and σ_z are called the horizontal and vertical dispersion parameters. They have traditionally been obtained empirically from observed data.

Sutton (1932) achieved similar results to Equation 2-23 by applying a statistical method first put forward by Taylor (1921). Taylor proposed that the variance of a group of particles about an origin after time T could be described as follows:

$$\sigma^2 = 2\,\overline{u'^2} \int_0^T\int_0^t R_L(\xi)\, d\xi\, dt \qquad (2\text{-}24)$$

where $\overline{u'^2}$ equals the rms value of the eddy velocity and $R_L(\xi)$ is the Lagrangian autocorrelation function. Invoking Taylor's Hypothesis and integrating $R(\xi)$ over t_1, where $R(\xi) \to 0$ as $t \to t_1$, leads to

$$\sigma^2 = \frac{2\,\overline{u'^2}\,x t_L}{\overline{u}}, \quad u' << \overline{u} \tag{2-25}$$

where t_L is defined as the Lagrangian time scale (equal to $\int_0^t R_L(\xi)d\xi$) and x is the downwind distance from the source.

Sutton was able to arrive at a practical solution to Taylor's description of turbulent diffusion by letting

$$K_z = \overline{w'^2} \int_0^{t_1} R_L(\xi)\, d\xi \tag{2-26}$$

and assuming the following functional form of $R_L(\xi)$:

$$R_L(\xi) = \left[\frac{\nu}{\nu + \overline{w'^2}\xi}\right]^n, \quad n \geq 0 \tag{2-27}$$

where ν equals the kinematic viscosity of the diffusing medium, and n is the exponent for the wind profile power law under neutral conditions given by

$$\bar{u}_2 = \bar{u}_1 (z_2/z_1)^{\frac{n}{2-n}} \tag{2-28}$$

This led to a solution for concentration, C, downwind from a continuous point source of the form

$$C(x,y,z) = \frac{Q}{\pi C_y C_z \bar{u} x^{2-n}} \exp\left\{-\left(\frac{y^2}{C_y^2} + \frac{z^2}{C_z^2}\right)\frac{1}{x^{2-n}}\right\} \tag{2-29}$$

where C_y and C_z were defined as generalized diffusion coefficients obtainable through measurement of wind velocity fluctuations in the y and z directions. Substitution of $C_y^2 = 2\sigma_y{}^2/x^{2-n}$ and $C_z^2 = 2\sigma_z{}^2/x^{2-n}$ into Equation 2-29 yields Equation 2-23.

2.3 Dispersion Parameters, σ_y and σ_z

The normalizing substitutions made to Equation 2-22 require that

$$\sigma_y = \left(\frac{2D_y x}{\bar{u}}\right)^{1/2}, \quad \sigma_z = \left(\frac{2D_z x}{\bar{u}}\right)^{1/2} \tag{2-30}$$

The proportionality of the root mean square displacements, σ_y and σ_z, to $(x/\overline{u})^{1/2} = t^{1/2}$ is analogous to Einstein's solution of molecular displacements cause by Brownian motion. This emphasizes the importance of a random turbulent flow field to the successful application of the Gaussian model. Spatial correlations of fluid motions in either the y or z directions over distances of the same order of magnitude as σ_y or σ_z will violate the assumed stochastic nature of the turbulent diffusive process. Thus, Gaussian models are unsuited for application to thermally unstable flows or flows over complex terrain.

Equations 2-30 clearly demonstrate the inherent consistency between the Gaussian and mixing length models of turbulent diffusion. The mixing length model can be used to show that turbulent diffusivity is proportional to the turbulence intensity and a length scale, ℓ, characterizing the dimensions of the dominant (largest) eddies contained in the flow (Tennekes and Lumley, 1972) so that

$$K_y \propto \overline{u} I_y \ell, \quad K_z \propto \overline{u} I_z \ell \tag{2-31}$$

where I_y and I_z represent relative intensities of turbulence.

In Equations 2-30, the variances of the concentration distribution in the y and z directions, σ_y^2 and σ_z^2, are proportional to D/u and x. D/u can be interpreted as a measure of the intensity of turbulence, akin to the relative value, I. Similarly, x can be thought of as an indicator of ℓ. As x increases, the plume size increases so that eddies characterized by larger values of ℓ become dominant in the mixing process.

The Sutton formulation implies that

$$\sigma_y = \frac{C_y x^{(1 - n/2)}}{\sqrt{2}}, \quad \sigma_z = \frac{C_z x^{(1 - n/2)}}{\sqrt{2}} \tag{2-32}$$

where

$$C_y^2 = \frac{4\nu^n}{(1-n)(2-n)\overline{u}^n}\left(\frac{\overline{v'^2}}{\overline{u}^2}\right)^{1-n} \tag{2-33}$$

$$C_z^2 = \frac{4\nu^n}{(1-n)(2-n)\overline{u}^n}\left(\frac{\overline{w'^2}}{\overline{u}^2}\right)^{1-n} \tag{2-34}$$

The difficulty with this method is that an increase in n, causing a decrease in σ, can result from either an increase in surface roughness or in atmospheric stability. Yet surface roughness and stability are known to have opposite effects on atmospheric dispersion rates. Also, the applicability of a common n to both C_y and C_z is seriously open to question (Barad and Haugen, 1959).

As has been mentioned, quantification of the dispersion parameters, σ_y and σ_z, has been accomplished solely through empirical methods. Such empiricism is, in fact, appropriate since Fickian diffusion and the mixing length model extension of the molecular analogy are gross approximations of an extremely complex natural phenomenon. Characterizing a turbulent flow, which contains a spectrum of eddy sizes and vorticity, by a single length and turbulence intensity is an inherently empirical approach. In addition, the Fickian assumption on which Gaussian models are based, i.e., diffusion rates as linear functions of local concentration gradients, can only be extended beyond neutrally stratified flows by empirical methods.

3. LITERATURE REVIEW

3.1 Generalized Dispersion Parameters

By the late 1950's, use of the Sutton coefficients, C_y, C_z and n, had been abandoned in favor of directly estimating values of σ_y and σ_z using bivane measurements of the horizontal (Θ) and vertical (ϕ) wind angles. Cramer (1957) published a series of graphs relating σ_y and σ_z to the standard deviation of the horizontal wind angle, σ_Θ. He also suggested the following power law relations between the dispersion parameters and wind fluctuation measurements:

$$\sigma_y = \sigma_\theta x^p \tag{3-1}$$

$$\sigma_z = \sigma_\phi x^q \tag{3-2}$$

where p and q are related to the atmospheric stability and x is the downwind distance from the source. Hay and Pasquill (1959) pointed out the difficulty of predicting the Lagrangian properties of σ_y and σ_z from the Eulerian measurements, σ_Θ and σ_ϕ. They realized that in order to equate the two, the ratio of the Lagrangian to Eulerian time scales, β, and the time of travel, $T=x/\overline{u}$, had to be considered. Furthermore, they noted that increased

sampling time (referred to as averaging time later in this paper) significantly increased the measured values of σ_y.

The following relations for lateral and vertical plume spread were later suggested by Pasquill (1961),

$$\sigma_y/x = (\sigma_\theta)_{\tau,T/\beta} \tag{3-3}$$

$$\sigma_z/x = (\sigma_\phi)_{\tau,T/\beta} \tag{3-4}$$

where σ_θ and σ_ϕ were measured over the sampling time τ, using readings averaged over the time period T/β, and σ_z was limited to elevated releases. In this method, T/β acted as a low-pass filter measuring ever larger scales of turbulence as T increased, corresponding to the larger scales of turbulence dominant in mixing the plume at greater distances.

Pasquill also introduced a method whereby values of vertical plume spread, h, could be inferred from measurements of surface wind speed, and insolation, while the horizontal plume spread, Θ, could be estimated from the range of an appropriately long wind direction trace (approximately one hour).

The parameters h and Θ were defined as encompassing plume spread out to a concentration of one-tenth the axial value. Assuming a Gaussian distribution, these parameters could then easily be used to compute σ_z and σ_y.

The classification scheme used by Pasquill to estimate vertical plume spread as a function of atmospheric stability is given in Table 1. While based largely on subjective considerations, the Pasquill stability classes represented an attempt to merge evolving similarity theories with experimental diffusion measurements. The scheme enjoyed wide application primarily because it used readily available meteorological observations. As similarity theory developed, some researchers tried to relate Pasquill's subjective system to quantitative similarity measurements. Luna and Church (1972) showed that the stability classes were linearly related to the intensity of turbulence, but poorly correlated to lapse rate and bulk Richardson number. Pasquill (1974) attributes this to the evolutionary aspects of atmospheric stability which can lead to the simultaneous occurrence of very different stability regimes at varying heights. The measurements used by Luna and Church were made at a height of 92 meters, while the Pasquill categories were based on surface measurements of wind speed (at 10 meters) and insolation. Golder (1972) analyzed a much

Table 1

Pasquill Stability Classification Scheme

Surface Wind Speed (at 10 m), m sec^{-1}	Day			Night	
	Incoming Solar Radiation			Thinly Overcast or $\geq$4/8 Low Cloud	$\leq$3/8 Cloud
	Strong	Moderate	Slight		
< 2	A	A-B	B		
2-3	A-B	B	C	E	F
3-5	B	B-C	C	D	E
5-6	C	C-D	D	D	D
> 6	C	D	D	D	D

(After Pasquill, 1961)

wider body of data comprised primarily of surface layer measurements. He had considerably greater success in relating a stability parameter, the Obukhov Length, L, to the Pasquill stability classes. His findings permitted conversion between the two stability methodologies with an allowance made for aerodynamic surface roughness, Z_0. However, he cautioned that no exact equivalence could be made since heat flux, used in estimating L, did not depend solely on insolation.

Gifford (1961) extended Pasquill's work by forming a family of dispersion curves directly relating σ_y and σ_z to downwind distance for various Pasquill stability categories. These became known as the Pasquill-Gifford (P-G) curves later popularized in the United States by Turner (1970) for use in air pollution modeling work (see Figures 1 and 2). It is noteworthy that these curves were derived for ground level releases, smooth terrain and extremely short averaging times (three minutes). Turner (1964) also proposed a seven class stability scheme using a more precise net radiation index in place of Pasquill's qualitative description of insolation. However, the wide acceptance of the P-G curves made Pasquill's A through F stability scheme the standard classification system for Gaussian dispersion modeling.

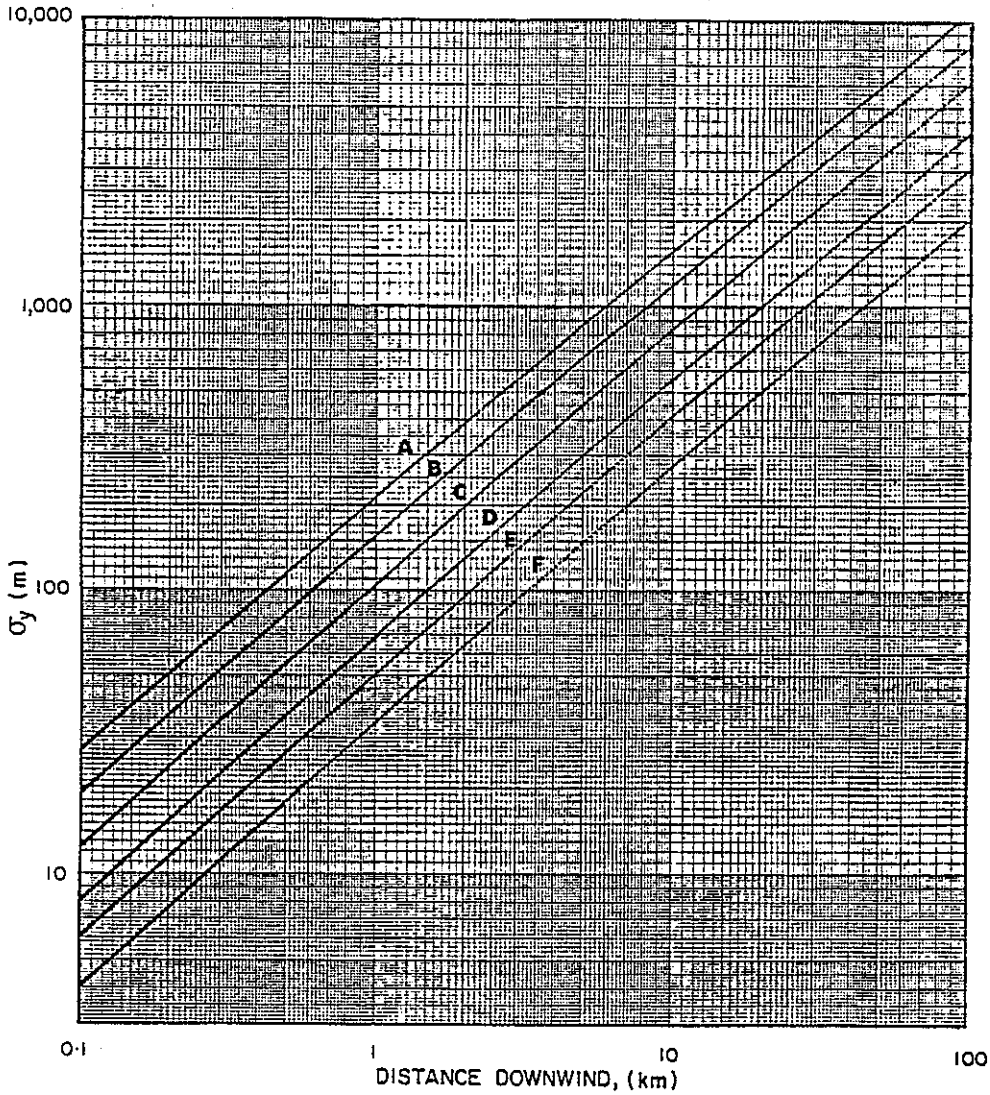

PASQUILL–GIFFORD CURVES
FOR THE HORIZONTAL DISPERSION PARAMETER, σ_y
(AFTER TURNER, 1970)

FIGURE 1

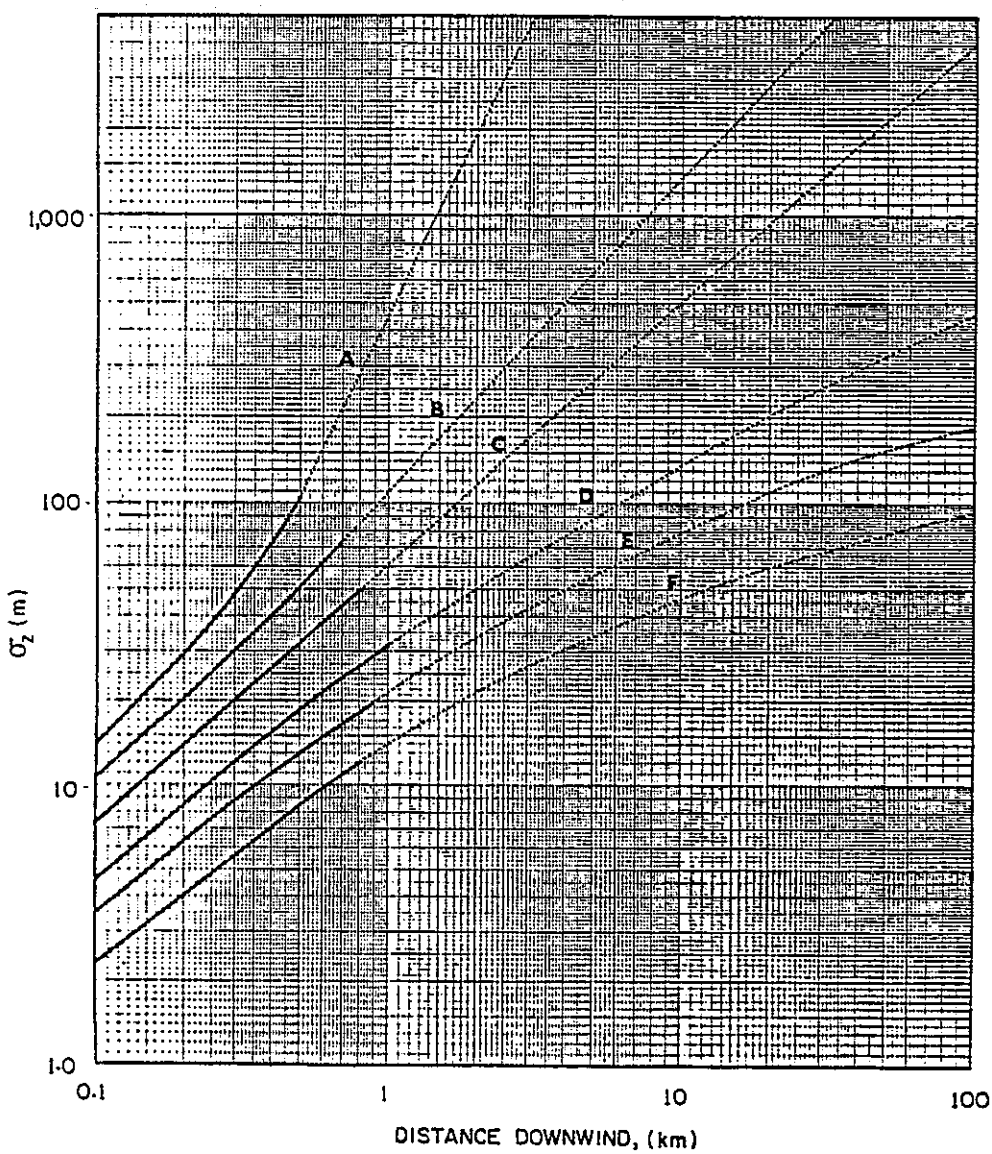

PASQUILL–GIFFORD CURVES
FOR THE HORIZONTAL DISPERSION PARAMETER, σ_z
(AFTER TURNER, 1970)

FIGURE 2

SGZ1 is adjusted in the model for averaging times other than 30 minutes (used in the GM study) by the following power law:

$$SGZ1_{ATIM} = SGZ1_{30} * (ATIM/30)^{0.2} \quad . \qquad (8\text{-}15)$$

Where, ATIM = Averaging time (minutes)

The value of SGZ1 is considered by CALINE3 to be independent of surface roughness and atmospheric stability class. The user should note that SGZ1 accounts for all the enhanced dispersion over and immediately downwind of the roadway. Thus, the stability class used to run the model should be representative of the upwind or ambient stability without any additional modifications for traffic turbulence.

8.4 Vertical Dispersion Curves

The vertical dispersion curves used by CALINE3 are formed by using the value of SGZ1 from the mixing zone model, and the value of σ_z at 10 kilometers (SZ10) as defined by Pasquill (1974) and Smith (1972). In effect, the power curve approximation suggested by Pasquill is elevated near the highway by the intense mixing zone turbulence (see Fig. 38). The significance of this added turbulence to

being proposed. Smith (1972) used two-dimensional, finite-difference solutions to the advection-diffusion equation (incorporating wind speed and diffusivity profiles) to develop a new set of vertical dispersion curves. These results were condensed into a family of power law relations of the form

$$\sigma_z = ax^s \tag{3-5}$$

and presented in Pasquill's revised edition of Atmospheric Diffusion (1974). Also proposed by Smith was a revised stability classification scheme essentially equivalent to Pasquill's original system, but directly incorporating heat flux and adding a seventh stability category, G.

In 1976, both Pasquill and Draxler proposed an adjustment factor, f(x), to account for the divergence in Lagrangian and Eulerian time scales with distance from the source when computing σ_y from σ_θ measurements using the original Hay and Pasquill scheme, so that

$$\sigma_y = \sigma_\theta x \cdot f(x) \tag{3-6}$$

where $f(x) = 1$ for $x = 0$, and decreases with increasing x. In the absence of wind fluctuation data from which to compute σ_θ, no modifications to the original P-G curves were suggested, however.

Application of standard sets of dispersion curves such as the P-G curves led to the use of modifying factors for surface roughness and averaging time. Hanna et. al. (1977) recommended the following power law adjustments to account for the differences between actual and standard conditions:

$$\sigma^A = \sigma^S (z_o^A / z_o^S)^p \ (T^A / T^S)^q \qquad (3\text{-}7)$$

where the superscripts A and S correspond to actual and standard conditions, respectively. From Smith's work, values of $p = 0.2$ near the source and decreasing to about 0.07 at ten kilometers result. Gifford (1975) has recommended values of $q = 0.25$ to 0.3 for $1 < T^A < 100$ hours and $q = 0.2$ for $3 < T^A < 60$ minutes.

A similarity theory approach to atmospheric diffusion first introduced by Monin (1959) has been paralleling the statistical approach through the 1960's and 70's, but lagging behind in practical application. The essence of this theory is that the Lagrangian behavior of particle

diffusion can be described by the Eulerian properties of momentum flux, measured by u_*, in a neutral flow, and heat flux, H, in a thermally stratified flow. Thus, average horizontal ($d\bar{y}/dt$) and vertical ($d\bar{z}/dt$) displacement velocities can be described by

$$\frac{d\bar{y}}{dt} = u(cz) \tag{3-8}$$

$$\frac{d\bar{z}}{dt} = bu_* \cdot \phi(z/L) \tag{3-9}$$

where b and c are universal constants, L is the Obukhov Length and ϕ represents a function of $\bar{z}/L$. Recent work in this area is outlined by Pasquill (1978). It is directed primarily at better quantification of vertical dispersion during unstable atmospheric conditions. While such meteorological conditions often lead to the highest observed pollutant concentrations downwind of large, stationary sources, they are of little or no concern when considering ground based mobile sources.

Solution of the advection-diffusion equation using 2nd-order closure techniques is another area where recent progress has been made, particularly in evaluating the

vertical dispersion parameter, σ_z. As reported by Pasquill (1978), results under neutral conditions have compared well with Smith's earlier work using simple gradient transport theory. Another interesting result of the 2nd-order closure technique is the relative lack of dependence of σ_z on stability within 100 meters of the source. Solutions for σ_z in this region follow closely those for neutral flow.

3.2 Traffic Induced Turbulence

Turbulence produced by the movement and thermal emissions of vehicles plays an important role in the initial mixing of vehicular pollutants. Spectral studies by Rao, Sedefian and Czapski (1979) have shown that the strongest contributions to turbulence from traffic sources occur for eddy sizes of about 4 to 8 meters. This corresponds well to the average scale of turbulence in stable air reported by Panofsky (1961), though it is nearly an order of magnitude below the scales for unstable air contained in Panofsky's article.

Turbulent diffusion near roadways received virtually no attention until the early 1960's. In 1960, Congress passed an amendment to the Air Pollution Control Act of 1955 that recognized the significance of mobile sources to the

nation's worsening urban air pollution problems, and directed the Surgeon General to study the effects of motor vehicle exhaust on human health. The results of that study (1962) indicated that severe congestion of motor vehicles in urban transportation corridors did pose a threat to human health.

Field measurements of near-roadway carbon monoxide levels have been available since the early 1920's. Wilkins (1956) gives a succinct, comprehensive review of this earlier work. After the Surgeon General's report was issued, a resurgence of interest in auto-related air pollutants led to many new field investigations. Among these, McCormick and Xintaras (1962) published results of curb-side carbon monoxide (CO) measurements. They identified traffic volume and wind speed as the main components affecting CO concentrations near the roadway. They also pointed out the importance of accounting for the underlying ambient concentrations, particularly in urban areas, when attempting to model curb-side levels.

Over the next decade, both Gaussian and numerical models were developed to assess air pollution impacts near roadways. These models, particularly the Gaussian ones, grew out of the large body of knowledge, already briefly reviewed here,

on plume dispersion from stationary sources at downwind distances of 100 meters and greater. Estimates of near source dispersion were made without rigorous study of the dynamics of the mixing process at the source. Beaton et. al. (1972), chose a value of 4 meters for σ_z at the roadway edge, and 8 meters for σ_y. These values were based on visual observations of smoke releases from a single vehicle. Calder (1973) assumed neutral stability and used the following power curves:

$$\sigma_y = 0.13\ x^{0.903} \tag{3-10}$$

$$\sigma_z = a(x + c)^b \tag{3-11}$$

where the σ_y curve was based on work by Geomet (1971), and a and b were chosen to fit the neutral vertical dispersion P-G curve. The value of c was assigned such that σ_z equaled an assumed value of 1.5 meters when x equaled 0. Zimmerman and Thompson (1974) later used this value of 1.5 meters for σ_z at the downwind edge of the roadway in their HIWAY model. They verified this initial σ_z as a conservative (low) estimate based on observed concentrations at a height of 2 meters near a roadway using

$$\sigma_z = \frac{Q}{Cu \cos(\theta)} \tag{3-12}$$

where Θ was the angle of the wind relative to the line source (note that this formulation assumes that C was measured at ground level).

Dabberdt (1975) examined intensities of turbulence and heat fluxes near the upwind and downwind edges of a 6-lane freeway. He discovered a significant increase in heat flux downwind of the freeway which he attributed to waste heat emissions from the vehicles. He felt that these emissions were sufficient to create an unstable regime over the roadway given normal traffic volumes. Dabberdt also found an increase in intensity of turbulence downwind of the freeway. While he could not correlate this with traffic speed, volume or spacing, there was some correlation exhibited with wind speed. Measurements of σ_z downwind of the roadway made later using this data behaved similarly (Benson and Squires, 1979).

Dabberdt explained this lack of dependence on traffic parameters by hypothesizing that virtually all the initial mixing of tailpipe emissions attributable to traffic

induced turbulence took place within the wake of each vehicle. He felt that mixing beyond this point was not efficiently carried out by the scales of turbulence created by additional vehicles so that traffic volumes and spacing did not have a significant effect on the initial mixing. However, Dabberdt did feel that the mean depth of the mixed zone over the roadway was related to vehicle density and speed insofar as those factors affected thermal instability. Another contributing factor mentioned by Benson and Squires is the inverse relation between traffic speed and volume. This could lead to possible offsetting effects between the mechanical and thermal turbulence created by the vehicles.

Chock (1977) reported findings on the effects of traffic turbulence near roadways based on measurements made during the General Motors Sulfate Dispersion Experiment (Cadle et. al., 1977). As in Dabberdt's work, he found a higher intensity of turbulence and heat flux downwind of the highway. Under low wind speed conditions (<1 m/s), Chock noted a persistent upward movement of air over the roadway which he attributed to vehicular thermal emissions. He also reported that traffic influence on low speed mean wind flows extended at least 15 meters upwind and downwind of the roadway edge, and that stability measurements made out

of the influence of the wake effect were consistently more unstable on the downwind side of the roadway than the upwind side.

During this same time period, efforts were being made by other researchers to define the turbulence envelope created by a vehicle wake using dynamic similarity arguments and physical model results. Fay and Eng (1975) formulated a two-dimensional crosswind turbulent wake model in which the downwind wake thickness and average concentration were related to the aggregated vehicle drag of the traffic stream. They assumed that the rate of entrainment of ambient air into the wake was proportional to the drag induced velocity component parallel to the roadway. Near field and far field expressions for wake thickness and concentration were non-dimensionalized by the factor, ξs, where ξ equaled the ratio of vehicular to ambient momentum in the wake, and s equaled the separation distance between opposing streams of traffic. Their results were verified with moderate success in a wind tunnel experiment in which the vehicle wake effects were simulated by an array of jets directed transverse to the mean flow. The results were so specialized, however, that they were of little practical use to the modeler.

Lane and Stukel (1976) published results of single vehicle wake experiments conducted in a low-speed water flume. Their experiments were run under conditions so as to be dynamically similar to vehicle speeds of 35 to 100 mph in air. They showed that for speeds greater than 35 mph, the distribution of pollutants within the wake was insensitive to vehicle speed, and that the radial distribution of pollutant concentrations normal to the vehicle direction followed a Gaussian curve. In addition, they found that emitted material dispersed rapidly within the wake so that near ambient levels were recorded by nine vehicle lengths downstream. These results tended to confirm some of Dabberdt's earlier reasoning regarding the lack of correlation in field data between traffic parameters and vertical dispersion.

Rao, Sedefian and Czapski (1979) presented results of a sophisticated field study including a spectral analysis of vehicle induced turbulence. They found the dominant frequency of vehicle induced turbulence for traffic speeds ranging from 35 to 60 mph to be in the order of 0.25 Hz (corresponding to horizontal eddy sizes of 4 to 8 meters). By studying the $\overline{w'T'}$ and $\overline{u'w'}$ cospectra, they concluded that contributions to near roadway turbulence from vehicular waste heat emissions was quickly disorganized

by the mechanical turbulence produced by each vehicle's motion. They also pointed out the importance of vehicle induced drag on wind flow near the roadway.

Recently, Eskridge and Hunt (1979) have developed a comprehensive model for predicting the velocity and turbulence field in the wake of a moving vehicle. They contend that the couple on the vehicle, and not its drag force, determines the wake strength. Solutions are obtained using finite differencing methods and summing the mean square components of velocity fluctuations due to wake passing, wake turbulence and ambient turbulence. Comparisons to observed results show that predictions of alongwind and vertical turbulence intensities, $\overline{u'^2}$ and $\overline{w'^2}$, are poor to marginal, while lateral turbulence, $\overline{v'^2}$, is predicted fairly well. The authors attribute this poor performance at predicting $\overline{u'^2}$ and $\overline{w'^2}$ to the small component of wake turbulence relative to ambient levels in these directions, and the consequent dominance of instrument noise. They also point out that the model does not incorporate the buoyancy effects suggested by Dabberdt and Chock. However, they do state that this effect should be negligible for wind speeds greater than 0.5 meters/second.

The Eskridge-Hunt vehicle wake theory is best suited for use in gridded numerical air quality models. The theory can be used to predict eddy diffusivities for multiple, overlapping wakes on the highway, thus providing the necessary detail to run the grid model with a minimum of input. Results of such an application reported by Eskridge et. al. (1979), indicated that the buoyancy effect did need to be accounted for under stable, low wind speed conditions. They considered a simple, dimensional parameterization to account for the buoyancy effect, and found it to be inadequate. Undoubtedly, the disruption of organized convective activity by the vehicle wakes makes application of conventional micrometeorological methods difficult.

3.3 Wind Speed Effect

A number of authors have noted a correlation between crossroad wind speed and initial vertical dispersion. As mentioned earlier, Dabberdt found some correspondence between wind speed and increased downwind turbulence intensity while finding no similar correlation for traffic parameters. Fay and Eng modeled their initial wake thickness as inversely proportional to the crossroad wind speed. Chock's analyses showed that the ratio of top-to-bottom level tower concentrations measured 30 meters downwind

tended to increase with decreasing crossroad wind speed. He felt that this was an indication of the greater role played by buoyancy in vertical mixing under low wind speed conditions.

Benson and Squires (1979) attempted to verify the CALINE2 model using several independent data bases. The inaccuracies that they found in the model led them to make more detailed analyses of the data in the hopes of finding explanations for the poor performance of CALINE2, especially under stable atmospheric conditions. This report is actually an extension and refinement of that earlier work. One particular area of interest was the initial vertical dispersion of vehicular emissions at the edge of the roadway. They found that the Gaussian distribution was able to fit roadside vertical concentration profiles reasonably well. However, the values of this initial σ_z did not correlate well with traffic volume or traffic volume times the square of the average vehicle speed (taken to be a gross measure of the mechanical turbulence created by the moving stream of traffic). Similarly, measures of σ_Θ and σ_ϕ showed little or no correspondance to these traffic parameters. It was concluded that for the range of traffic volumes and speeds studied (4000 to 8000 vehicles/hour and 30 to 60 miles/hour) little difference in initial vertical mixing

was to be expected. It was hypothesized that at vehicle speeds above 35 miles/hour the wake thickness was relatively insensitive to speed (Lane and Stukel, 1976), and at lower speeds, and correspondingly higher traffic densities, the loss of mechanically generated turbulence was offset by an increase in thermal turbulence.

Benson and Squires also presented correlated measurements of initial σ_z and wind speed for the three independent data bases they studied. The results were strikingly similar, suggesting some sort of underlying physical basis. The authors concluded that the initial vertical dispersion was dependent upon the residence time of emitted pollutants within the intensely turbulent region occupied by the moving stream of traffic. This physical interpretation was also suggested by Rao and Keenan (1980) in their work on improving the Environmental Protection Agency's line source Gaussian model, HIWAY.

DeTar (1979) took the concept one step further and developed a Gaussian model in which σ_z was solely a function of time of travel from roadway to receptor, with a higher rate of plume growth assigned for travel time spent over the roadway. This had the interesting consequence of $\sigma_z \to \infty$ as $u \to 0$ rather than the conventional result of $C \to \infty$

as $u \to 0$. Unfortunately, DeTar did not incorporate σ_y into his model, so that lateral dispersion was not realistically accounted for. His model does present a provocative alternative to the classical Gaussian plume method, however, particularly in flows where the dominant turbulence generating mechanism is independent of distance traveled (i.e., convective versus shear flows).

Another important aspect of wind speed which must be considered when using the Gaussian dispersion model, as derived in Section 2.2, is the assumption of zero wind shear. Drivas and Shair (1974) have shown that this assumption is totally inappropriate for an instantaneous crosswind line source. However, they note that the assumption is much more viable for a continuous source. Because of the quasi-empirical nature of the Gaussian model, inconsistencies between model assumptions and actual conditions, such as the omission of wind shear, can be at least partially accounted for by reliable field measurements of σ_y and σ_z, and by rational application of the model to situations similar to those from which the dispersion parameters were derived.

4. FIELD MONITORING PROGRAMS

Development of the CALINE3 model has relied heavily upon comprehensive field monitoring programs conducted independently by several organizations during the 1970's. These programs are briefly described here along with the recently completed Caltrans Intersection Study in Sacramento.

4.1 General Motors Sulfate Dispersion Experiment

The General Motors (GM) Sulfate Experiment (Cadle et. al., 1977) was conducted at the GM Milford, Michigan, proving grounds straightaway track during the month of October, 1975. The track is 5 kilometers long and is surrounded by lightly wooded, rolling hills. Three hundred and fifty-two cars, including 8 vehicles emitting tracer gas, were driven at constant speeds of 80 km/hr around the track. This simulated a traffic flow of 5,462 vehicles per hour along a four lane freeway with a median width of approximately 12 meters.

Monitoring probes were stationed at 2 upwind locations and 5 downwind locations out to a distance of 113 meters from the track centerline (see Fig. 3). In addition, a monitoring location was situated in the track median. The

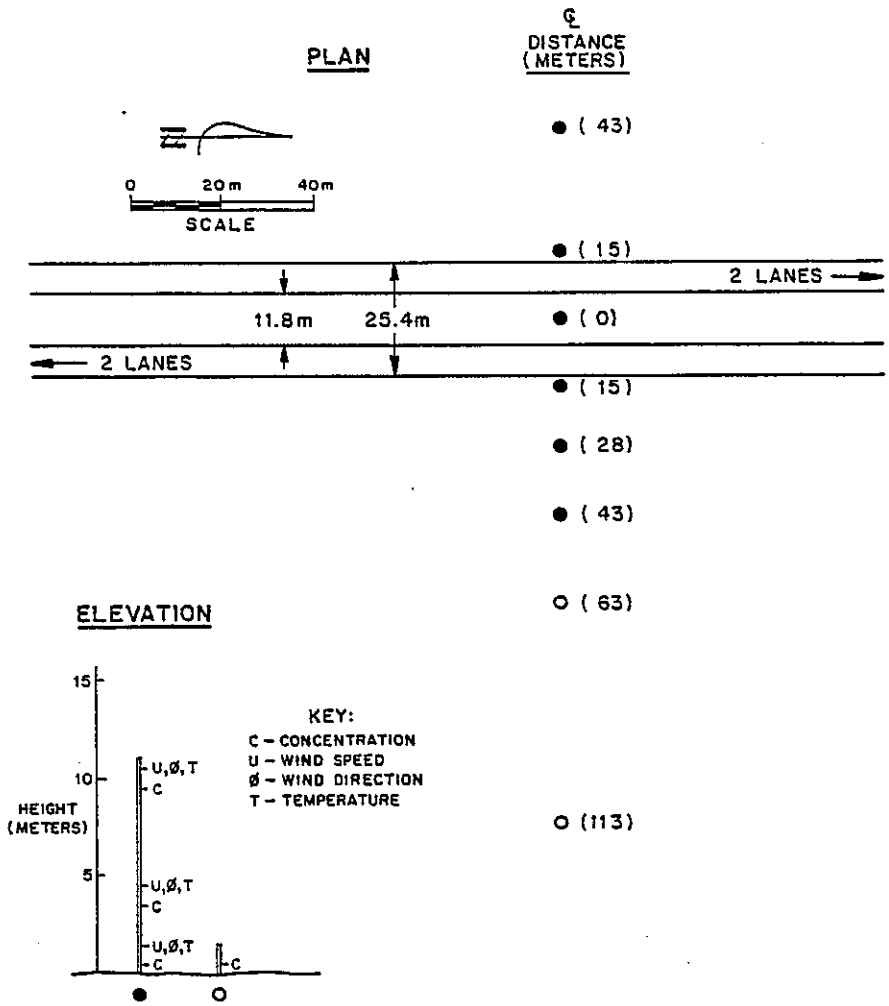

GENERAL MOTORS (GM) SULFATE
EXPERIMENT TEST SITE

FIGURE 3

westerly, median and closest 3 easterly locations were equipped with tower mounted sampling probes at elevations (z) of 0.5, 3.5 and 9.5 meters above the ground. The two additional more distant downwind probes were positioned at z = 0.5 meter. Wind speed and direction measurements were made at each probe location using Gill UVW anemometers. Temperature profiles were recorded at the two outermost towers, 43 meters from the track centerline. The use of sulfur hexafluoride (SF_6) as a tracer gas in 8 of the vehicles eliminated interference from background pollutant levels. SF_6 is a highly inert gas found in only insignificant amounts in ambient air.

Data from over 60 half hour test runs was compiled. Most of these were conducted during early morning hours to take advantage of the stable atmospheric conditions prevalent then. The cars were grouped into 32 single lane packs of 11 cars each and distributed over the track so that two packs from each direction passed the sampling area simultaneously at approximately 30 second intervals.

The experimental procedure in the GM study was carefully controlled, resulting in one of the most reliable highway air quality data bases yet compiled. The only shortcoming

in the experiment was the lack of variability in the traffic parameters of speed, volume and occupancy.

4.2 Stanford Research Institute Bayshore Freeway Study

The site chosen for the Stanford Research Institute (SRI) field study (Dabberdt, 1975) was located along U.S. Highway 101 in Santa Clara, California. The highway is a six lane, at-grade section with an approximate 10 meter median strip. It carries a relatively high volume of traffic (around 100,000 ADT) with traffic speed and directional volume varying considerably throughout the day.

The area surrounding the sampling location for a radius of 0.75 kilometer is essentially flat and composed of level fields containing short grasses. Monitoring was carried out during selected days in January and February of 1975. Eight ground level probes (z = 1 meter) were located on each side of the highway along a line perpendicular to the highway (see Fig. 4). Two vertical probe arrays were also located on either side of the highway with probes situated at elevations of 1, 3, 6.1 and 13.6 meters. A similar tower was located in the highway median. Wind speed and direction measurements were made at each probe location on the 5 towers using either UVW anemometers or propeller

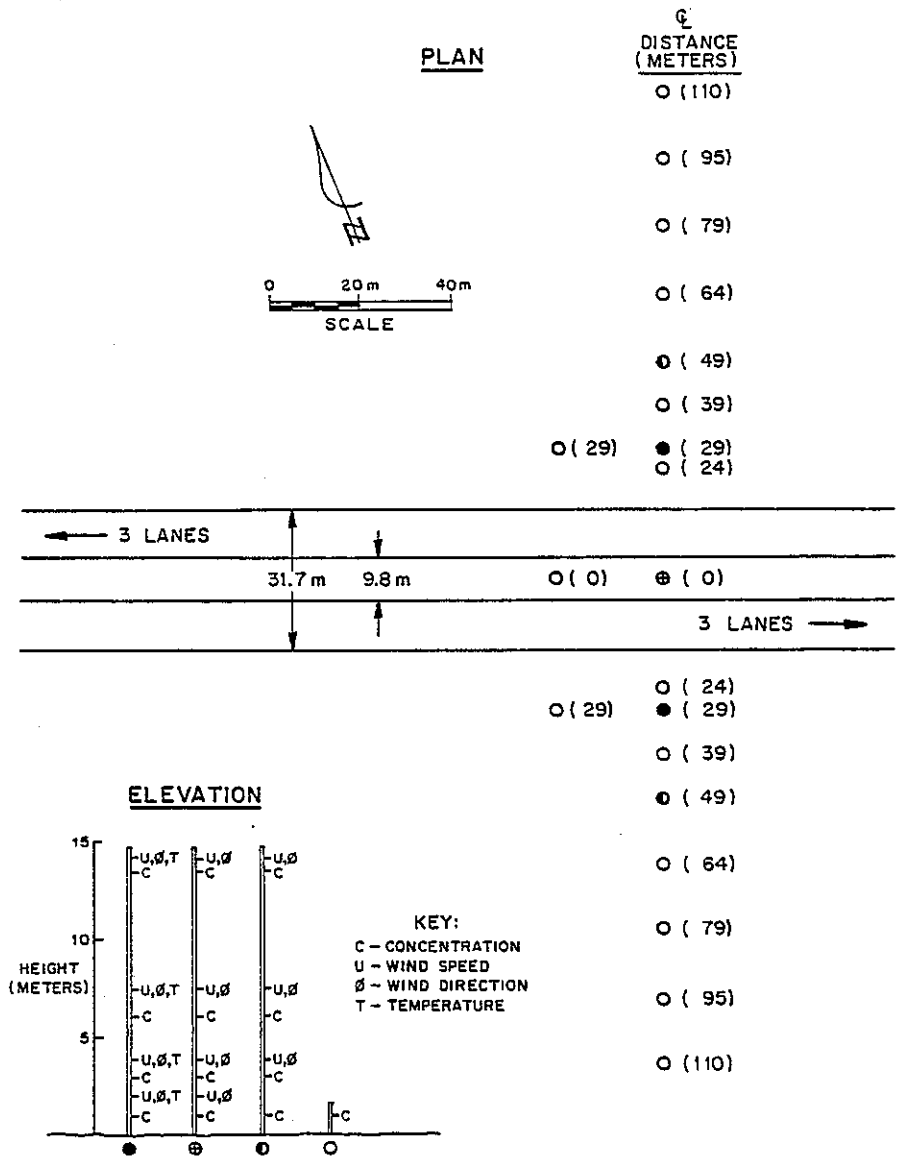

STANFORD RESEARCH INSTITUTE (SRI)
AT GRADE TEST SITE
FIGURE 4

vanes. Temperature profiles were measured at the innermost two towers. Samples were taken using sequential multibag samplers, thus obtaining integrated hourly air samples. Two vans were equipped to release two types of tracer gases, SF_6 and freon-13B1. Concentrations of the two tracer gases, methane and nonmethane hydrocarbons, and carbon monoxide were measured at each sampling location. Because of the small number of tracer vehicles and variable traffic conditions, the carbon monoxide measurements (less ambient levels) were used in this paper rather than the tracer results.

4.3 New York State Long Island Expressway Tracer Study

The New York State Department of Environmental Conservation performed a detailed series of tracer release experiments during October and November of 1976 on a segment of the Long Island Expressway (Rao et. al., 1978). For a radius cf about one kilometer around the site the topography is essentially flat, with small farms the predominant land use. The expressway runs approximately east-west with three lanes in each direction and a 20 meter grass median. The sampling network ran perpendicular to the expressway with three ground level (z = 2.0 meters) probes on each side out to a distance of 80 meters from the median centerline and a single probe in the median (see Fig. 5). Also,

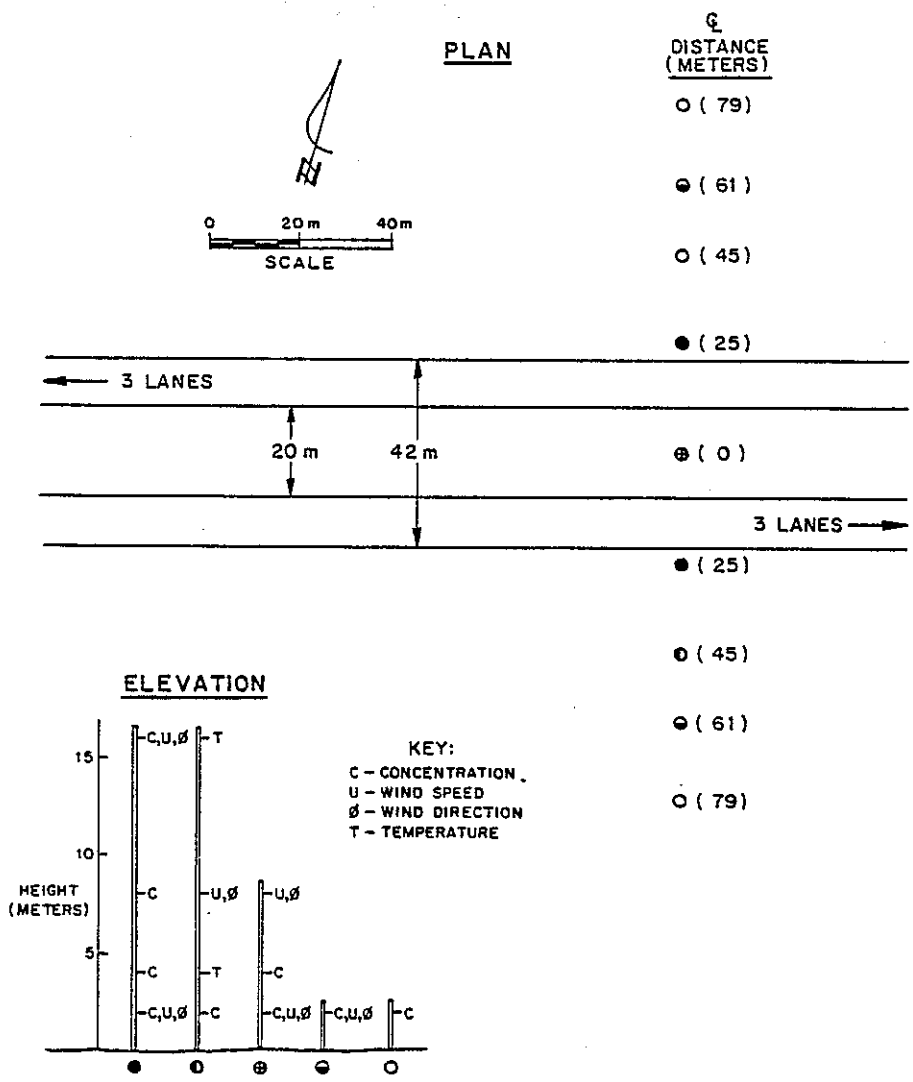

NEW YORK STATE (NY)
AT GRADE TEST SITE

FIGURE 5

vertical probe arrays (z = 2, 4, 8, 16 meters) were situated on each side of the expressway 25 meters from the centerline or within about 4 meters of the traveled way. Wind shear measurements were made at these towers while temperature gradient was measured at a single tower 45 meters south of the expressway centerline.

A total of 23 tracer runs of 1 hour duration each were made using SF_6. Six station wagons following a closed loop route at approximate 90 second intervals were used to release the tracer. Release occurred from 0.8 kilometer east to about 0.3 kilometer west of the sampling network. Sample recovery was made using 44 liter bag samplers operating at a 0.7 liter/minute flow rate.

All but one of the 23 runs were made under neutral to unstable conditions. Wind speeds varied from 0.9 to 7.5 meter/second as measured in the median at a height of 8 meters. A variety of crosswind, parallel and oblique wind directions with respect to the expressway were reported.

4.4 Caltrans Los Angeles Freeway Study

During 1974 and 1975, the California Department of Transportation conducted a detailed monitoring program for pollutants near freeways in the Los Angeles area (Bemis et. al., 1977). Comprehensive amounts of meteorologic and aerometric data were compiled for two sites in particular: a depressed portion of the Santa Monica Freeway (LA1), and an elevated (fill) segment of the San Diego Freeway (LA3). The configurations of meteorological sensors and concentration probes used for the two sites are shown in Figures 6 and 7.

Two specially equipped air quality research vans were built for the LA study. Each contained a computer linked to a variety of analyzers which recorded concentrations of carbon monoxide, oxides of nitrogen, methane, non-methane hydrocarbons and ozone. Up to 15 probe locations could be monitored simultaneously for carbon monoxide. Also, wind shear and lapse rates could be measured and recorded at two separate locations.

A single research van was used at each site. Traffic data for the sites was obtained from the Los Angeles surveillance loop, a 42 mile freeway loop containing permanently installed

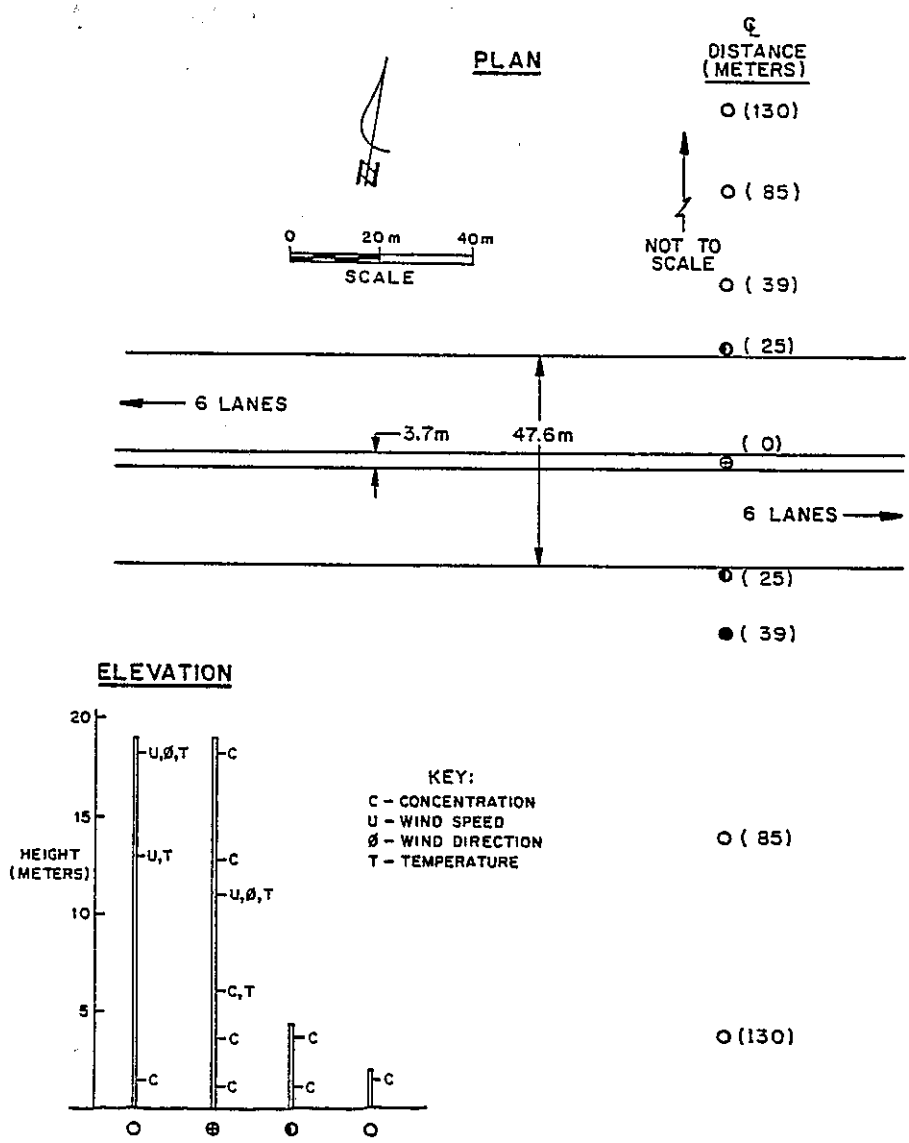

CALTRANS LOS ANGELES DEPRESSED
(LA I) TEST SITE

FIGURE 6

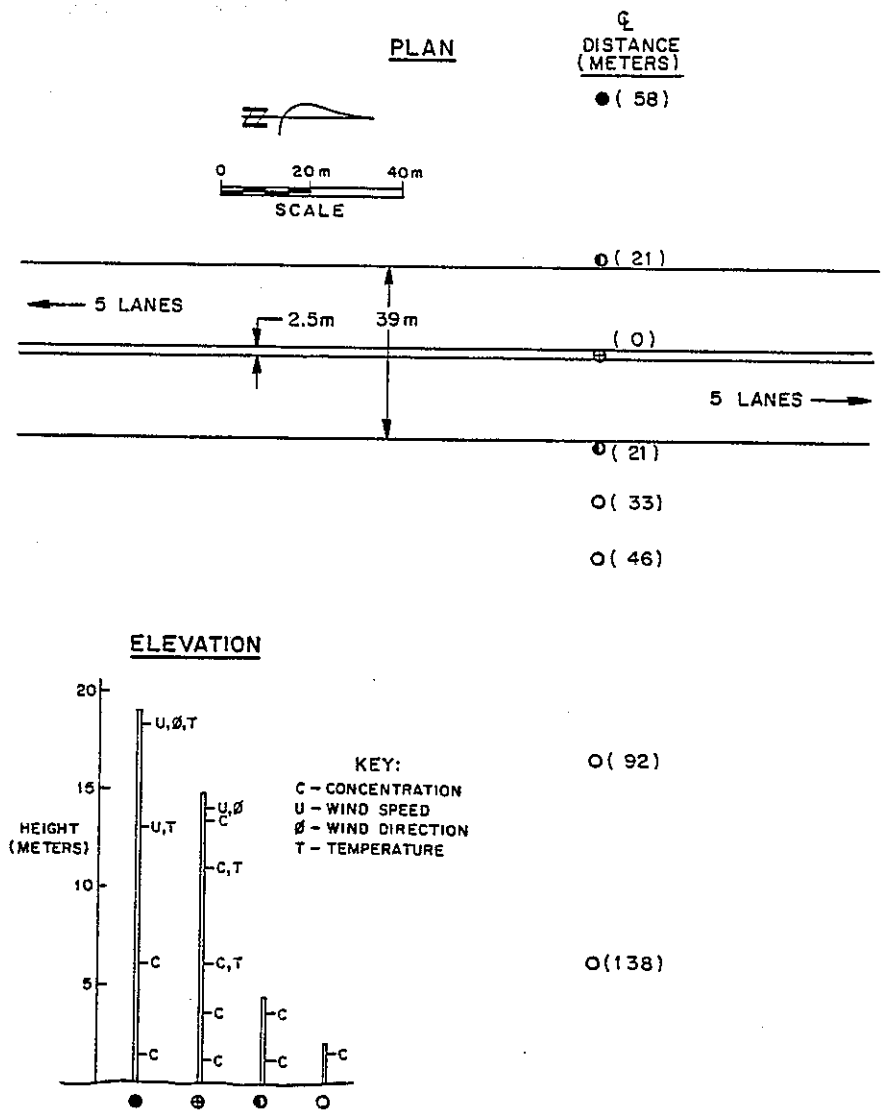

CALTRANS LOS ANGELES FILL
(LA 3) TEST SITE

FIGURE 7

traffic counting devices. Monitoring at the LA1 site started in early April, 1974, and continued through mid-July of the same year for approximately 3-1/2 months worth of data. The LA3 site was monitored for approximately 8 months, starting in late August, 1974 and ending April, 1975. Both sites were representative of urban residential locations, and were far removed from isolated pollutant sources such as power plants and industrial complexes. The LA1 site was located approximately 10 miles inland from the ocean in a mixed single and double story residential area. The LA3 site was situated about 3 miles from the ocean with a resulting crosswind sea/land breeze wind pattern prevailing. The area surrounding the LA3 site was open and flat on the west (seaward) side of the freeway, and light density, single story residential on the east side.

4.5 Caltrans Intersection Study

During the first three months of 1980, the California Department of Transportation conducted an extensive aerometric survey at the intersection of Florin Road and Freeport Boulevard in Sacramento. One of the purposes of this study was to evaluate the extent of the near roadway vertical dispersion of CO under stop-and-go traffic conditions, and compare this to similar results for free flow

highway conditions. As yet, only preliminary results are available from the study.

The intersection site chosen consisted of bare or grass covered ground on all four quadrants for a distance of at least 50 meters back from the traveled ways. The surrounding terrain was level and occupied by scattered single story residential developments. The intersection was oriented with Freeport Boulevard running due North-South and Florin Road due East-West. A small community shopping center was located well back from the intersection in the northwest quadrant. The site offered a reasonably high traffic flow without the interfering background sources of gas stations and parking lots normally associated with busy intersections. Also, the openness of the site promised a low level of entering mechanical turbulence in the surface layer flow. This made it easier to isolate vehicle induced turbulence.

Fifteen probe locations were chosen--eight in the northwest quadrant and the remainder in the southwest quadrant (see Fig. 8). Also, a sequential bag sampler was placed in the southeast quadrant. The two towers innermost to Florin Road contained vertical probe arrays with four probes on the southern tower at 1, 2, 4 and 10 meter heights, and five on the northern tower at 1, 2, 4, 10 and 15 meter heights.

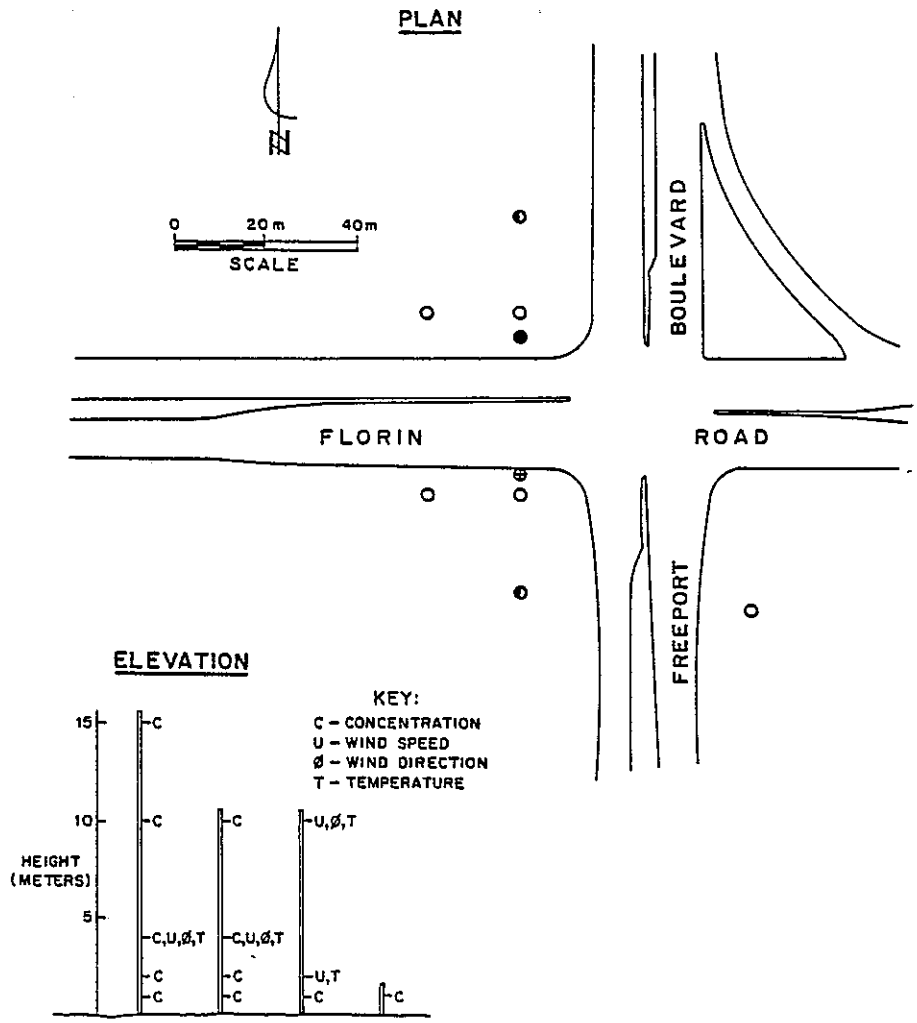

CALTRANS SACRAMENTO (SACTO)
INTERSECTION TEST SITE

FIGURE 8

Three additional ground level probes (z = 1.0 meter) were located on each side of Florin Road. The outermost meteorological towers had cup anemometers and temperature probes mounted at 2 and 10 meter heights to provide wind shear and temperature profile estimates. Wind direction was measured with wind vanes mounted at the 10 meter level. Traffic counts were made using pneumatic counters for inflow and outflow on each leg of the intersection.

One of the Caltrans air quality research vans constructed in 1974 for the freeway study in Los Angeles was used to monitor and record the various air quality and meteorological parameters. Of consequence to this study are the CO and meteorological measurements made by the van. Sampling of CO was accomplished using two separate systems: Non-dispersive Infrared (NDIR) and gas chromatography with flame ionization detection. Three NDIR analyzers were used, each dedicated to five probe lines. An on-board minicomputer performed switching at one minute intervals so that each line was sampled one minute out of every five by an NDIR analyzer at line velocities of 10 feet/second. The gas chromatography samples were taken as bag samples over the first 15 minutes of each hour, thus providing an integrated concentration measurement rather than the temporally stratified sample taken by the NDIR analyzers. The gas

chromatography analysis was run only for the nine probes in the vertical arrays next to Florin Road. Sums and sums of squares of 0.1 second wind speed and direction readings were stored by the minicomputer and written out on magnetic tape every 10 seconds. Temperature readings were recorded once every 60 seconds. Further information on the operation of the research van and its data acquisition system has been reported by Peter et. al., (1977) and Winter and Farrockhrooz (1976).

A second minicomputer housed outside of the research van was used to record 0.1 second readings from a pair of bivane anemometer-fast response thermistor units mounted at the four meter level on the two vertical probe array towers adjacent to Florin Road. The purpose of these units was to provide eddy correlation measures of atmospheric turbulence and heat flux upwind and downwind of one leg of the intersection.

Climet model 018-10 bivane anemometer units combined with fast response thermistor probes mounted 15 centimeters above the bivane pivot were used (see Fig. 9). The bivane air-foils respond to wind speeds as low as 0.34 m/s and provide a damping ratio of 0.6. The propellers have a starting threshold of 0.22 m/s and a distance constant of 0.91 meters.

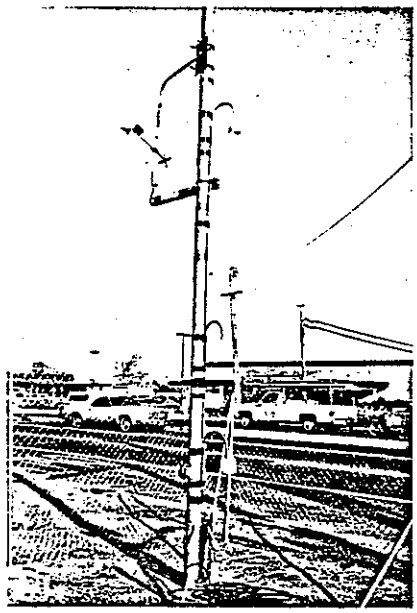

BIVANE ANEMOMETER AND
THERMISTOR PROBE AT 4 METERS

Figure 9

Kaimal et. al., (1964) compared vertical wind velocity spectra measured using a bivane anemometer and two sonic anemometers. The bivane anemometer sensed wind speed using a hot thermistor anemometer rather than the propeller device used in this study. Coherence plots showed good agreement between the three instruments up to 0.15 cycles/second. Results reported by Rao et. al, (1979) indicate that traffic induced contributions to turbulent energy are strongest at about 0.25 cycles/second. Thus, measurements obtained at the Florin-Freeport installation will be somewhat limited in their resolution of mechanically induced vehicular turbulence. The instrumentation package should, however, be able to adequately sense the larger scale thermal contributions to roadside turbulence.

Analysis of the bivane anemometer data is still in the preliminary stage, and therefore will not be presented in this report. A recent article by Chimonas (1980) has indicated the need to adjust for systematic errors inherent in the bivane anemometer system when measuring eddy correlation fluxes. These adjustments will have to be made before the analysis can proceed.

5. METEOROLOGICAL ANALYSIS

Measurements of horizontal wind speed and temperature at two heights upwind of the roadway were available for all but the New York (NY) Data Base. These measurements were used to make site specific estimates of the Obukhov Length (L), friction velocity (u_*), sensible heat flux (H) and vertical momentum diffusivity (K_z) for the surface layer.

5.1 Methodology

Atmospheric turbulence generally may be classified as either mechanical or thermal in origin. Mechanical turbulence is produced by fluid instabilities generated in regions of shear or uneven flow. In the atmosphere, shear flow is created by the frictional drag of the Earth's surface. The friction velocity, u_*, is a parameter which characterizes the downward flux of atmospheric momentum toward the surface of the Earth (see Equation 2-14). As such, it is an indicator of the amount of mechanical turbulence being produced at the location where it is measured. For a neutrally stratified isothermal shear flow, the momentum flux is directly proportional to the shear, with the constant of proportionality being defined as the momentum diffusivity. Thus,

both u_* and K_z are measures of the mechanical production of turbulence.

Thermal turbulence is produced by density instabilities caused by either convective transfer of heat away from the Earth's surface (sensible heat flux) or by delayed release of latent heat of evaporation. The former process is dominant over arid land masses while the latter is most important over oceans, lakes, etc.

Thermal turbulence produced over land is typified by vertical, convective cells of a much larger scale than mechanical turbulence. Because of this, thermal turbulence is a more energetic diluting mechanism for air pollution than mechanical turbulence. However, while thermally induced density instabilities do much to disperse air pollutants, thermal and radiative processes can also produce stably stratified conditions in which density stability acts to inhibit dispersion by suppressing turbulence.

Meteorologists use similarity parameters such as the Richardson Number and Obukhov Length as measures of atmospheric stability or instability. The Richardson Number represents a ratio of the mechanical production of turbulence to the thermally induced production or suppression of

turbulence. The Obukhov Length is interpreted as the height above the surface at which effects of thermal stratification become dominant over mechanical sources of turbulence. Similarity parameters are most useful in analyzing meteorological data because they provide a quantitative means of classifying complex and seemingly diverse atmospheric events into categories with similar dynamic properties.

Monin and Obukhov (1954) reasoned that relationships established for neutrally stratified flows could be extended to non-neutral conditions using empirically derived functions of the dimensionless quantity z/L. These functions, called ϕ-functions, provided a means of estimating the vertical fluxes of momentum, heat and water vapor during stably or unstably stratified atmospheric conditions. Conversely, given field measurements of these fluxes, the relationships could be used to determine the Obukhov Length, L.

Businger et. al. (1971) performed a comprehensive study in which ϕ-functions for momentum and heat flux were determined from both profile measurements and direct, eddy correlation flux measurements. Their results were based on 15 minute averages of meteorological observations made to a height of 32 meters over a uniform field of wheat stubble extending 2400 meters upwind. The large fetch to height ratio of

nearly 100 was considered necessary to assure that the boundary layer had attained equilibrium with respect to the homogeneous surface.

None of the sites studied in this paper could be termed homogeneous by strict micrometeorological standards. Fetch to height ratios were typically an order of magnitude below those for which the Businger ϕ-functions were derived. However, in most cases, surface roughness elements surrounding the sites were considerably larger than at the wheat stubble site used by Businger, and were of the same order of magnitude as the vehicles using the roadway. Thus, the assumption of site homogeniety was made for locations both upwind and downwind of the roadway. This assumption, though seriously open to question, permitted the use of the Businger ϕ-functions for estimating L, u_*, H and K_z.

An initial value of u_*, assuming neutral stratification, was computed using,

$$u_* = \frac{k(u_2 - u_1)}{\ln(z_2/z_1)} \qquad (5\text{-}1)$$

where k is the von Karman constant (0.35 used) and u_1 and u_2 are horizontal wind speeds measured at heights z_1 and z_2, respectively. Continuing to assume neutral conditions,

$$L = \frac{-u_*^3 C_p \rho T}{kgH} \tag{5-2}$$

and

$$H = -C_p \rho K_h \frac{\partial \theta}{\partial z} \tag{5-3}$$

where θ represents potential temperature, K_h signifies sensible heat diffusivity, g is the standard acceleration of gravity, and T is the absolute temperature. θ was estimated using,

$$\theta = T + \gamma_d z \tag{5-4}$$

where γ_d is the dry adiabatic lapse rate (approximately 1° C/100 meters). Since all of the field experiments were conducted during the winter months, and the majority of runs were made during early morning and late evening, evapotranspiration was assumed to be negligible. Thus, no adjustments for latent heat release were made to the

potential temperature estimates. Combining Equations 5-2 and 5-3 yields,

$$L = \frac{u_*^3 \, T}{kgK_h \frac{\partial\theta}{\partial z}} \tag{5-5}$$

Under neutral conditions, $u_*^2 = K_z \frac{\partial u}{\partial z}$.

Thus,

$$L = \frac{u_* \frac{\partial u}{\partial z}}{\frac{kg}{T} \frac{\partial\theta}{\partial z}} \left(\frac{K_z}{K_h}\right) \tag{5-6}$$

A value of 1 for K_z/K_h was initially assumed.

Using the value of L computed from Equation 5-6 and the Businger ϕ-functions, a revised estimate of u_* was made.

$$\left(\frac{\partial u}{\partial z}\right) \frac{kz}{u_*} = \phi_m(z/L) \tag{5-7}$$

where $\phi_m(z/L) = 1 + 4.7\ z/L$ for stable conditions ($\partial\theta/\partial z>0$) and $\phi_m(z/L) = (1 - 15\ z/L)^{-1/4}$ for unstable conditions ($\partial\theta/\partial z<0$). Integrating Equation 5-7 from u_1 to u_2 and z_1

to z_2 yields,

$$u_* = \frac{k(u_2 - u_1)}{\ln(z_2/z_1) + \frac{4.7}{L}(z_2 - z_1)} \tag{5-8}$$

for $\partial\theta/\partial z>0$, and

$$u_* = \frac{k(u_2 - u_1)}{\ln\left\{\left[\frac{\psi_2 - 1}{\psi_2 + 1}\right]\left[\frac{\psi_1 + 1}{\psi_1 - 1}\right]\right\} + 2(\tan^{-1}\psi_2 - \tan^{-1}\psi_1)} \tag{5-9}$$

for $\partial\theta/\partial z<0$, where $\psi_1 = (1 - 15\ z_1/L)^{1/4}$ and $\psi_2 = (1 - 15\ z_2/L)^{1/4}$.

L was then recalculated using the revised value for u_* and the ϕ-function methodology. For all stability conditions,

$$u_*^2 = \frac{kzu_*}{\phi_m(z/L)}\left(\frac{\partial u}{\partial z}\right) \tag{5-10}$$

and

$$H = \frac{-kzu_*C_p\rho}{\phi_h(z/L)}\left(\frac{\partial\theta}{\partial z}\right) \tag{5-11}$$

Substituting Equations 5-10 and 5-11 into Equation 5-2 gives

$$L = \frac{u_* \frac{\partial u}{\partial z}}{\frac{kg}{T} \frac{\partial \theta}{\partial z}} \left(\frac{\phi_h(z/L)}{\phi_m(z/L)} \right) \tag{5-12}$$

where $z = (z_1/z_2)^{1/2}$ and L is the Obukhov length from the previous iteration. For $\partial\theta/\partial z>0$, $\phi_h\ (z/L) = 1 + 17\ z/L$, while for $\partial\theta/\partial z<0$, $\phi_h\ (z/L) = (1 - 15\ z/L)^{-0.55}$.

If $|1/L^{NEW} - 1/L^{OLD}| < 0.0005$, the iterative solution was considered closed. If not, a revised value for L was determined by,

$$1/L = \{(1/L^{NEW})(1/L^{OLD})\}^{1/2} \tag{5-13}$$

where the proper sign of L was retained. The revised value of L was then reapplied to either Equation 5-8 or 5-9 to determine a new value for u_* which was then used in Equation 5-12. This series of computations was repeated until convergence was achieved. At that time, H was determined using Equation 5-11 and K_z was computed by,

$$K_z = \frac{ku_* z}{\phi_m(z/L)} \tag{5-14}$$

Golder [1972] studied the relationship between the classes of the Pasquill stability method and some commonly used atmospheric similarity parameters. His study was based on observations made independently at five meteorologically diverse sites. Golder's findings, presented in nomographic form, organized the Pasquill stability classes in terms of inverse Obukhov Length ranges for sites of varying aerodynamic roughness length, z_o. In this paper, the Golder nomograph was used to estimate Pasquill stability classes from computed values of L.

Under low wind speeds (u<1 m/s), the iterative method for computing L oftentimes would not converge to a solution. This was primarily due to the difficulty in measuring wind shear accurately under such conditions. In order to assign a Pasquill stability class, the Bulk Richardson Number (Ri_B) was computed for these cases as follows,

$$Ri_B = \frac{g}{T} \frac{\partial\theta/\partial z}{u^2} \bar{z}^2 \tag{5-15}$$

where $\bar{z}$ equals the geometric mean of the two heights at which temperature measurements are made to estimate $\partial\theta/\partial z$ and u is the horizontal wind speed measured at $\bar{z}$. Nomographs also developed by Golder (1972) were then used to determine the Richardson Number (Ri) from Ri_B and z_0. As suggested by Golder, L was computed by $1/L = Ri/z_2(1 - 7Ri)$ for $\partial\theta/\partial z>0$, and $1/L = Ri/z_2$ for $\partial\theta/\partial z<0$.

5.2 Results

For both the GM and Caltrans Sacramento (SACTO) studies, values of L, u_*, H and K_z were computed at meteorological towers upwind and downwind of the roadway. These towers, located 30 meters from the roadway edge, were outside the influence of vehicle drag flows, yet close enough to sense traffic induced modifications to the stability of the surface layer. Temperature and wind speed measurements taken at heights of 1.5 and 10.5 meters for the GM study, and 2.0 and 10.0 meters for the SACTO study were used to apply the methods described in section 5.1. The results are given in Tables 2 and 3. As mentioned before, the Pasquill stability classes were assigned according to Golder's method. Stability entries containing no values for 1/L, etc., were assigned using the Bulk Richardson Number method. Also noted in the tables are the wind

TABLE 2

METEOROLOGICAL ANALYSIS
GENERAL MOTORS SULFATE EXPERIMENT
INSTRUMENT ELEVATIONS: 1.5 AND 10.5 METERS
TOWER LOCATIONS: 30 METERS FROM EDGE OF ROADWAY

	UPWIND					DOWNWIND						
RUN NO.	U* (M/S)	H (LY/MIN)	KZ (SQM/S)	1/L (1/M)	STAB	U* (M/S)	H (LY/MIN)	KZ (SQM/S)	1/L (1/M)	STAB	U (M/S)	PHI (DEG)
2720820	----	----	----	----	F	----	----	----	----	F	1.0	59
2720850	----	----	----	----	F	----	----	----	----	A	1.2	78
2720920	----	----	----	----	F	----	----	----	----	A	.6	75
2720950	----	----	----	----	A	----	----	----	----	A	.7	64
2741410	.281	.056	.474	-.020	C	.259	.038	.427	-.017	C	3.7	69
2741440	.261	.080	.481	-.035	C	.261	.057	.456	-.025	C	3.2	68
2741510	.260	.023	.407	-.010	D	.252	.069	.460	-.034	C	3.6	69
2741540	.278	.016	.416	-.006	D	.288	.060	.484	-.020	C	3.9	68
2750810	.132	-.003	.151	.011	D	.107	.001	.158	-.004	D	1.7	39
2760915	.262	.021	.405	-.009	D	.286	.041	.461	-.014	C	3.5	47
2760945	.297	.048	.481	-.014	C	.327	.068	.533	-.015	C	4.0	56
2790810	.046	-.002	.021	.110	F	.082	-.002	.081	.022	E	1.5	71
2790840	.052	-.001	.031	.072	F	.132	.003	.205	-.010	D	1.5	67
2790910	.133	.008	.235	-.027	C	.185	.037	.356	-.045	C	1.8	73
2790940	.180	.028	.336	-.038	C	.228	.066	.435	-.043	C	2.3	70
2810805	.099	-.004	.085	.033	E	.201	.006	.300	-.006	D	2.3	36
2810905	.020	-.000	.008	.132	F	.098	.003	.166	-.021	C	1.2	78
2810935	.103	-.001	.124	.008	D	.187	.046	.373	-.055	B	2.4	86
2830820	.091	-.002	.095	.017	E	.142	.008	.243	-.022	C	1.7	74
2830850	.064	-.000	.075	.010	D	.117	.027	.279	-.130	A	1.2	83
2830920	.111	.006	.206	-.037	C	.145	.026	.301	-.067	B	1.4	62
2830950	.138	.019	.277	-.056	B	.174	.032	.339	-.048	C	1.6	40
2900810	.074	-.002	.061	.036	E	.198	.014	.320	-.014	C	2.5	68
2900840	.098	-.003	.092	.026	E	.241	.022	.384	-.012	C	2.6	58
2900910	.093	-.002	.096	.018	E	.227	.031	.385	-.020	C	2.5	62
2900940	.127	-.002	.159	.006	D	.249	.043	.426	-.022	C	2.8	56
2931035	.174	.004	.261	-.006	D	.224	.030	.381	-.021	C	2.5	88
2931105	.183	.011	.294	-.014	C	.224	.059	.424	-.041	C	2.6	89
2940805	.099	-.006	.076	.043	E	.173	-.005	.209	.008	D	2.2	50
2940835	.103	-.005	.088	.033	E	.192	-.002	.255	.003	D	2.2	55
2940935	.146	.024	.298	-.062	B	.176	.032	.340	-.046	C	1.7	39
2950810	----	----	----	----	F	----	----	----	----	F	.4	51
2950840	----	----	----	----	F	----	----	----	----	F	.8	75
2950910	----	----	----	----	F	----	----	----	----	E	.9	49

TABLE 3

METEOROLOGICAL ANALYSIS
FLORIN-FREEPORT INTERSECTION
INSTRUMENT ELEVATIONS: 2.0 AND 10.0 METERS
TOWER LOCATIONS: 30 METERS FROM EDGE OF ROADWAY

	UPWIND					DOWNWIND						
RUN NO.	U* (M/S)	H (LY/MIN)	KZ (SQM/S)	1/L (1/M)	STAB	U* (M/S)	H (LY/MIN)	KZ (SQM/S)	1/L (1/M)	STAB	U (M/S)	BRG (DEG)
6014	.235	.023	.430	-.013	C	.270	.226	.681	-.085	B	4.0	336
6015	.153	.009	.294	-.019	C	.206	.112	.532	-.095	B	2.8	316
6016	.093	-.000	.132	.005	D	.169	.026	.366	-.041	B	2.5	330
6017	.032	-.000	.020	.076	F	.099	.002	.184	-.015	C	1.7	339
6018	----	----	----	----	F	----	----	----	----	F	.9	262
6107	----	----	----	----	F	----	----	----	----	F	.5	20
6108	.096	.006	.219	-.052	B	.107	.004	.210	-.023	C	1.1	58
6109	.066	.003	.167	-.087	B	.107	.002	.195	-.013	C	1.2	23
6110	.051	.004	.162	-.243	A	.122	.016	.292	-.068	B	1.2	19
8116	.359	.009	.576	-.001	D	.330	.100	.642	-.021	C	6.1	329
8117	.191	-.007	.259	.007	D	.196	.013	.358	-.013	C	4.0	337
8118	.095	-.002	.104	.020	E	.056	-.001	.049	.038	E	1.9	330
8119	.111	-.003	.133	.015	E	.056	-.002	.037	.065	F	2.0	319
8120	.127	-.006	.134	.023	E	.129	-.006	.138	.022	E	2.9	0
8121	.157	-.006	.194	.012	E	.253	-.015	.343	.007	D	4.5	19
8706	.059	-.001	.051	.038	E	.055	-.001	.054	.028	E	1.2	4
8707	.061	-.000	.085	.005	D	.131	.035	.354	-.117	A	1.5	339
8708	.168	.013	.327	-.021	C	.249	.211	.652	-.102	B	3.0	328
8715	.433	.033	.710	-.003	D	.442	.145	.804	-.012	C	7.2	325
8716	.372	.015	.603	-.002	D	.354	.095	.663	-.016	C	6.4	333
8717	.251	-.008	.362	.004	D	.242	.031	.455	-.016	C	4.8	334
8718	.097	-.002	.109	.018	E	.002	-.000	.000	2.341	F	2.0	312
8913	.236	.389	.737	-.221	A	.199	.070	.476	-.066	B	2.5	159
8914	.220	.300	.679	-.209	A	.191	.082	.484	-.089	B	2.4	191
8915	.167	.167	.546	-.267	A	.181	.071	.461	-.089	B	2.1	203
8916	.175	.054	.429	-.075	B	.168	.047	.410	-.073	B	2.2	190
8917	.073	-.001	.074	.026	E	.109	.008	.242	-.047	B	1.8	194
8918	.091	-.004	.076	.041	E	.224	.005	.369	-.003	D	2.4	164
8919	.108	-.007	.095	.037	E	.185	-.002	.278	.002	D	2.4	162
8920	.122	-.006	.127	.024	E	.179	-.002	.261	.003	D	2.4	148
8921	.066	-.002	.047	.057	F	.142	-.001	.212	.002	D	1.7	149
8922	.037	-.001	.018	.107	F	.133	-.002	.181	.007	D	1.9	175
8923	.106	-.005	.100	.031	E	.190	.001	.301	-.001	D	2.3	163
9114	.215	.322	.685	-.243	A	.177	.078	.466	-.104	B	2.4	179
9115	.230	.169	.605	-.103	B	.234	.089	.533	-.052	B	3.1	177
9116	.263	.085	.557	-.035	C	.227	.081	.517	-.052	B	3.6	181
9117	.153	.001	.249	-.002	D	.225	.059	.486	-.039	C	2.9	160
9516	.192	-.004	.277	.004	D	.247	.032	.461	-.016	C	3.2	149
9517	.205	-.003	.303	.003	D	.230	.025	.428	-.015	C	3.3	148
9518	.281	-.010	.409	.003	D	.273	.011	.453	-.004	D	4.5	151
9519	.231	-.008	.326	.005	D	.246	.007	.405	-.003	D	4.4	143
9520	.207	-.009	.280	.007	D	.213	.002	.343	-.002	D	3.9	143

speed (U) and wind direction measured at the higher, upwind instrument location. In Table 2, the wind direction is given relative to the roadway (PHI, 0° = Parallel wind, 90° = crosswind) while in Table 3 it is given as the azimuth bearing with respect to true North (note that the Florin-Freeport intersection is oriented north-south, east-west).

Table 4 gives similar results for the SRI study. However, only the upwind tower was analyzed because the tower locations, 10.7 meters from the roadway edge, was close enough so that advected drag flow velocity components sometimes caused negative wind shear measurements at the downwind tower. The micrometeorological relationships discussed in Section 5-1 are not valid for such transient boundary layer flows.

Tables 5 and 6 summarize results from the upwind meteorological analyses for the LA1 and LA3 sites. The second meteorological tower for both these sites was located in the freeway median, and therefore was not analyzed because of the same drag flow problem experienced with the SRI data.

Stability classes for the NY study were taken from Rao et. al., (1979). These were based on temperature gradient and

TABLE 4

METEOROLOGICAL ANALYSIS
STANFORD RESEARCH INSTITUTE AT-GRADE SITE
INSTRUMENT ELEVATIONS: 2.0 AND 7.3 METERS
TOWER LOCATION: 10.7 METERS FROM EDGE OF ROADWAY

DATE-TIME	U P W I N D U* (M/S)	H (LY/MIN)	KZ (SQM/S)	1/L (1/M)	STAB	U (M/S)	PHI (DEG)
21 JAN 0700	----------				F	.7	46
21 JAN 0900	.054	.007	.152	-.294	A	.9	79
24 JAN 0600	.077	-.005	.044	.075	F	1.3	44
24 JAN 0700	.114	-.011	.080	.051	F	1.8	37
24 JAN 0800	.022	-.000	.007	.161	F	.8	47
24 JAN 1200	.131	.091	.365	-.294	A	1.6	44
28 JAN 0700	.147	-.007	.152	.017	E	3.5	46
28 JAN 0900	.180	.019	.302	-.023	C	3.1	51
28 JAN 1100	.129	.145	.406	-.487	A	.9	78
30 JAN 1400	.164	.106	.406	-.174	A	1.6	49
30 JAN 1500	.176	.262	.512	-.349	A	2.3	50
30 JAN 1600	.160	.395	.551	-.692	A	2.0	66
30 JAN 1900	.076	-.006	.037	.098	F	1.0	87
5 FEB 1200	.184	.018	.304	-.021	C	2.9	46
5 FEB 1300	.190	.008	.283	-.008	C	4.0	63
5 FEB 1400	.233	.012	.342	-.007	D	3.8	67
5 FEB 1500	.314	.006	.435	-.002	D	5.3	72
5 FEB 1600	.336	-.006	.446	.001	D	5.2	72
5 FEB 1700	.330	-.005	.439	.001	D	3.9	69
5 FEB 1800	.215	-.020	.231	.014	E	2.4	55

TABLE 5

METEOROLOGICAL ANALYSIS
CALTRANS LOS ANGELES STUDY - SITE 1
INSTRUMENT ELEVATIONS: 13.4 AND 18.6 METERS
TOWER LOCATION: 15 METERS FROM EDGE OF ROADWAY

DATE-TIME				UP WIND U* (M/S)	H (LY/MIN)	KZ (SQM/S)	1/L (1/M)	STAB	U (M/S)	PHI (DEG)
74	4	23	5	.348	.006	2.022	-.001	D	2.0	86
74	5	1	9	.430	.097	3.092	-.008	B	2.5	83
74	5	1	11	.352	.356	3.764	-.055	A	2.2	81
74	5	8	5	.353	.027	2.306	-.004	C	1.5	80
74	5	8	6	.149	-.000	.768	.001	D	1.2	89
74	5	8	7	.287	.005	1.706	-.001	C	1.6	80
74	5	8	8	.277	.026	1.992	-.008	B	1.3	87
74	5	14	8	.279	.014	1.826	-.004	C	1.5	85
74	5	17	10	.647	.172	4.243	-.004	C	3.3	83
74	5	23	7	.142	.004	1.050	-.009	B	1.4	76
74	5	23	9	.312	.116	2.808	-.025	B	1.8	82
74	5	23	10	.358	.104	2.892	-.015	B	2.0	88
74	5	23	12	.387	.125	3.096	-.015	B	2.6	77
74	5	28	7	.348	.041	2.415	-.006	B	1.9	77
74	5	28	8	.315	.026	2.137	-.006	B	1.9	77
74	5	29	6	.611	.051	3.642	-.002	C	2.5	84
74	5	29	8	.277	.026	1.987	-.008	B	1.9	78

TABLE 6

METEOROLOGICAL ANALYSIS
CALTRANS LOS ANGELES STUDY - SITE 3
INSTRUMENT ELEVATIONS: 13.4 AND 18.6 METERS
TOWER LOCATION: 40 METERS FROM EDGE OF ROADWAY

DATE-TIME				UP WIND U* (M/S)	H (LY/MIN)	KZ (SQM/S)	1/L (1/M)	STAB	U (M/S)	PHI (DEG)
74	8	21	14	.447	.324	3.983	-.024	C	5.1	78
74	8	23	13	.495	.593	4.703	-.033	B	5.3	79
74	8	23	15	.404	.262	3.668	-.027	C	5.7	77
74	8	26	13	.441	.424	4.200	-.033	B	4.9	78
74	8	26	14	.372	.331	3.762	-.044	B	5.1	78
74	8	26	17	.394	.099	2.983	-.011	C	5.1	79
74	8	29	14	.354	.295	3.611	-.045	B	4.9	79
74	8	30	6	.074	.007	.945	-.117	A	1.2	78
74	8	30	14	.382	.325	3.779	-.039	B	4.8	78
74	11	13	12	----	----	----	----	E	1.9	78
74	11	13	14	.279	.211	3.109	-.065	B	2.0	79
74	11	13	18	----	----	----	----	F	.5	78
74	12	16	17	----	----	----	----	F	.8	75
75	1	16	16	----	----	----	----	E	1.0	80
75	1	16	18	----	----	----	----	F	.9	81
75	1	17	17	----	----	----	----	F	.9	79
75	1	17	18	----	----	----	----	F	.5	81
75	1	21	12	.182	.498	3.416	-.563	A	1.2	77
75	1	21	18	----	----	----	----	F	.8	76
75	2	26	15	.187	.015	1.504	-.015	C	2.2	77
75	2	26	16	.092	-.001	.339	.007	E	2.2	77
75	3	13	15	.302	.090	2.630	-.022	C	2.1	77
75	3	14	16	.234	-.005	1.054	.003	D	3.9	77
75	3	14	17	.148	-.003	.540	.007	E	2.8	78
75	3	14	18	.141	-.002	.544	.006	E	2.1	79
75	3	17	18	----	----	----	----	F	.9	77
75	3	18	18	.051	-.001	.090	.029	E	1.3	76
75	3	21	10	.242	.027	1.888	-.013	C	2.1	78
75	3	24	18	.071	-.001	.200	.013	E	1.6	78
75	3	25	8	.279	.014	1.831	-.004	D	3.0	79
75	3	25	9	.172	-.004	.664	.006	E	3.2	78
75	3	27	10	.304	.121	2.809	-.029	C	2.2	77
75	3	28	16	.522	.047	3.203	-.002	D	5.6	79
75	3	28	17	.394	-.012	1.963	.001	D	4.3	79

wind speed measurements obtained at the site.

5.3 Discussion

Examination of Tables 2 and 3 indicates a general tendency for more unstable conditions to prevail immediately downwind of the roadway during neutral to stable upwind episodes. During extremely unstable episodes, the reverse effect is seen in a limited number of cases. Table 7 shows the distribution of GM and SACTO runs cross-classified by upwind stability class (A = most unstable, F = most stable) and net change in number of classes between the upwind and downwind towers. The table contains only those cases computed by the iterative method. It is clear that either the traffic or the roadway itself is altering the stability of at least the first 10 meters of the surface layer. The downwind extent of this modification cannot be ascertained from the data because of the lack of more distant meteorological towers.

Possible explanations for the observed pattern of stability modifications involve the contributions of traffic motion and heat to the level of turbulence of the mean flow immediately downwind of the roadway. Under stable conditions, the mechanical mixing resulting from numerous, superimposed

TABLE 7

FREQUENCY DIAGRAM OF
ATMOSPHERIC STABILITY CLASS MODIFICATION
DOWNWIND OF ROADWAY – GM & SACTO DATA

NET CHANGE DOWNWIND (NO. OF CLASSES)	UPWIND STABILITY CLASS A	B	C	D	E	F	
+3				2	1	2	More Unstable
+2				2	4	3	↑
+1		2	5	13	8	1	
0		2	6	4	3		No Change
−1	5	2			2		↓
−2							More Stable

vehicle wakes could cause a downward flux of sensible heat in the lower 10 meters, thus lessening the strength of the stable, upwind temperature gradient. Also, additions of vehicular waste heat near the surface might be strong enough to destabilize a stably stratified upwind flow. Under strongly unstable conditions, the mechanical mixing is likely to disrupt organized convective air movements by rapidly dissipating ground level heat build up through forced convection.

Figures 10 and 11 show the ratio of downwind to upwind vertical momentum diffusivity plotted against the inverse Obukhov Length for the GM and SACTO data, respectively. For both data sets, the points group about a ratio of unity for unstable conditions ($1/L<0$), and climb steadily with increasing stability. Similar plots were obtained for the ratio of downwind to upwind friction velocity. The graphs provide a clear indication of the importance of traffic induced mechanical mixing under stable atmospheric conditions. Based on these findings, one would expect conventional vertical dispersion estimates to accurately predict dispersion downwind of roadways under unstable conditions, but significantly underpredict during stable episodes.

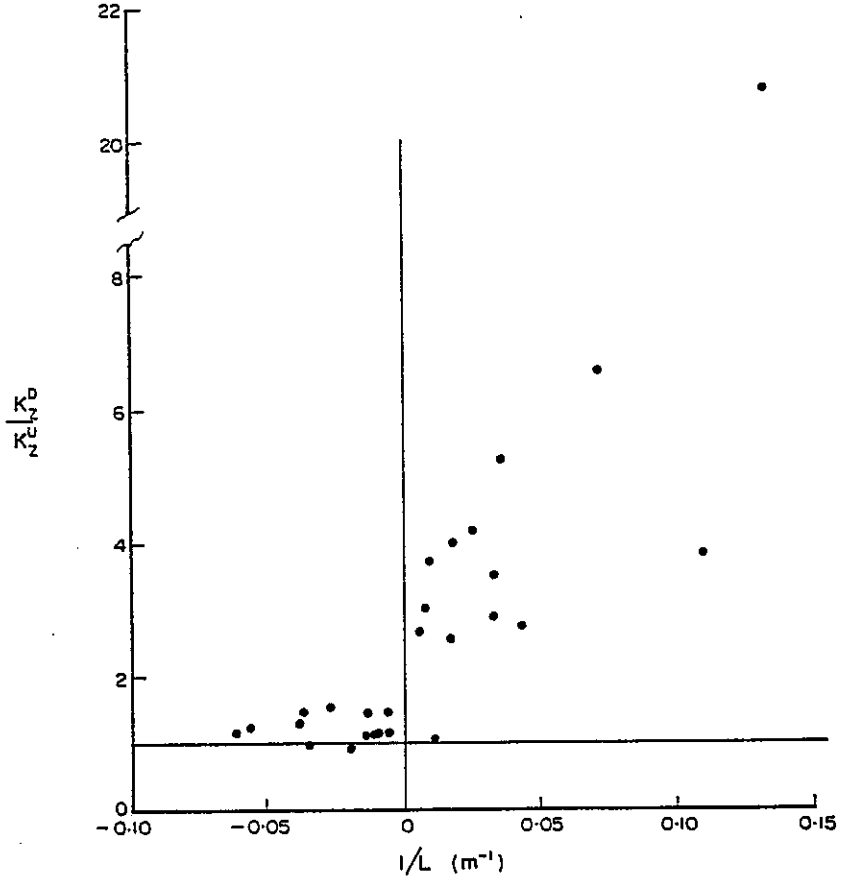

RATIO OF DOWNWIND TO UPWIND VERTICAL DIFFUSIVITY (K_z) VERSUS STABILITY — GM DATA

FIGURE 10

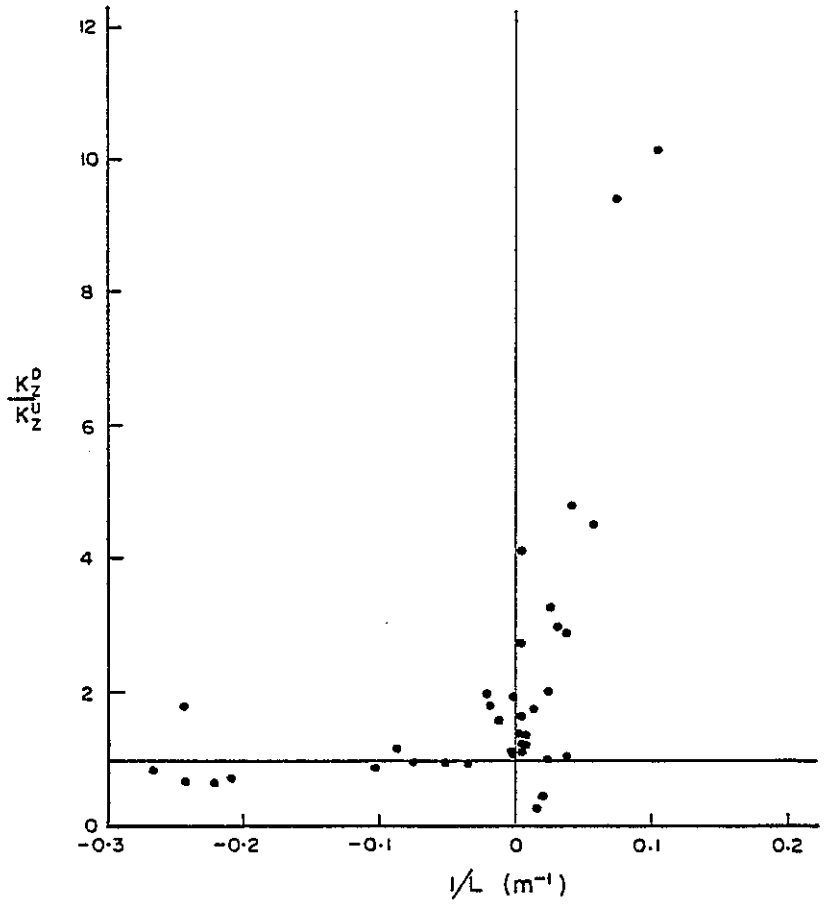

RATIO OF DOWNWIND TO UPWIND VERTICAL DIFFUSIVITY (K_z) VERSUS STABILITY— CALTRANS DATA (SACTO)

FIGURE 11

In Figures 12 and 13, the difference between downwind and upwind heat flux is plotted against the inverse Obukhov Length for GM and SACTO data. An interesting pattern emerges from these two graphs. For strongly unstable cases, diminished heat flux is observed downwind of the roadway, presumably due to the disruption of convective heat transfer from the surface by vehicle induced turbulence. Under near-neutral conditions thermal contributions from the traffic apparently become significant leading to enhanced heat flux downwind. For strongly stable conditions, the amounts of thermal turbulence added for the traffic volumes studied are unable to cause any significant change in the downwind heat flux.

The results of the meteorological analysis show that stability and dispersion downwind of roadways are significantly altered by traffic for cases of neutral to stable flows, but relatively unperturbed for unstable regimes. The mechanism of mechanical turbulence appears to be most important in modifying strongly stable flows, while thermal contributions in the form of vehicular waste heat are significant only under near-neutral conditions.

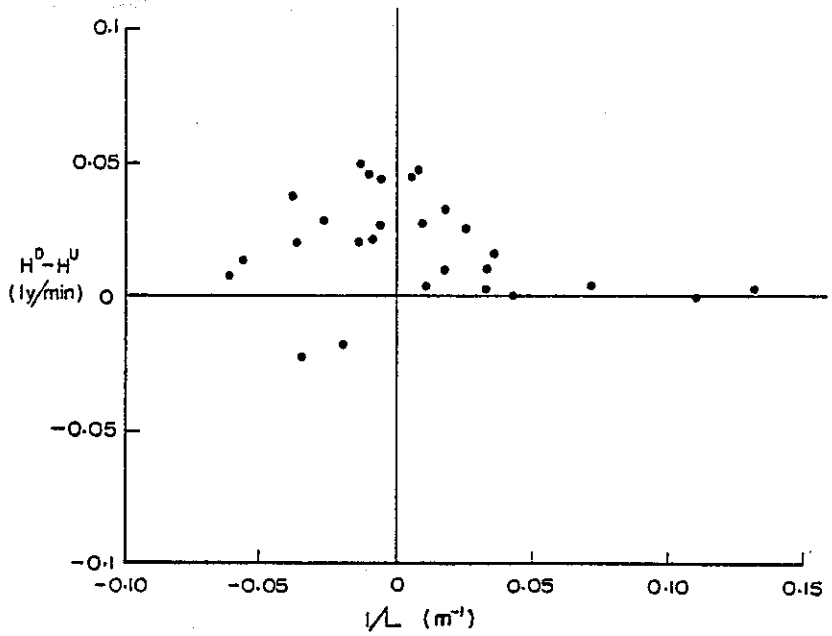

DOWNWIND MINUS UPWIND HEAT FLUX (H)
VERSUS STABILITY — GM DATA

FIGURE 12

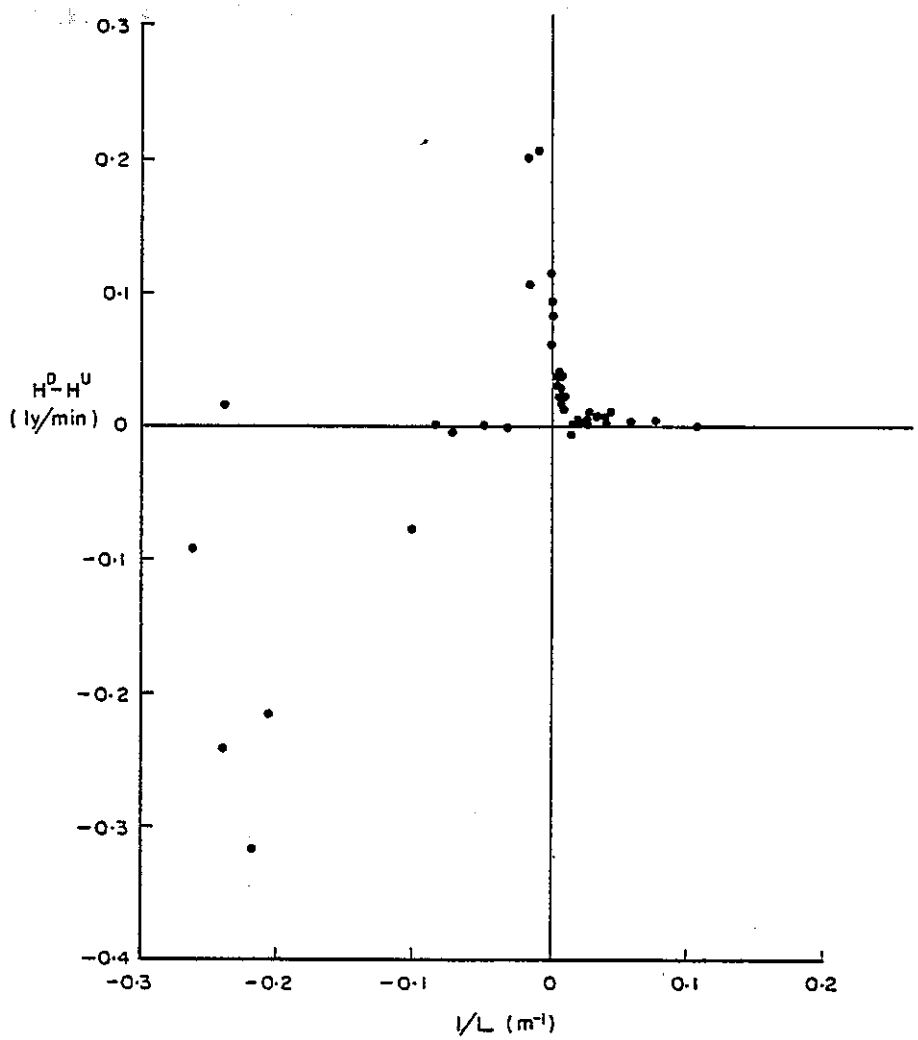

DOWNWIND MINUS UPWIND HEAT FLUX (H)
VERSUS STABILITY— CALTRANS DATA (SACTO)

FIGURE 13

6. DISPERSION PARAMETER ANALYSIS

Vertical concentration profiles and ground level concentration measurements were available for each of the data bases studied. Under crosswind conditions (PHI$\geq$ 35°) these measurements could be used to directly estimate the vertical dispersion parameter, σ_z. A comparison between the measured values of σ_z and the predicted values using the Pasquill-Smith methodology could then be made.

6.1 Methodology

For a ground level, semi-infinite line source under crosswind conditions Equation 2-23 can be rewritten as,

$$C(x,z) = \frac{2q}{\sqrt{2\pi}\sigma_z u} \exp\left[\frac{-1}{2}\left(\frac{z}{\sigma_z}\right)^2\right] \qquad (6\text{-}1)$$

where q is the source strength/unit length. Equation 6-1 can also be written as,

$$C(A_o,\sigma_z) = \frac{A_o}{\sigma_z} \exp\left[\frac{-1}{2}\left(\frac{z}{\sigma_z}\right)^2\right] \qquad (6\text{-}2)$$

where A_o represents a variable that remains constant with respect to x and z in accordance with the Gaussian assumption of vertical and horizontal wind speed homogeneity, and σ_z is constant with respect to z. Given a set of n concentration measurements at varying heights a distance x from the roadway centerline, a least squares estimate for the variables A_o and σ_z may be obtained by the simultaneous solution of the following two normal equations,

$$\sum_{i=1}^{n} (Y_i - \hat{Y}_i) \frac{\partial C(A_o, \sigma_z)}{\partial A_o} = 0 \qquad (6\text{-}3)$$

and

$$\sum_{i=1}^{n} (Y_i - \hat{Y}_i) \frac{\partial C(A_o, \sigma_z)}{\partial \sigma_z} = 0 \qquad (6\text{-}4)$$

where Y_i is the observed concentration and $\hat{Y}_i$ is the concentration predicted by Equation 6-2 (Draper and Smith, 1966). The two partial differentials may be written as,

$$\frac{\partial C}{\partial A_o} = \frac{1}{\sigma_z} \exp\left[\frac{-1}{2}\left(\frac{z}{\sigma_z}\right)^2\right] \qquad (6\text{-}5)$$

$$\frac{\partial C}{\partial \sigma_z} = \frac{A_o}{\sigma_z^2}\left[\left(\frac{z}{\sigma_z}\right)^2 - 1\right] \exp\left[\frac{-1}{2}\left(\frac{z}{\sigma_z}\right)^2\right] \tag{6-6}$$

Substituting into Equations 6-3 and 6-4 and solving for A_o yields the following equations,

$$A_o = \frac{\sigma_z \sum_{i=1}^{n} Y_i \exp\left[\frac{-1}{2}\left(\frac{z_i}{\sigma_z}\right)^2\right]}{\sum_{i=1}^{n} \exp\left[-\left(\frac{z_i}{\sigma_z}\right)^2\right]} \tag{6-7}$$

$$A_o = \frac{\sigma_z \sum_{i=1}^{n} Y_i\left[\left(\frac{z_i}{\sigma_z}\right)^2 - 1\right] \exp\left[\frac{-1}{2}\left(\frac{z_i}{\sigma_z}\right)^2\right]}{\sum_{i=1}^{n}\left[\left(\frac{z_i}{\sigma_z}\right)^2 - 1\right] \exp\left[-\left(\frac{z_i}{\sigma_z}\right)^2\right]} \tag{6-8}$$

A simultaneous solution to these two equations for each given vertical array of concentration readings was then obtained using a computerized trial and error procedure.

At locations where only ground level concentrations were available, a more simplified method of computing σ_z was used. Solving Equation 6-1 for σ_z gives,

$$\sigma_z = \frac{2q}{\sqrt{2\pi}Cu} \exp\left[\frac{-1}{2}\left(\frac{z}{\sigma_z}\right)^2\right] \tag{6-9}$$

Since the "ground level" probes for the various data bases actually ranged in height from 0.5 to 2.0 meters, a simple iterative routine was necessary to solve Equation 6-9. An initial value of σ_z was determined assuming z = 0. This value was then lessened in increments until adjacent computations converged to within 0.01 meter.

While the method for estimating σ_z from vertical probe arrays was independent of the source strength, q, the ground level method was not. For the SRI and NY data bases, mass balance calculations indicated serious inconsistencies in the reported source strengths and the observed concentrations. These same calculations for the GM data base agreed to within an average of $\pm$12% of the reported tracer release rates. Similar results were obtained by Bullin et. al. (1980) for the GM and SRI data bases. Therefore, when estimating σ_z from ground level concentrations, the reported source strength was used for the GM results only.

For the SRI and NY data bases, the value of A_o measured at the nearest downwind tower was used in place of the reported source strength so that,

$$\sigma_z = \frac{A_o}{C} \exp\left[\frac{-1}{2}\left(\frac{z}{\sigma_z}\right)^2\right] \qquad (6\text{-}10)$$

The values of C for the SRI study were in terms of carbon monoxide concentrations less upwind ambient levels. The NY study consisted of tracer concentrations so that no ambient adjustments were necessary. Ground level results for the SACTO study were not considered in this report.

6.2 Results

Tables 8 thru 10 summarize the vertical dispersion parameters derived from ground level concentrations for the GM, SRI and NY data bases. The wind speed (U) and relative direction (PHI) measured upwind of the roadway at heights of 10.5 and 7.5 meters for the GM and SRI results, respectively, are listed to the right. For the NY results, U and PHI were measured in the median at a height of 8.0 meters. The stability classes (STAB) given in the tables were based on upwind measurements using the techniques described in Section 5.1. Missing results were caused by

TABLE 8

VERTICAL DISPERSION PARAMETER (SIGMA Z)
CALCULATED FROM GROUND LEVEL SF6 CONCENTRATIONS
GENERAL MOTORS SULFATE EXPERIMENT DATA

RUN NO.	SIGMA Z (METERS) 15M	28M	43M	63M	113M	U (M/S)	PHI (DEG)	STAB
2720820	-----	-----	-----	-----	-----	1.0	59	F
2720850	-----	-----	-----	-----	-----	1.2	78	F
2720920	-----	-----	-----	-----	-----	.6	75	F
2720950	-----	-----	-----	-----	-----	.7	64	A
2741410	1.7	2.5	3.5	5.6	7.4	3.7	69	C
2741440	1.5	2.8	5.2	5.4	11.5	3.2	68	C
2741510	1.9	2.7	4.7	6.4	8.7	3.6	69	D
2741540	1.5	2.2	3.7	5.9	10.5	3.9	68	D
2750810	2.0	3.8	11.0	7.2	13.9	1.7	39	D
2760915	1.3	1.9	2.4	3.8	7.5	3.5	47	D
2760945	1.3	2.3	3.1	4.3	6.2	4.0	56	C
2790810	2.0	2.9	3.9	5.1	7.0	1.5	71	F
2790840	1.7	3.0	4.3	5.4	6.9	1.5	67	F
2790910	2.2	3.1	4.5	5.9	11.9	1.8	73	C
2790940	1.9	3.1	4.4	6.3	11.5	2.3	70	C
2810805	1.7	-----	4.1	-----	-----	2.3	36	E
2810905	2.7	-----	7.1	-----	-----	1.2	78	F
2810935	1.9	-----	4.1	-----	-----	2.4	86	D
2830820	2.4	3.7	5.0	6.6	12.9	1.7	74	E
2830850	3.2	4.7	8.1	10.9	20.9	1.2	83	D
2830920	3.3	4.2	6.1	8.4	13.5	1.4	62	C
2830950	2.6	4.2	6.4	40.5	20.4	1.6	40	B
2900810	1.7	-----	4.1	-----	-----	2.5	68	E
2900840	1.8	-----	3.4	-----	-----	2.6	58	E
2900910	1.8	-----	4.5	-----	-----	2.5	62	E
2900940	1.7	-----	4.2	-----	-----	2.8	56	D
2931035	2.6	3.1	4.8	7.7	11.3	2.5	88	D
2931105	2.3	3.5	3.9	6.2	10.4	2.6	89	C
2940805	1.6	2.0	2.9	4.0	6.1	2.2	50	E
2940835	1.6	2.6	3.3	4.6	6.3	2.2	55	E
2940935	2.0	3.0	4.6	6.8	11.8	1.7	39	B
2950810	6.8	-----	-----	-----	-----	.4	51	F
2950840	4.1	-----	9.1	-----	-----	.8	75	F
2950910	2.[illegible]	-----	7.7	-----	-----	.9	49	F

TABLE 9

VERTICAL DISPERSION PARAMETER (SIGMA Z)
CALCULATED FROM GROUND LEVEL CO CONCENTRATIONS
AND BEST FIT AO
STANFORD RESEARCH INSTITUTE AT-GRADE SITE DATA

DATE-TIME	SIGMA Z (METERS) 24M	39M	64M	79M	95M	110M	U (M/S)	PHI (DEG)	STAB
21 JAN 0700	8.8	15.6	17.4	20.3	21.4	18.3	.7	46	F
21 JAN 0900	4.8	12.9	-----	23.3	25.8	-----	.9	79	A
24 JAN 0600	4.0	7.8	8.2	13.4	-----	14.5	1.3	44	F
24 JAN 0700	4.2	7.9	7.9	13.2	-----	18.2	1.8	37	F
24 JAN 0800	10.9	21.3	-----	31.0	75.8	25.2	.8	47	F
24 JAN 1200	4.7	9.0	16.1	-----	24.2	24.2	1.6	44	A
28 JAN 0700	2.9	5.4	8.6	7.9	-----	11.3	3.4	46	E
28 JAN 0900	3.8	7.8	-----	-----	25.5	20.4	3.1	51	C
28 JAN 1100	4.0	10.0	-----	50.0	25.1	50.0	.9	78	A
30 JAN 1400	4.5	9.3	-----	23.2	-----	-----	1.6	49	A
30 JAN 1500	4.6	6.5	13.7	-----	23.5	-----	2.3	50	A
30 JAN 1600	2.4	5.2	9.2	10.5	11.6	13.8	2.0	66	A
30 JAN 1900	6.3	8.8	13.3	13.3	22.8	26.6	1.0	87	F
5 FEB 1200	4.1	6.9	10.9	15.2	19.0	25.4	2.9	46	C
5 FEB 1300	3.4	5.3	9.9	8.5	11.9	14.9	4.0	63	C
5 FEB 1400	3.7	5.6	8.8	10.0	11.4	13.3	3.8	67	D
5 FEB 1500	2.8	3.2	8.6	11.1	7.7	11.1	5.5	72	D
5 FEB 1600	3.4	4.7	7.0	8.6	-----	10.0	5.2	72	D
5 FEB 1700	4.2	5.3	7.8	9.7	-----	10.3	3.9	69	D
5 FEB 1800	3.6	5.4	8.5	-----	10.4	-----	2.4	55	E

TABLE 10

VERTICAL DISPERSION PARAMETER (SIGMA Z)
CALCULATED FROM GROUND LEVEL SF6 CONCENTRATIONS
AND BEST FIT AO ESTIMATES
NEW YORK AT-GRADE SITE

RUN NO.	SIGMA Z (METERS) 25M	45M	61M	79M	U (M/S)	PHI (DEG)	STAB
1006R2	3.9	5.8	8.7	11.0	1.8	76	D
1008R1	3.7	7.9	9.8	12.1	2.5	64	B
1018R1	2.5	5.1	7.5	6.3	4.6	80	C
1019R2	4.6	8.9	13.7	16.4	1.9	74	B
1019R3	4.1	5.1	7.2	10.4	1.8	66	C
1021R1	3.8	6.0	7.8	10.8	7.5	48	D
1116R1	2.8	6.7	8.2	9.6	5.0	59	B
1116R2	3.7	7.6	9.3	11.2	5.0	76	B
1116R3	4.3	-----	7.2	6.7	.9	75	F
1118R1	3.2	6.8	7.6	9.6	6.5	65	D

several factors including suspected tracer release system failure, contaminated bag samples and lack of ground level probes for particular wind direction configurations.

A similar set of tables (11 thru 20) list results for the least squares estimate of the two variables, A_0 and σ_z, contained in Equation 6-2. A_0 is given in length units because the concentration measurements used are in volumetric form. A separate table is used for each downwind, vertical probe array. For the GM data base, four towers at 0, 15, 28 and 43 meters from the roadway centerline are analyzed. Results from two towers at 29.0 and 48.8 meters are summarized for the SRI data base. Both the NY and SACTO data bases have results given for a single, downwind tower near the roadway edge while results for the LA1 and LA3 sites are given for a single tower located in the freeway median. The differences in Tables 11 thru 15 between the number of runs analyzed for different towers of the same data base can be explained in two ways: 1) tower results with fewer than three concentration measurements were not analyzed, and 2) only two towers were established on the west side of the GM test track so that the 28 meter tower result was not available for runs made during easterly crosswind conditions.

TABLE 11

BEST FIT GAUSSIAN DISTRIBUTION - TWO VARIABLES
6M SULFATE EXPERIMENT TRACER MEASUREMENTS (SF6 IN PPHB)
MEDIAN TOWER

RUN NO.	SIGMA Z (M)	AO (M)	YHAT-Y (PPHB) 0.5M	3.5M	9.5M	SYX (PPHB)	U (M/S)	PHI (DEG)	STAB
2720820	5.0	1271	-10	15	-9	20.0	1.0	59	F
2720850	4.1	549	1	-1	2	2.7	1.2	78	F
2720920	4.6	572	5	-8	7	11.5	.7	75	F
2720950	4.5	625	1	-2	2	2.6	.7	64	A
2741410	3.1	241	-0	1	-6	6.3	3.7	69	C
2741440	3.5	291	-1	3	-9	9.2	3.2	68	C
2741510	3.9	250	-1	2	-3	3.9	3.6	69	D
2750810	4.2	500	2	-3	3	4.6	1.7	39	D
2760915	2.7	336	-0	0	-1	1.1	3.6	47	D
2760945	3.9	401	2	-3	5	6.0	4.0	56	C
2790810	3.7	624	1	-2	5	5.7	1.5	71	F
2790840	3.5	590	0	-1	2	2.6	1.4	67	F
2790910	3.5	416	0	-1	2	2.4	1.8	73	C
2790940	3.4	343	0	-0	2	2.0	2.3	70	C
2810805	3.0	480	-0	0	0	.5	2.3	36	E
2810905	4.1	776	-2	3	-4	5.7	1.2	78	F
2810935	2.5	290	-0	0	-0	.3	2.4	86	D
2830820	3.2	411	-0	0	1	.8	1.7	74	E
2830850	3.3	468	-0	0	-1	.8	1.2	83	D
2830920	3.4	549	-1	2	-7	7.5	1.4	62	C
2830950	5.2	881	-7	10	-6	13.8	1.6	40	B
2900810	3.1	302	0	-0	1	.8	2.5	68	E
2900840	3.0	340	-0	0	1	.6	2.6	58	E
2900910	2.6	383	-0	0	-0	.3	2.5	62	E
2900940	3.2	319	-0	0	-1	.8	2.9	56	D
2931035	2.4	283	-0	0	-0	.3	2.6	88	D
2931105	2.9	276	-0	0	0	.3	2.6	89	C
2940805	3.3	627	0	-0	2	1.9	2.2	50	E
2940835	2.9	543	-0	0	-0	.3	2.2	55	E
2940935	3.6	739	-1	2	-4	4.9	1.7	39	B
2950810	5.5	944	-7	10	-5	13.4	.4	51	F
2950840	3.9	744	-0	0	0	.3	.8	75	F
2950910	4.5	1042	-3	5	-4	7.7	.9	49	F

TABLE 12

BEST FIT GAUSSIAN DISTRIBUTION - TWO VARIABLES
GM SULFATE EXPERIMENT TRACER MEASUREMENTS (SF6 IN PPHB)
TOWER 15 METERS DOWNWIND FROM ROADWAY CENTERLINE

RUN NO.	SIGMA Z (M)	AO (M)	YHAT-Y (PPHB) 0.5M	3.5M	9.5M	SYX (PPHB)	U (M/S)	PHI (DEG)	STAB
2720820	6.6	1849	-33	43	-14	56.3	1.0	59	F
2720850	2.9	748	-1	2	-28	28.1	1.2	78	F
2720920	2.8	792	-1	2	-28	28.4	.7	75	F
2720950	2.4	752	-0	0	-26	26.4	.7	64	A
2741410	2.3	365	-0	0	-10	9.6	3.7	69	C
2741440	2.1	409	-0	0	-9	9.1	3.2	68	C
2741510	2.3	341	-0	0	-7	6.9	3.6	69	D
2741540	2.1	359	-0	0	-11	10.8	3.9	68	D
2750810	2.8	733	-0	1	-18	18.3	1.7	39	D
2760915	2.8	585	-0	1	-9	9.2	3.6	47	D
2760945	2.3	434	-0	0	-7	7.1	4.0	56	C
2790810	3.2	903	-1	2	-12	11.8	1.5	71	F
2790840	2.8	967	-0	1	-12	11.8	1.4	67	F
2790910	2.6	566	-0	1	-5	4.8	1.8	73	C
2790940	2.5	489	-0	0	-2	2.5	2.3	70	C
2810805	2.9	764	-0	0	-4	4.0	2.3	36	E
2810905	3.1	998	-2	4	-36	36.4	1.2	78	F
2810935	2.4	535	-0	0	-1	1.2	2.4	86	D
2830820	3.2	707	-0	0	-2	2.5	1.7	74	E
2830850	3.4	790	-1	2	-8	7.9	1.2	83	D
2830920	3.7	691	-4	7	-17	18.7	1.4	62	C
2830950	5.1	1016	-14	21	-13	28.5	1.6	40	B
2900810	2.3	484	-0	0	-2	1.6	2.5	68	E
2900840	2.6	505	-0	0	-3	3.1	2.6	58	E
2900910	2.6	499	-0	0	-4	4.1	2.5	62	E
2900940	2.4	468	-0	0	-5	4.8	2.9	56	D
2931035	2.9	463	-0	0	-1	.5	2.6	88	D
2931105	2.4	412	-0	0	-2	1.7	2.6	89	C
2940805	3.1	860	-1	2	-12	12.6	2.2	50	E
2940835	2.8	820	-0	1	-12	12.2	2.2	55	E
2940935	3.1	911	-1	3	-21	21.7	1.7	39	B
2950810	6.4	1866	-31	42	-14	54.2	.4	51	F
2950840	3.3	939	-4	8	-40	40.8	.8	75	F
2950910	5.0	1629	-21	32	-20	43.2	.9	49	F

TABLE 13

BEST FIT GAUSSIAN DISTRIBUTION - TWO VARIABLES
GM SULFATE EXPERIMENT TRACER MEASUREMENTS (SF6 IN PPHB)
TOWER 28 METERS DOWNWIND FROM ROADWAY CENTERLINE

RUN NO.	SIGMA Z (M)	AO (M)	YHAT-Y (PPHB) 0.5M	3.5M	9.5M	SYX (PPHB)	U (M/S)	PHI (DEG)	STAB
2741410	4.7	506	0	-1	1	1.1	3.7	69	C
2741440	4.1	433	-3	5	-7	9.3	3.2	68	C
2741510	4.4	440	-2	2	-2	3.6	3.6	69	D
2741540	2.8	333	-0	1	-13	13.2	3.9	68	D
2750810	5.2	733	-2	3	-1	3.7	1.7	39	D
2760915	4.3	602	-2	3	-4	5.2	3.6	47	D
2760945	4.1	452	0	-0	0	.6	4.0	56	C
2790810	5.3	1042	-2	3	-2	4.0	1.5	71	F
2790840	4.7	994	9	-14	11	19.8	1.4	67	F
2790910	5.0	732	-10	15	-9	20.3	1.8	73	C
2790940	4.2	527	1	-1	1	1.8	2.3	70	C
2830820	4.2	600	-4	6	-7	9.7	1.7	74	E
2830850	5.3	787	-10	14	-8	19.2	1.2	83	D
2830920	5.6	827	-5	7	-3	9.7	1.4	62	C
2830950	7.0	895	-4	5	-1	6.4	1.6	40	B
2931035	2.6	347	-0	0	-6	6.0	2.6	88	D
2931105	3.9	445	-0	0	-1	.9	2.6	89	C
2940805	4.4	969	-7	11	-11	17.4	2.2	50	E
2940935	6.7	1342	-0	0	-0	.6	1.7	39	B

TABLE 14

BEST FIT GAUSSIAN DISTRIBUTION - TWO VARIABLES
GM SULFATE EXPERIMENT TRACER MEASUREMENTS (SF6 IN PPHB)
TOWER 43 METERS DOWNWIND FROM ROADWAY CENTERLINE

RUN NO.	SIGMA Z (M)	A0 (M)	YHAT-Y (PPHB) 0.5M	3.5M	9.5M	SYX (PPHB)	U (M/S)	PHI (DEG)	STAB
2720850	9.0	807	8	-9	2	12.3	1.2	78	F
2720920	7.0	674	-0	0	-0	.6	.7	75	F
2720950	10.7	701	-1	1	-0	1.7	.7	64	A
2741410	4.8	358	-3	5	-4	7.3	3.7	69	C
2741440	5.7	366	4	-5	2	6.8	3.2	68	C
2741510	5.7	327	-3	4	-2	5.3	3.6	69	D
2741540	4.7	312	-3	4	-4	6.5	3.9	68	D
2750810	9.8	672	19	-24	5	31.0	1.7	39	D
2760915	5.4	588	-8	11	-6	14.9	3.6	47	D
2760945	4.5	348	-3	4	-4	6.8	4.0	56	C
2790810	6.5	970	1	-1	0	1.7	1.5	71	F
2790840	6.2	883	1	-1	0	1.2	1.4	67	F
2790910	5.9	644	1	-1	0	1.5	1.8	73	C
2790940	4.8	416	-0	0	-0	.6	2.3	70	C
2810805	5.3	575	-2	2	-1	3.2	2.3	36	E
2810905	9.2	1123	-1	1	-0	1.6	1.2	78	F
2810935	4.1	431	-1	2	-3	4.2	2.4	86	D
2830820	5.7	586	-5	7	-3	9.5	1.7	74	E
2830850	7.7	741	4	-5	1	6.6	1.2	83	D
2830920	6.5	659	-4	5	-2	6.7	1.4	62	C
2830950	8.1	669	-5	6	-1	7.9	1.6	40	B
2900810	4.3	385	-1	1	-1	2.0	2.5	68	E
2900840	4.4	432	-4	7	-7	10.4	2.6	58	E
2900910	5.1	417	1	-1	1	1.2	2.5	62	E
2900940	5.6	429	-1	1	-1	1.7	2.9	56	D
2931035	4.4	362	-4	6	-5	8.5	2.6	88	D
2931105	3.1	320	-1	2	-18	18.0	2.6	89	C
2940805	5.7	856	-7	10	-4	13.0	2.2	50	E
2940835	5.3	717	-8	12	-6	15.8	2.2	55	E
2940935	7.7	988	-3	4	-1	5.4	1.7	39	B
2950840	9.8	1339	6	-7	1	9.1	.8	75	F
2950910	12.0	1638	4	-5	1	6.4	.9	49	F

TABLE 15

BEST FIT GAUSSIAN DISTRIBUTION - TWO VARIABLES
STANFORD RESEARCH INSTITUTE AT-GRADE SITE (CO IN PPM)
TOWER 29.0 METERS DOWNWIND FROM ROADWAY CENTERLINE

DATE-TIME	SIGMA Z (M)	AO (M)	YHAT-Y (PPM) 1.0M	3.0M	6.1M	13.6M	SYX (PPM)	U (M/S)	PHI (DEG)	STAB
21 JAN 0700	10.5	75.6	-.4	----	.6	-.2	.70	.7	46	F
21 JAN 0900	10.2	23.4	.1	-.0	-.1	.0	.09	.9	79	A
24 JAN 0600	5.1	17.5	-.0	-.0	.1	-.2	.16	1.3	44	F
24 JAN 0700	6.4	38.6	.7	-1.5	1.1	-.8	1.49	1.8	37	F
24 JAN 0800	29.7	68.7	2.3	-1.2	-1.5	.4	3.02	.8	47	F
24 JAN 1200	6.3	14.7	.2	-.3	.2	-.2	.35	1.6	44	A
28 JAN 0700	3.9	21.7	-.2	.3	-.2	-.1	.28	3.4	46	E
28 JAN 0900	3.3	10.3	----	.1	-.5	-.2	.59	3.1	51	C
28 JAN 1100	7.0	5.0	.0	----	-.0	.0	.02	.9	78	A
30 JAN 1400	6.6	9.4	-.1	-.0	.2	-.2	.24	1.6	49	A
30 JAN 1500	4.3	16.6	.1	-.2	.1	----	.26	2.3	50	A
30 JAN 1600	3.6	22.3	.1	-.2	.2	-.1	.24	2.0	66	A
30 JAN 1900	7.2	16.1	.0	-.1	.1	-.0	.06	1.0	87	F
5 FEB 1200	5.0	7.7	.0	-.0	.0	-.1	.05	2.9	46	C
5 FEB 1300	4.2	6.0	-.0	.0	-.0	.0	.01	4.0	63	C
5 FEB 1400	4.6	8.1	-.0	.0	.0	-.2	.13	3.8	67	D
5 FEB 1500	3.3	7.8	-.3	.5	-.4	----	.65	5.3	72	D
5 FEB 1600	4.1	12.2	-.2	.3	-.1	-.2	.26	5.2	72	D
5 FEB 1700	4.3	16.7	-.0	.0	.0	-.3	.20	3.9	69	D
5 FEB 1800	4.6	9.5	.0	-.0	.0	-.2	.13	2.4	55	E

TABLE 16

BEST FIT GAUSSIAN DISTRIBUTION - TWO VARIABLES
STANFORD RESEARCH INSTITUTE AT-GRADE SITE (CO IN PPM)
TOWER 48.8 METERS DOWNWIND FROM ROADWAY CENTERLINE

DATE-TIME	SIGMA Z (M)	AO (M)	YHAT-Y (PPM) 1.0M	3.0M	6.1M	13.6M	SYX (PPM)	U (M/S)	PHI (DEG)	STAB
21 JAN 0700	9.3	41.1	-.4	----	.7	-.3	.83	.7	46	F
21 JAN 0900	12.8	15.7	.2	-.3	.1	-.0	.28	.9	79	A
24 JAN 0600	9.0	15.2	.4	-.4	.0	.0	.40	1.3	44	F
24 JAN 0700	10.0	34.3	.1	-.1	.0	----	.17	1.8	37	F
24 JAN 0800	12.4	45.4	.3	-.8	.5	-.1	.70	.8	47	F
24 JAN 1200	12.4	13.6	-.1	.2	-.0	----	.20	1.6	44	A
28 JAN 0700	6.2	19.3	-.0	.1	----	-.0	.07	3.4	46	E
28 JAN 0900	7.2	8.6	.1	-.1	.0	----	.14	3.1	51	C
28 JAN 1100	9.1	3.9	.1	-.1	-.1	.0	.12	.9	78	A
30 JAN 1400	15.0	8.9	-.0	-.0	.0	-.0	.04	1.6	49	A
30 JAN 1600	3.3	15.3	----	.2	-.9	-.2	.91	2.0	66	A
30 JAN 1900	8.4	11.3	-.2	.2	.0	-.0	.17	1.0	87	F
5 FEB 1200	9.1	8.5	.0	-.0	----	.0	.03	2.9	46	C
5 FEB 1300	5.1	4.2	.0	-.0	-.0	.0	.03	4.0	63	C
5 FEB 1400	5.8	6.9	-.0	.0	-.0	----	.06	3.8	67	D
5 FEB 1500	12.5	12.9	-.1	-.0	.1	-.0	.10	5.3	72	D
5 FEB 1600	5.8	12.3	-.0	-.0	.1	-.2	.15	5.2	72	D
5 FEB 1700	5.8	14.8	.1	-.2	.1	----	.21	3.9	69	D
5 FEB 1800	3.0	7.3	-.2	.4	-.4	.0	.58	2.4	55	E

downwind of the roadway. This is probably attributable to the thorough mixing of the lower 10 meters of air imparted by the vehicle induced mechanical turbulence.

The statistical methodology used to fit Gaussian distributions to observed vertical concentration profiles revealed that the Gaussian model is flexible enough to simulate observed vertical distributions as close to the source as the roadway edge. It also showed that the relationship between σ_z and the downwind distance, x, can be adequately described by a power curve of the form $\sigma_z = ax^b$ for distances up to at least 200 meters downwind from the roadway centerline.

The unusually high values of initial vertical dispersion measured under low wind speed, F stability conditions are attributed to the increased residence time of pollutants within the turbulent mixing zone. Results from the comparison of upwind and downwind heat fluxes made in the meteorological analysis seem to indicate that thermal turbulence and plume rise are not important factors under such conditions. Instead, the mixing zone model used in CALINE3 was derived from the reasonably strong correlations exhibited between initial σ_z and residence time.

TABLE 19

BEST FIT GAUSSIAN DISTRIBUTION - TWO VARIABLES
CALTRANS LOS ANGELES STUDY - SITE 3 (CO IN PPM)
MEDIAN TOWER

DATE-TIME				SIGMA Z (M)	AO (M)	YHAT-Y (PPM) 1.2M	3.7M	6.1M	11.0M	SYX (PPM)	U (M/S)	PHI (DEG)	STAB
74	8	21	14	3.6	26.3	-.3	.8	-.7	.1	.79	5.1	78	C
74	8	23	13	3.4	19.0	.0	-.1	.1	-.3	.22	5.3	79	B
74	8	23	15	3.9	42.1	.3	-.8	.7	-.4	.85	5.7	77	C
74	8	26	13	4.0	26.8	-.0	.1	.0	-.2	.18	4.9	78	B
74	8	26	14	3.9	38.2	-.0	.1	.0	-.3	.24	5.1	78	B
74	8	26	17	3.3	24.2	-.4	1.1	-1.1	-.3	1.15	5.1	79	C
74	8	29	14	3.9	38.9	-.0	.1	.0	-.2	.16	4.9	79	B
74	8	30	6	5.4	50.7	-.3	.5	-.2	-.0	.47	1.2	78	A
74	8	30	14	3.5	43.4	-.2	.4	-.3	-.4	.47	4.8	78	B
74	11	13	12	5.4	19.0	.1	-.2	.2	-.0	.22	1.9	78	E
74	11	13	14	4.5	21.5	-.0	.0	.0	-.1	.04	2.0	79	B
74	11	13	18	4.9	60.4	-.6	1.0	-.1	-.7	.96	.5	78	F
74	12	16	17	3.8	70.9	-.1	.2	-.2	.3	.30	.8	75	F
75	1	16	16	3.4	54.4	.1	-.3	.4	-1.2	.92	1.0	80	E
75	1	16	18	3.3	36.6	.0	-.1	.2	-1.1	.76	.9	81	F
75	1	17	17	3.3	82.2	-.2	.5	-.4	-.9	.79	.8	79	F
75	1	17	18	3.8	68.7	-.4	.8	-.4	-1.2	1.10	.5	81	F
75	1	21	12	4.9	26.0	-.1	.0	.3	-.6	.48	1.2	77	A
75	1	21	18	4.1	40.3	-.2	.4	-.1	-.5	.52	.8	76	F
75	2	26	15	4.2	31.7	.3	-.6	.3	.2	.54	2.2	77	C
75	2	26	16	3.3	35.1	-.1	.4	-.4	.0	.39	2.2	77	E
75	3	13	15	2.7	35.1	-.0	.1	-.1	-.4	.29	2.1	77	C
75	3	14	16	3.6	32.9	-.1	.2	-.2	-.0	.19	3.9	77	D
75	3	14	17	3.4	27.6	-.1	.2	-.2	-.1	.20	2.8	78	E
75	3	14	18	3.8	25.9	-.1	.1	-.1	-.1	.14	2.1	79	E
75	3	17	18	4.7	27.9	.1	-.1	-.1	.3	.23	.9	77	F
75	3	18	18	3.5	15.7	-.1	.4	-.3	.0	.36	1.3	76	E
75	3	21	10	3.4	14.6	-.2	.5	-.4	.0	.47	2.1	78	C
75	3	24	18	3.5	15.3	-.2	.5	-.4	.0	.49	1.6	78	E
75	3	25	8	3.5	14.7	.0	-.1	.1	-.2	.17	3.0	79	D
75	3	25	9	3.8	16.9	.1	-.1	.1	.1	.14	3.2	78	E
75	3	27	10	4.1	20.2	.0	-.0	.0	-.1	.05	2.2	77	C
75	3	28	16	3.1	32.3	-.1	.4	-.5	-.1	.47	5.5	79	D
75	3	28	17	4.1	20.0	.0	-.0	-.0	.1	.10	4.3	79	D

TABLE 20

BEST FIT GAUSSIAN DISTRIBUTION - TWO VARIABLES
FLORIN-FREEPORT INTERSECTION SITE
TOWER 3 METERS DOWNWIND FROM EDGE OF ROADWAY

RUN NO.	SIGMA Z (M)	AO (M)	YHAT-Y (PPM) 1.0M	2.0M	4.0M	10.0M	SYX (PPM)	U (M/S)	BRG (DEG)	STAB
6014	1.7	4.0	-.0	.0	-.0	-.1	.08	4.0	336	C
6015	3.2	8.9	-.2	.2	-.1	-.0	.21	2.8	316	C
6016	3.0	14.0	.1	-.2	.1	-.1	.18	2.5	330	D
6017	2.4	19.0	-.4	.7	-.4	-.1	.64	1.7	339	F
6018	4.9	40.7	.3	-.3	-.1	.2	.35	.9	262	A
6107	7.5	13.9	.3	.2	-.5	.2	.44	.5	20	A
6108	5.7	13.9	-.1	.4	-.4	.2	.39	1.1	58	B
6109	3.0	13.4	-.2	.3	-.1	-.4	.38	1.2	23	B
6110	3.0	23.3	-.3	.4	-.1	-.6	.56	1.2	19	A
8116	1.6	5.0	-.1	.1	-.2	-.1	.19	6.1	329	D
8117	1.5	8.8	-.0	.1	-.3	-.1	.24	4.0	337	D
8118	2.3	9.1	-.0	.1	-.0	-.1	.12	1.9	330	E
8119	4.3	15.7	-.2	.2	.0	-.1	.20	2.0	319	E
8120	2.6	6.6	.1	-.1	.1	-.2	.17	2.9	0	E
8121	1.3	4.8	-.0	.0	-.1	-.1	.11	4.5	19	E
8706	2.7	5.4	-.2	.3	-.2	-.1	.30	1.2	4	E
8707	6.9	24.7	-.2	.3	-.1	-.0	.27	1.5	339	D
8708	2.3	8.2	-.1	.2	-.1	-.4	.36	3.0	328	C
8715	2.0	6.0	-.1	.2	-.2	-.2	.26	7.2	325	D
8716	1.9	4.9	.0	-.0	.0	-.1	.11	6.4	333	D
8717	1.4	5.9	-.0	.1	-.2	-.1	.16	4.8	334	D
8718	2.6	10.9	-.0	.0	.0	-.2	.14	2.0	312	E
8913	2.4	9.5	.2	-.3	.2	.0	.26	2.5	159	A
8914	2.9	5.8	-.0	.1	-.0	-.0	.06	2.4	191	A
8915	1.6	4.2	-.1	.2	-.4	-.2	.37	2.1	203	A
8916	2.1	4.8	-.1	.2	-.1	.0	.15	2.2	190	B
8917	2.1	6.8	-.1	.2	-.1	-.0	.15	1.8	194	E
8918	2.1	10.0	-.1	.1	-.1	-.1	.15	2.4	164	E
8919	2.4	8.6	.5	-.9	.5	.0	.80	2.4	162	E
8920	2.6	9.9	.1	-.1	.1	.0	.10	2.4	148	E
8921	3.1	9.7	.1	-.1	.1	-.0	.13	1.7	149	F
8922	2.9	5.8	.0	-.0	.0	-.1	.07	1.9	175	F
8923	1.9	3.2	-.0	.0	-.0	.0	.01	2.3	163	E
9114	4.7	3.4	-.1	.1	.1	-.1	.10	2.4	179	A
9115	2.2	7.0	.0	-.1	.0	.0	.05	3.1	177	B
9116	2.1	7.7	.0	-.1	.1	-.1	.13	3.6	181	C
9117	2.3	13.9	.2	-.3	.2	-.1	.31	2.9	160	D
9516	2.5	15.2	-.2	.4	-.2	.0	.32	3.2	149	D
9517	2.4	14.2	.2	-.3	.2	.0	.32	3.3	148	D
9518	1.9	6.8	-.2	.3	-.4	.0	.39	4.5	151	D
9519	1.5	3.7	-.0	.0	-.1	.0	.05	4.4	143	D
9520	2.3	3.1	.0	-.1	.0	.0	.07	3.9	143	D

In addition to the best fit values for A_o and σ_z, Tables 11 thru 20 contain the differences between predicted (using Equation 6-2) and observed concentrations for each probe level on the tower, and the standard error (SYX) computed as follows,

$$SYX = \left[\frac{\sum_{i=1}^{n} (\hat{Y}_i - Y_i)^2}{n - 2} \right]^{1/2} \qquad (6\text{-}11)$$

These results provide a measure of how well the Gaussian distribution is modeling the actual vertical concentration profile.

After careful review of Tables 8 thru 20, a small fraction of the results presented therein were deleted from further consideration. These results deviated significantly from the trends exhibited by the rest of the data, and could not possibly be explained using the Gaussian model. Table 21 lists the deleted results.

Table 21

DELETED DISPERSION PARAMETER RESULTS

Data Base	Run No. or Date-Time	Ground Level Analysis	Tower Analysis
GM	2830950	63 meters	
SRI	24 JAN 0800	All	All
SRI	28 JAN 1100	79 & 110 meters	

6.3 Discussion

The results shown in Tables 11 thru 20 can be used to test the assumption that the Gaussian formulation (Equation 6-2) adequately describes the vertical distribution of pollutant concentrations near a roadway. The residuals (YHAT-Y) for towers immediately adjacent to the roadway indicate a greater amount of kurtosis (higher concentrations in the central and tail areas of the distribution) in the observed vertical concentration profile than can be explained by the Gaussian distribution. This condition is the result of a low ratio of receptor distance to source dimension (roadway width) which violates the geometric description of the source, used in deriving Equation 6-1, as a line of infinitesimal width.

Figures 14 thru 16 illustrate this effect. They show observed and best fit Gaussian estimates for the vertical

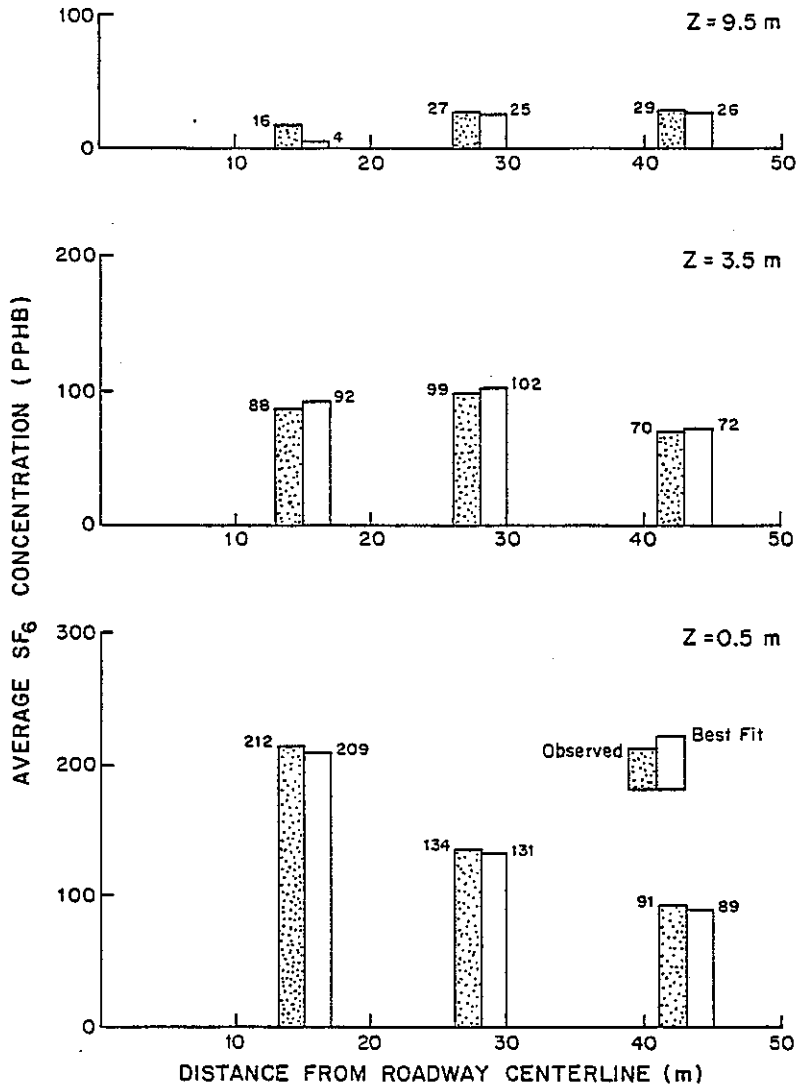

COMPARISON OF AVERAGE OBSERVED AND BEST FIT CONCENTRATION PROFILES FOR THE GM DATA BASE (UNSTABLE CONDITIONS)

FIGURE 14

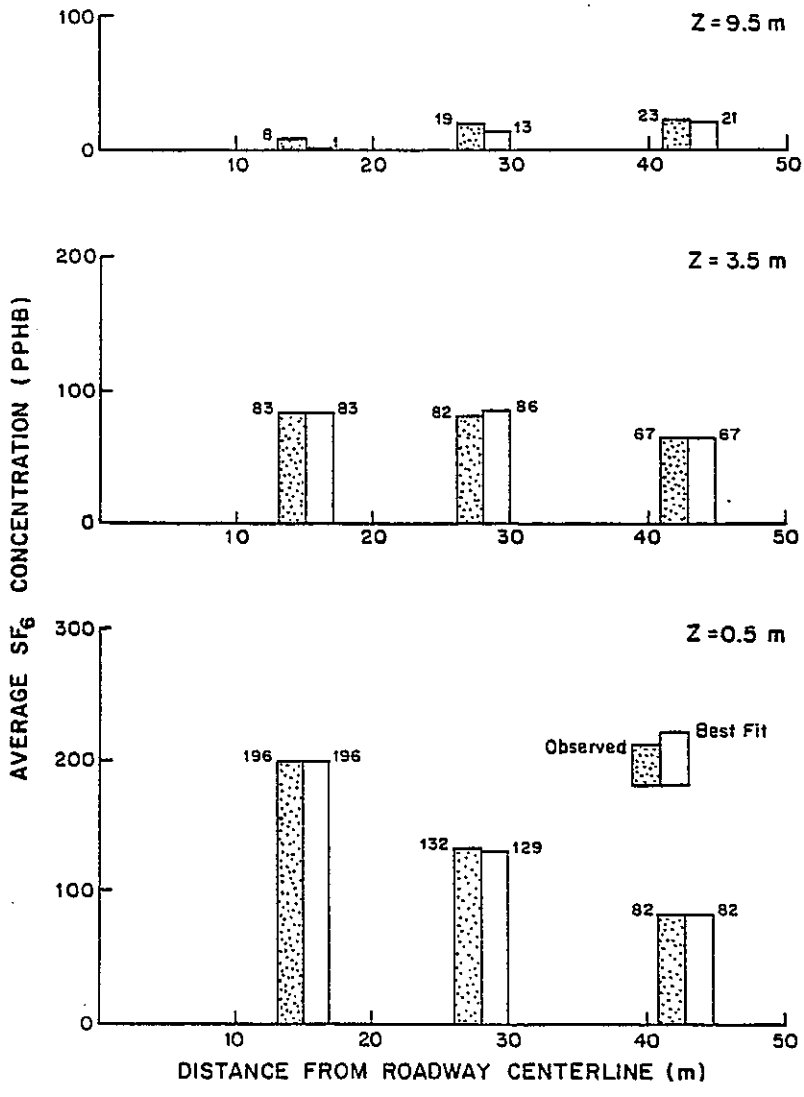

COMPARISON OF AVERAGE OBSERVED AND BEST FIT CONCENTRATION PROFILES FOR THE GM DATA BASE (NEUTRAL CONDITIONS)

FIGURE 15

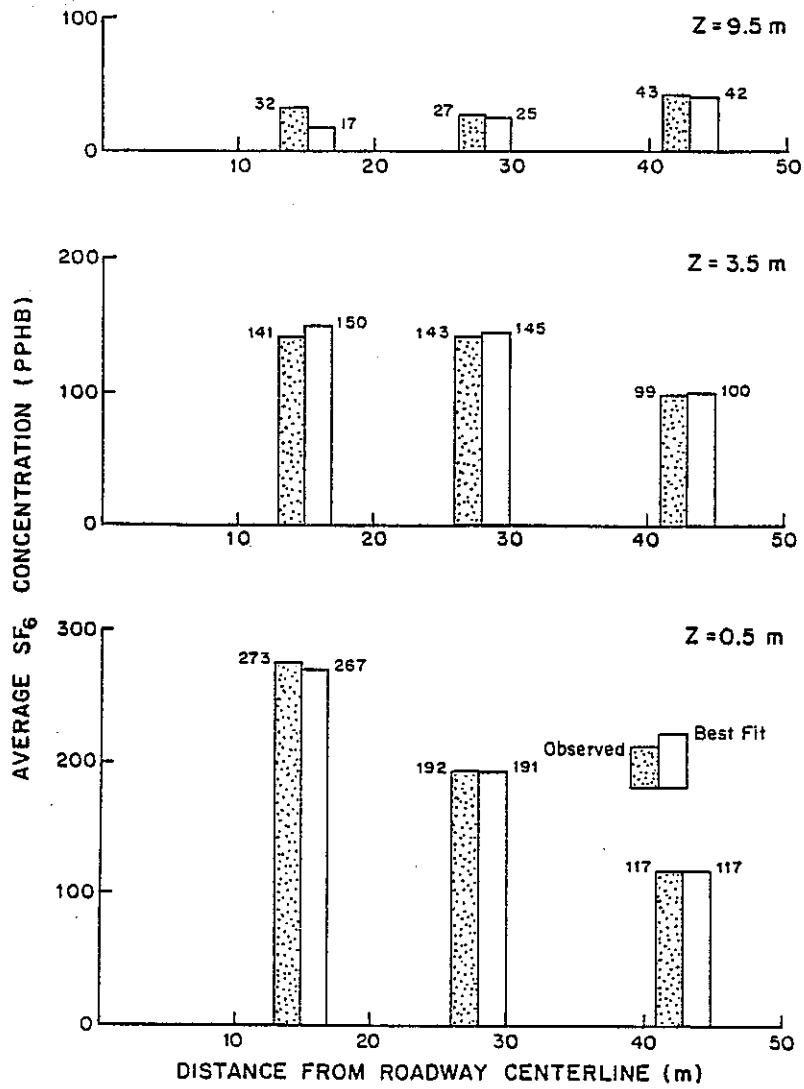

COMPARISON OF AVERAGE OBSERVED AND BEST FIT CONCENTRATION PROFILES FOR THE GM DATA BASE (STABLE CONDITIONS)

FIGURE 16

concentration profile of SF_6 at each downwind tower of the GM experiment. The values shown are averages of all cases for unstable (A thru C), neutral (D) and stable (E and F) atmospheric conditions. The best fit Gaussian distribution has difficulty matching the average observed concentration at z = 9.5 meters on the 15 meter tower (located approximately 4 meters from the roadway edge). However, by the time the 28 meter tower is reached, this effect has almost disappeared. The close matches attained at all other probes under varying atmospheric stability conditions provides strong support for the use of the Gaussian model near roadways.

An interesting comparison of the values of σ_z measured within the roadway median can be made by studying Tables 11, 18 and 19. Values for σ_z measured under similar wind speed and stability conditions are 2 to 3 times higher for the LA1 depressed section site (Table 18) than for either the at-grade GM site (Table 11) or the LA3 fill site (Table 19). Possible explanations include the existence of a "chimney" effect over the depressed section, or a "dead" air space within the section permitting more thorough mixing of emitted pollutants via vehicle induced turbulence.

Plots of σ_z versus downwind distance from the roadway centerline for crosswind cases of the GM, SRI and NY data bases are shown by stability class in Figures 17 thru 22. These plots were used to compare the dispersion curves for passive, ground level releases proposed by Pasquill (1974) and Smith (1972) to the observed measures of σ_z near roadways. Both ground level and tower analysis values for σ_z were plotted except when both measures of σ_z were available at the same location. Then the tower results were used exclusively. Downwind distances were computed by dividing the perpendicular probe or tower distance by the sine of the roadway-wind angle, ϕ. The plots are in log-log format, and contain best fit dispersion curves, derived by least squares regression, of the form, $\sigma_z = ax^b$. The power law approximations for the growth of vertical spread with distance suggested by Pasquill and Smith for z_o = 10 centimeters are also plotted, and denoted by the label, P-S.

All of the plots are characterized by well organized trends with significantly high correlation coefficients (r) despite the independent origins of the three data bases. Comparison of the best fit curves (shown as dashed) and the P-S curves for increasingly stable conditions reveals an interesting divergence in results. For the most unstable classes (A and B) agreement between the curves is close

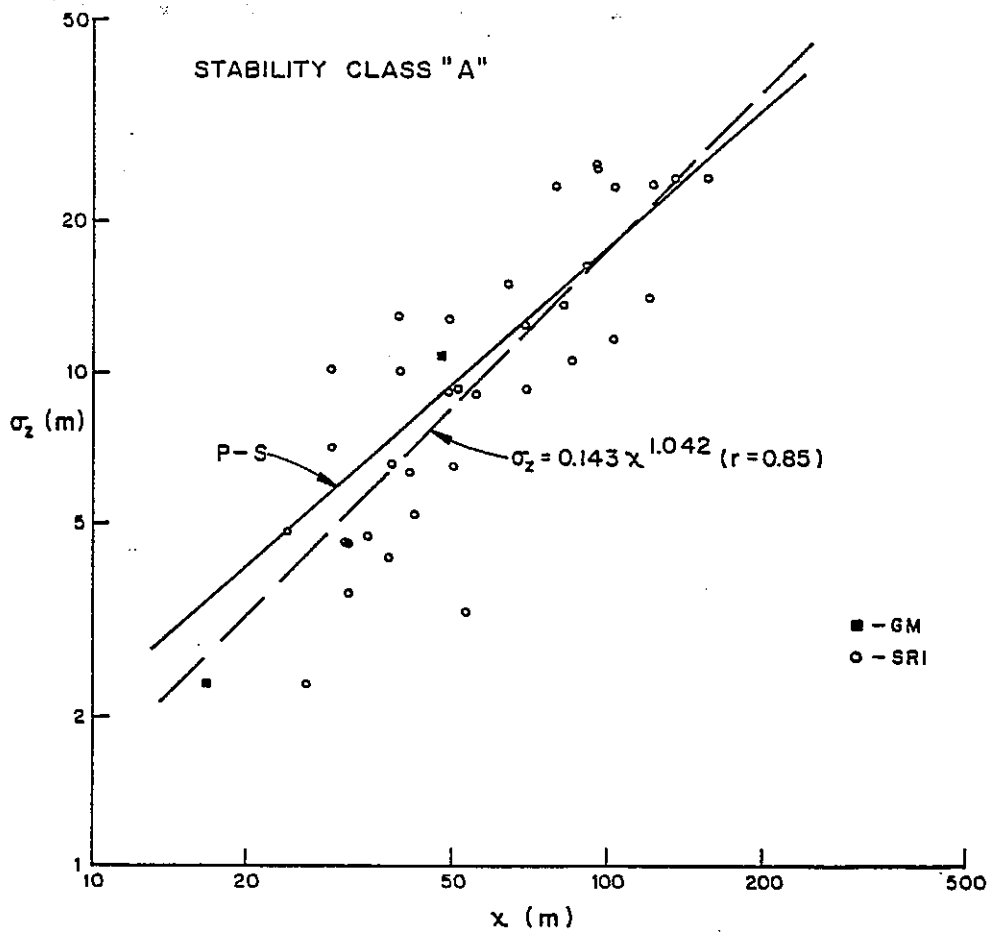

MEASURED VALUES OF THE GAUSSIAN VERTICAL DISPERSION PARAMETER (σ_z) AT VARIOUS DISTANCES DOWNWIND FROM THE ROADWAY CENTERLINE UNDER CROSSWIND CONDITIONS ($\phi \geq 35°$)

FIGURE 17

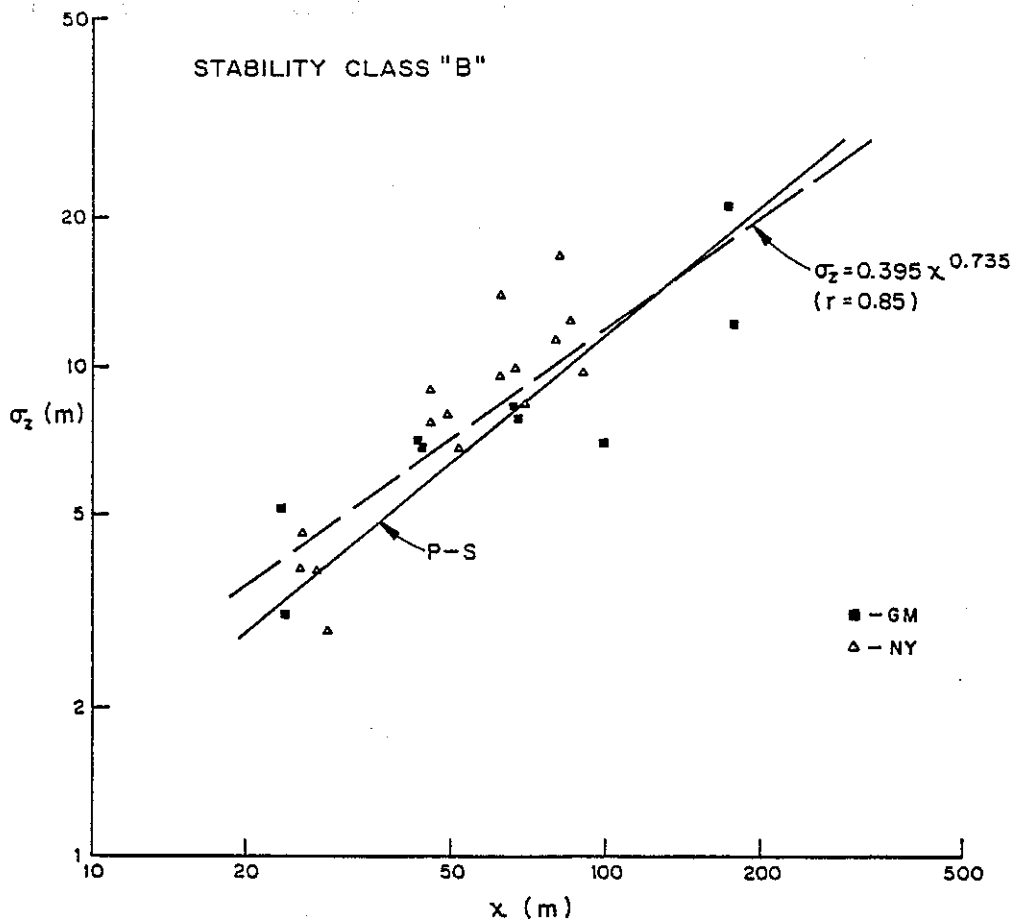

MEASURED VALUES OF THE GAUSSIAN VERTICAL DISPERSION PARAMETER (σ_z) AT VARIOUS DISTANCES DOWNWIND FROM THE ROADWAY CENTERLINE UNDER CROSSWIND CONDITIONS ($\phi \geq 35°$)

FIGURE 18

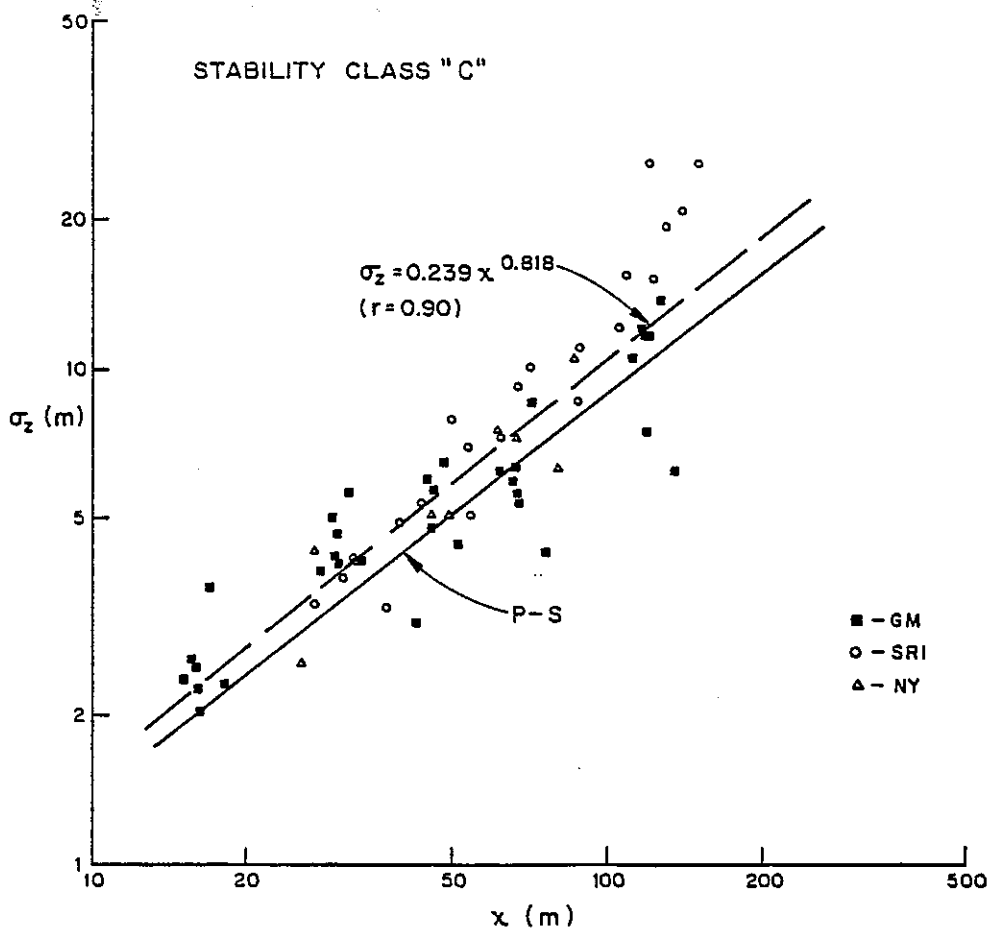

MEASURED VALUES OF THE GAUSSIAN VERTICAL DISPERSION PARAMETER (σ_z) AT VARIOUS DISTANCES DOWNWIND FROM THE ROADWAY CENTERLINE UNDER CROSSWIND CONDITIONS ($\phi \geq 35°$)

FIGURE 19

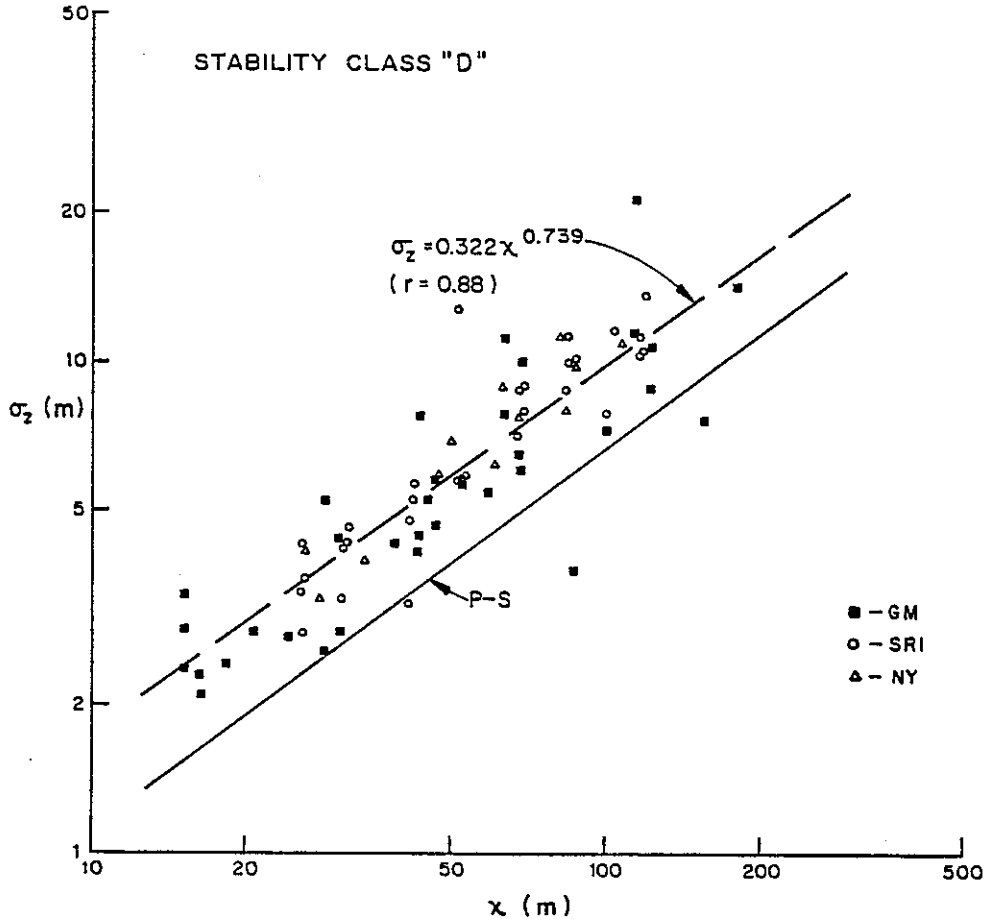

MEASURED VALUES OF THE GAUSSIAN VERTICAL DISPERSION PARAMETER (σ_z) AT VARIOUS DISTANCES DOWNWIND FROM THE ROADWAY CENTERLINE UNDER CROSSWIND CONDITIONS ($\phi \geq 35°$)

FIGURE 20

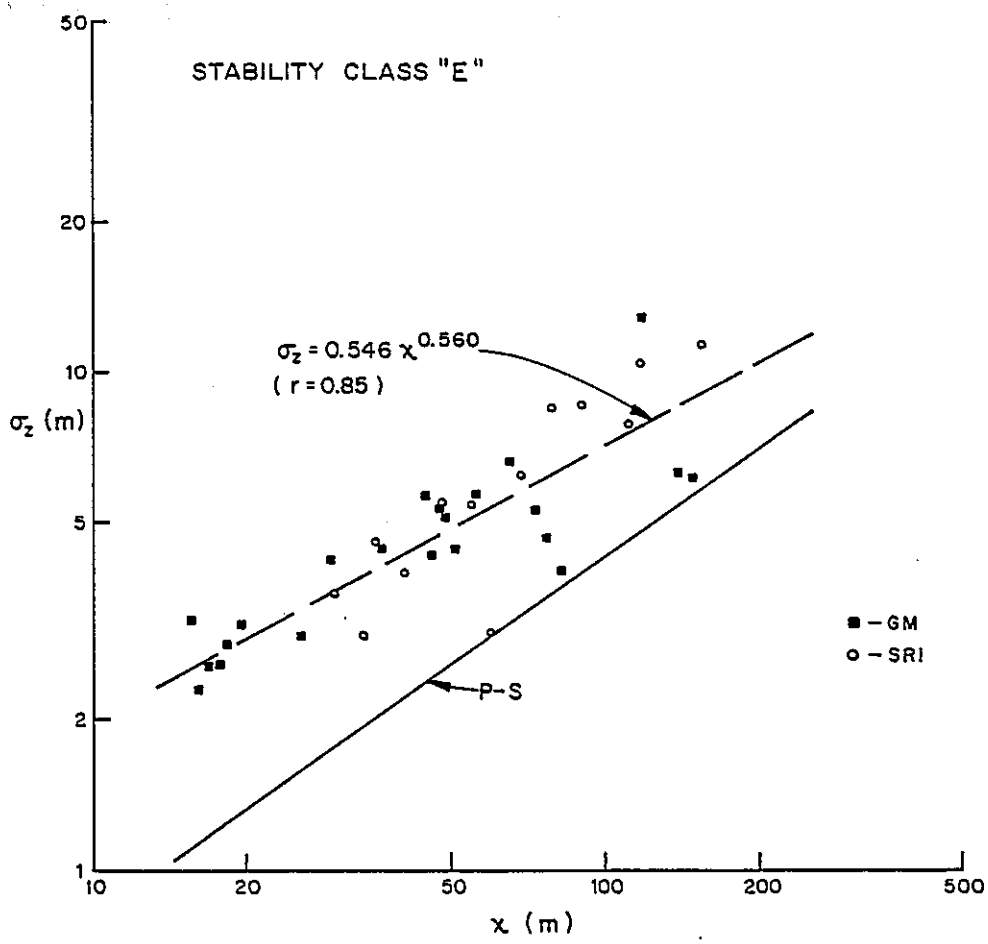

MEASURED VALUES OF THE GAUSSIAN VERTICAL DISPERSION PARAMETER (σ_z) AT VARIOUS DISTANCES DOWNWIND FROM THE ROADWAY CENTERLINE UNDER CROSSWIND CONDITIONS ($\phi \geq 35°$)

FIGURE 21

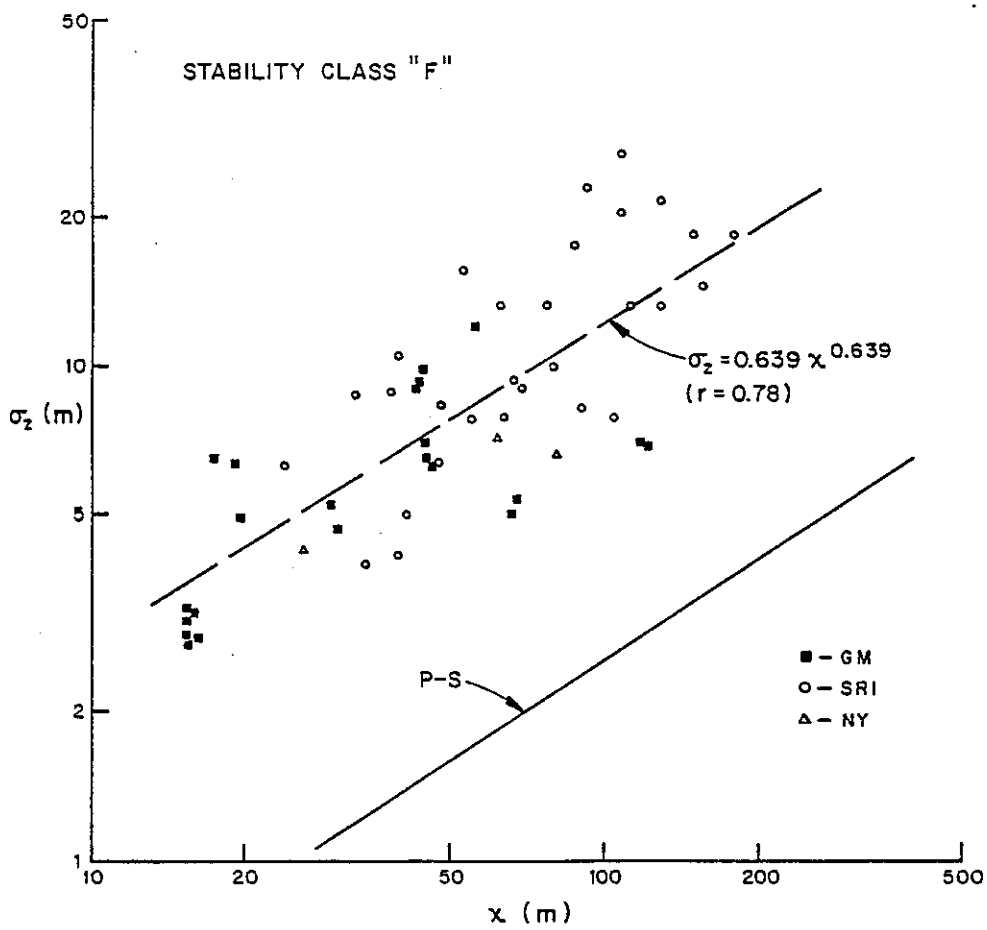

MEASURED VALUES OF THE GAUSSIAN VERTICAL DISPERSION PARAMETER (σ_z) AT VARIOUS DISTANCES DOWNWIND FROM THE ROADWAY CENTERLINE UNDER CROSSWIND CONDITIONS ($\phi \geq 35°$)

FIGURE 22

and certainly within the confidence limits of the data. But for each increasingly stable class thereafter, the P-S curve falls further below the best fit curve. This illustrates the increasing importance of roadway turbulence contributions to short range downwind mixing as ambient conditions become more stable.

The best fit vertical dispersion curves for stability classes A through F are shown on a single graph in Figure 23. With the exception of the most stable class, F, the curves tend to have a common origin at the roadway edge of approximately 2.5 meters for σ_z. Further downwind they tend to diverge with greater vertical mixing occurring for the more unstable classes. This suggests that the dominant mixing processes near the roadway are relatively independent of stability class, and that the influence of the ambient stability gradually reasserts itself 50 to 100 meters downwind of the roadway centerline. The elevated values of σ_z near the roadway for stability class F may be attributable to either plume bouyancy or enhanced traffic induced initial mixing under low wind speed conditions.

Assuming the validity of the power curve relationship, $\sigma_z = ax^b$, for short range dispersion, the vertical rate of plume growth with respect to distance may be expressed as,

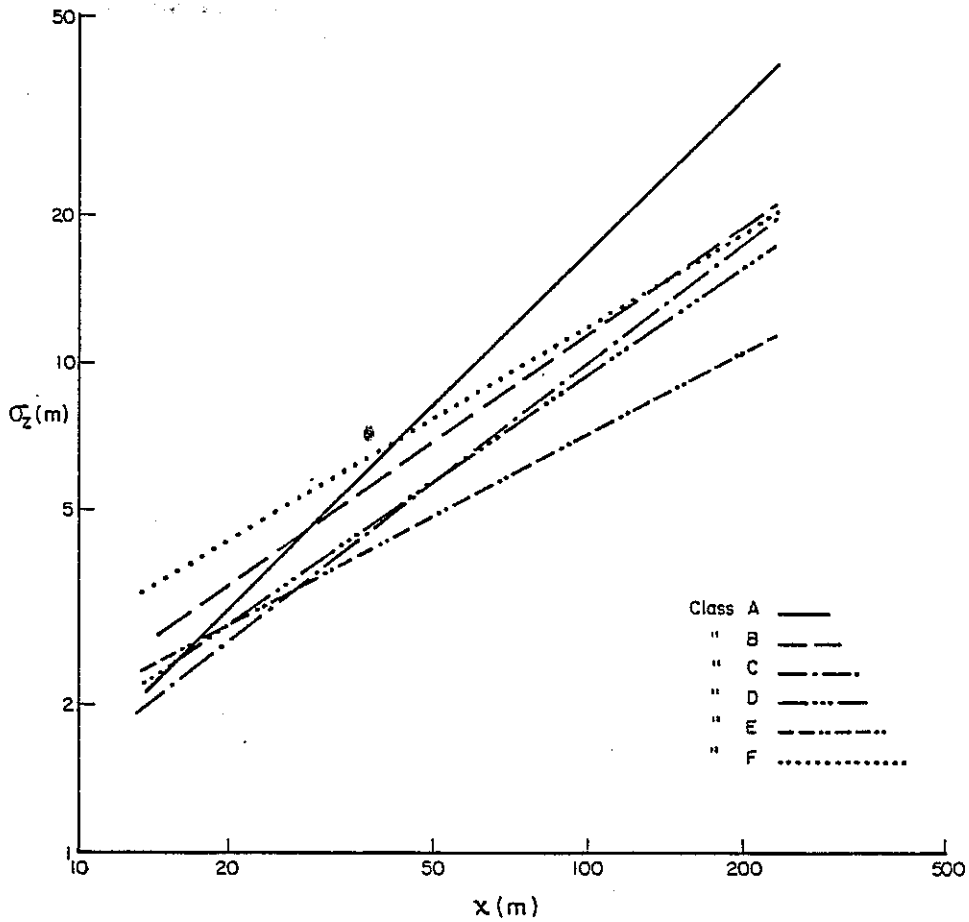

BEST FIT VERTICAL DISPERSION CURVES
BY STABILITY CLASS BASED ON GM, SRI AND NY DATA BASES

FIGURE 23

$$\frac{d\sigma}{dx} = abx^{(b-1)} \qquad (6\text{-}12)$$

This relationship was used to further compare the P-S and overall best fit dispersion curves. Table 22 lists values for $d\sigma_z/dx$ at 50 meters for both types of curves, and gives the ratio of the results.

Table 22

PASQUILL-SMITH (P-S) AND BEST FIT VERTICAL RATES OF PLUME GROWTH ($d\sigma_z/dx$) AT 50 METERS

Stability Class	$d\sigma_z/dx$ Best Fit (1)	$d\sigma_z/dx$ P-S (2)	Ratio (1)/(2)
A	0.176	0.170	1.03
B	0.103	0.109	0.95
C	0.096	0.080	1.19
D	0.086	0.059	1.44
E	0.055	0.038	1.44
F	0.099	0.022	4.50

The table clearly shows that a faster rate of plume growth is to be expected under most conditions for pollutants released from a moving stream of traffic than for the passive

releases on which the P-S curves are based, and that this effect becomes more pronounced under increasingly stable conditions. The other interesting aspect of the table is the expected downward trend in best fit values of $d\sigma_z/dx$ for increasing stability, and the departure from this trend for stability class F. This departure again suggests an interaction between stable, low wind speed regimes and either thermal or mechanical sources of traffic induced turbulence.

To explore this idea further, values of a, b and $d\sigma_z/dx$ were computed for individual runs of the GM data base. To assure consistency in the results, values from ground level analyses with four or more estimates of σ_z were used exclusively. The plume growth rate, $d\sigma_z/dx$, was evaluated at the location of the downwind meteorological tower, 43 meters from the roadway centerline.

Plots of $d\sigma_z/dx$ against the downwind values of K_z and H obtained during the meteorological analysis revealed no significant correlation. A slight tendency for a slowing of vertical plume growth with increasing upwind stability is shown in Figure 24, though it is not statistically significant. As in the overall analysis, the two F stability cases shown are above the general downward trend.

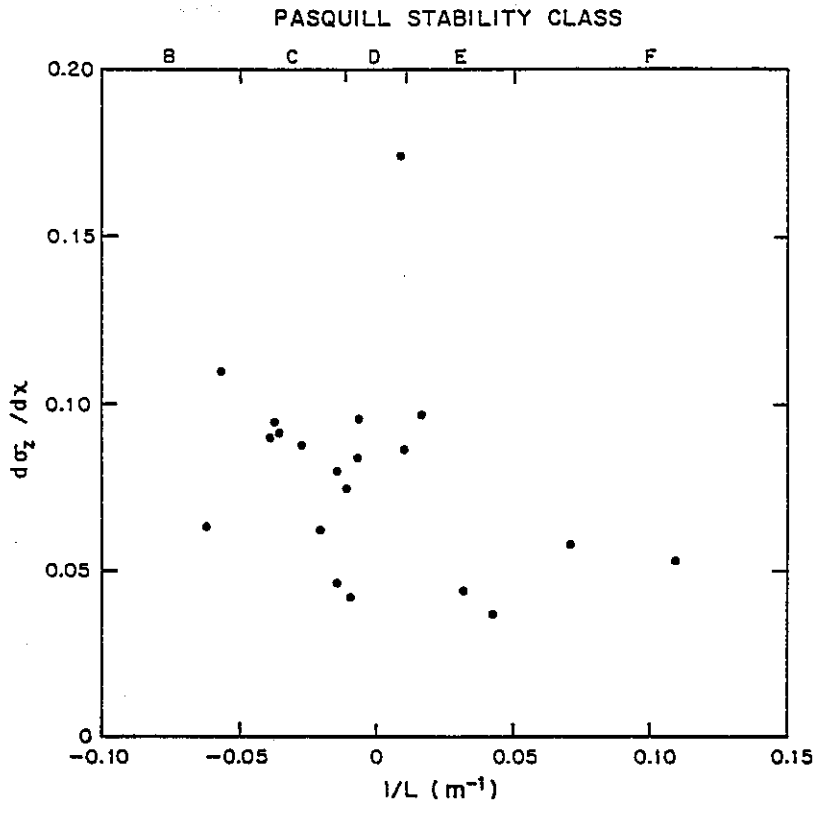

RATE OF VERTICAL PLUME GROWTH ($d\sigma_z/dx$)
VERSUS STABILITY
GM GROUND LEVEL DATA

FIGURE 24

Unfortunately, none of the F stability cases with wind speeds less than 1 m/s could be plotted because of lack of ground level and Obukhov length results.

At this point it was decided that the simplest means to bridge the gap between the P-S curves and the near roadway measurements of σ_z was to determine a method of predicting the initial vertical dispersion parameter at the roadway edge, SGZ1, and then modifying the P-S curves to fit this value. If the lower wind speeds characteristic of F stability could be correlated with higher values of initial vertical dispersion, then an explanation for the high values of $d\sigma_z/dx$ observed for F stability could also be made.

Earlier studies made by Benson and Squires (1979) concluded that SGZ1 was independent of traffic speed, volume and ambient stability, given neutral to stable conditions and traffic volumes of at least 4000 vehicles per hour. It was argued that vehicle induced mechanical turbulence dominated near the roadway under free flow traffic conditions, and that thermal turbulence from vehicular waste heat supplanted the mechanical turbulence when traffic flows became congested. A strong inverse correlation between SGZ1 and wind speed was observed, however, and gave rise to the mixing zone residence time model used in CALINE3.

The mixing zone residence model simply assumes that SGZ1 is proportional to the amount of time a parcel of air spends over the intensely turbulent mixing zone. The width of the mixing zone is given as the width of the active roadway plus 3 meters on each side to account for the vehicle wake effect. The time of residence (TR) is arbitrarily defined as the quotient of the perpendicular distance from centerline to mixing zone edge and the wind speed measured upwind at a height of approximately 5 to 10 meters.

Figures 25 thru 27 contain plots of SGZ1 versus TR for the GM, SACTO and NY data bases. The SACTO intersection site has a much lower intercept than the two freeway sites. This can be attributed to the stop-and-go nature of traffic movement through the intersection which tends to diminish initial mixing of tailpipe emissions due to the vehicle wake effect. The slope of the linear relationship between SGZ1 and TR appears to be inversely related to mixing zone width (W). This indicates that a wide roadway is not very sensitive to the residence time effect since, for the range of normal wind speeds, there is always sufficient time for the full mixing effect of the roadway turbulence to be felt. For the opposite reason, SGZ1 for a narrow roadway can be expected to be much more sensitive to TR. Note that the apparent lack of a significant vehicle wake effect for the

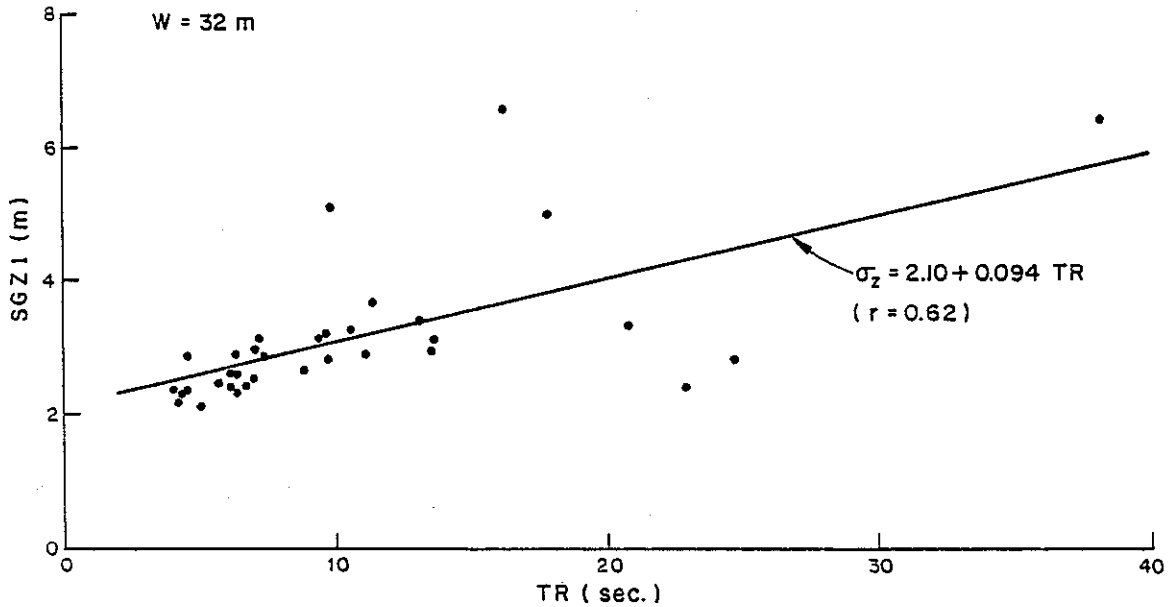

INITIAL VERTICAL DISPERSION PARAMETER SGZ1
MEASURED AT 15 METER TOWER AS A FUNCTION OF
RESIDENCE TIME (TR) — GM DATA

FIGURE 25

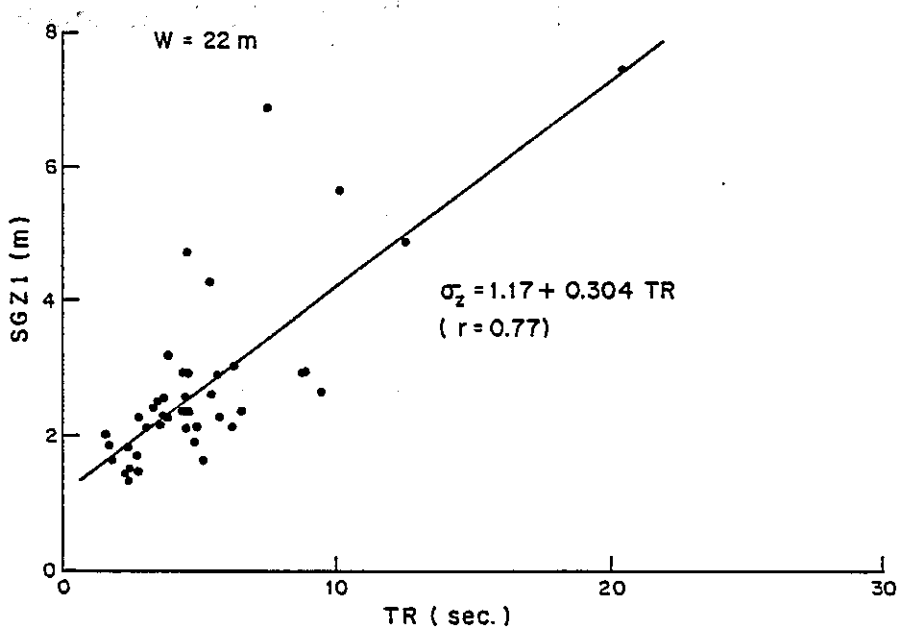

INITIAL VERTICAL DISPERSION PARAMETER SGZ1
MEASURED AT 11 METER TOWER AS A FUNCTION OF
RESIDENCE TIME (TR) – CALTRANS DATA (SACTO)

FIGURE 26

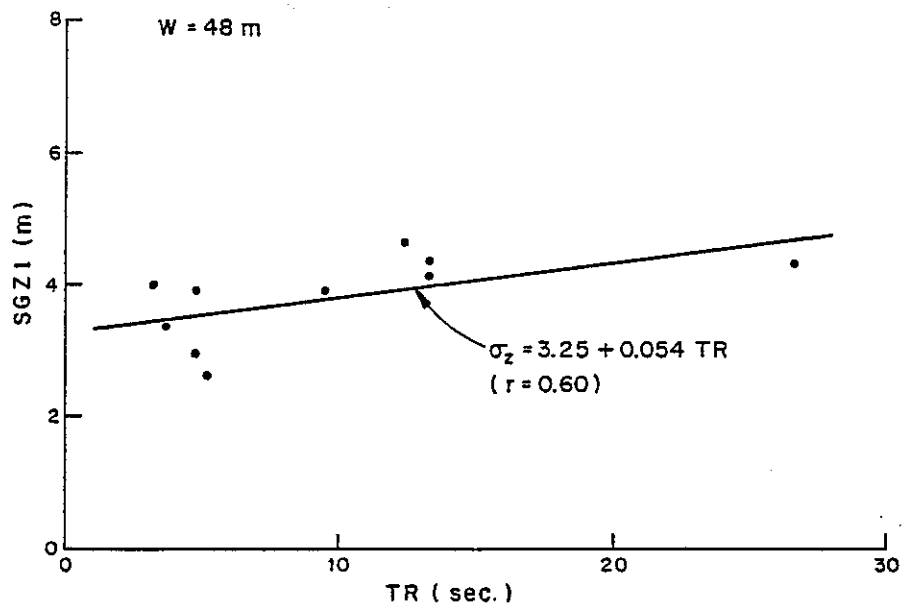

INITIAL VERTICAL DISPERSION PARAMETER SGZ1
MEASURED AT 25 METER TOWER AS A FUNCTION OF
RESIDENCE TIME (TR) — NY DATA

FIGURE 27

SACTO intersection site was accounted for by omitting the 3 meter per side addition to W.

The dispersion parameter analysis demonstrates that vertical concentration profiles measured near roadways under cross-wind conditions can be adequately described by a Gaussian distribution, and that traffic induced turbulence significantly enhances the amount of vertical mixing taking place near the roadway under neutral to stable atmospheric conditions. Also, the relationship between pollutant residence time within the roadway mixing zone and initial vertical dispersion is shown. The CALINE3 model, described in the Section 8, was based on these findings combined with a revised geometrical interpretation of the roadway as a series of finite line sources.

7. SUMMARY OF FINDINGS AND CONCLUSIONS

The preceeding sections have considered the significance and extent of vehicle induced turbulence, particularly as it relates to the vertical dispersion of inert gases near roadways. This was done by analyzing changes in surface layer stability, diffusivity and heat flux measured upwind and downwind of test roadways. Direct measurements of carbon monoxide and tracer gas concentrations were also analyzed in terms of the Gaussian dispersion model. By classifying these results into conventional Pasquill stability categories, insights regarding the mechanisms of pollutant dispersion near roadways were obtained. Also, practical information was gathered on how to modify the Gaussian model to account for vehicle induced turbulence. In Section 8, the CALINE3 line source dispersion model, which was developed from the findings of this research, is described in detail. In this section a brief summary of the findings and conclusions of the meteorological and dispersion parameter analyses is made.

Results of the meteorological analysis make it clear that vehicle induced turbulence can alter surface layer stability within the immediate vicinity of the roadway. However, this effect is only significant during neutral to stable regimes.

In support of this, the dispersion parameter analysis shows no significant difference between the Pasquill-Smith vertical dispersion curves and those derived from observed values of σ_z under unstable conditions. But, for neutral to stable conditions, the Pasquill-Smith curves seriously underpredict σ_z.

The importance of the two types of vehicle induced turbulence, mechanical and thermal, is also studied. Comparison of upwind to downwind values of diffusivity and friction velocity indicate that mechanical turbulence, originating within the roadway zone, is unimportant compared to ambient levels of turbulence during unstable conditions, but becomes increasingly important as conditions move from neutral to stable. Measurement and comparison of upwind and downwind heat fluxes using the same data bases suggest that thermal effects are significant during near-neutral conditions when relatively small additions of heat can initiate vertical movements of air. Apparently, during stable regimes, vehicular sources of thermal energy are not of sufficient magnitude to overcome the prevailing thermal stability. Naturally, during unstable conditions, vehicular thermal emissions do not add significantly to the thermal turbulence created by surface heating. In fact, the measurements indicate a tendency for more neutral conditions to exist

downwind of the roadway. This is probably attributable to the thorough mixing of the lower 10 meters of air imparted by the vehicle induced mechanical turbulence.

The statistical methodology used to fit Gaussian distributions to observed vertical concentration profiles revealed that the Gaussian model is flexible enough to simulate observed vertical distributions as close to the source as the roadway edge. It also showed that the relationship between σ_z and the downwind distance, x, can be adequately described by a power curve of the form $\sigma_z = ax^b$ for distances up to at least 200 meters downwind from the roadway centerline.

The unusually high values of initial vertical dispersion measured under low wind speed, F stability conditions are attributed to the increased residence time of pollutants within the turbulent mixing zone. Results from the comparison of upwind and downwind heat fluxes made in the meteorological analysis seem to indicate that thermal turbulence and plume rise are not important factors under such conditions. Instead, the mixing zone model used in CALINE3 was derived from the reasonably strong correlations exhibited between initial σ_z and residence time.

8. MODEL DEVELOPMENT AND DESCRIPTION

8.1 Improvements of CALINE3 Over CALINE2

The first formal, computerized version of the California Line Source Dispersion Model, called CALINE2, was introduced by Ward et. al. (1976). CALINE2 was used extensively by transportation agencies across the country for assessing air quality impacts of proposed transportation projects. Noll et. al. (1978) reported serious overpredictions made by CALINE2 for results measured under stable conditions with winds parallel to the roadway. Benson (1978) confirmed these findings and also noted a tendency for the model to underpredict during neutral to unstable, crosswind conditions. The development of CALINE3 was in response to these findings, and was a result of a total reexamination of the assumptions and algorithams contained in CALINE2.

The first and most critical area in which CALINE2 seemed deficient involved the horizontal (σ_y) and vertical (σ_z) dispersion parameter curves. The σ_y and σ_z curves used in CALINE2 were developed for averaging times of approximately 3 minutes and smooth terrain (z_o = 10 centimeters). This led to extremely conservative predictions for 1 hour

averaging times and rough terrain such as normally encountered in urban areas.

CALINE3 solves this problem by applying power law corrections for averaging time and surface roughness to the σ_y and σ_z dispersion parameters. CALINE3 also adjusts the value of σ_z at the roadway edge, set at a constant 4 meters in CALINE2, to be a function of pollutant residence time in the mixing zone. This corrects for the CALINE2 underpredictions that were observed for neutral to unstable, crosswind conditons by recognizing that lower initial values of σ_z occur at the higher windspeeds typical of Pasquill stability classes C and D. A special adjustment is made by CALINE3 to account for the apparent increased residence time for pollutants emitted in depressed sections. This is in contrast to the CALINE2 depressed section reduction factor which was derived from concentration profiles measured directly over the roadway, but applied in blanket fashion to all receptors regardless of location.

Another difficulty with CALINE2 involved its indirect handling of wind directions oblique to the roadway and its assumption of a single, 5 mile long line source of constant emissions. The model could only directly calculate receptor concentrations for roadway-wind angles, PHI, of 0° (parallel

wind) and 90° (crosswind). The parallel wind concentration, C_p, was computed by summing elemental contributions for a 1/2 mile length of roadway, and then extrapolating to 5 miles. This gave no allowance for a change in roadway alignment or emissions. The crosswind concentration, C_c, was computed by assuming the line source was of infinite length. These two results were then combined using,

$$C_{PHI} = C_c \sin (PHI) + C_p \cos (PHI) \qquad (8\text{-}1)$$

where C_{PHI} equaled the receptor concentration for the roadway-wind angle, PHI.

This problem is solved in CALINE3 by adopting a uniform method of computing incremental contributions from each roadway element. The contributions are computed as a direct function of wind-roadway angle, and summed to yield a total receptor concentration. The roadway or link length can be adjusted by the user, and multiple links can be used to simulate changes in alignment or source strength.

CALINE2 computed its value for C_p by modeling each elemental area source of the roadway as if it were emitted from a point source. This "virtual" point source was located sufficiently upwind of the element such that the plume width,

defined as $4\sigma_y$, equaled the mixing cell width, defined as the roadway width plus 10 feet on each side, as the plume traveled over the element. The mixing cell itself was treated as a box model with a height of 4 meters and a constant concentration throughout. The basic incompatability between the box model and the Gaussian point source model led to an unavoidable discontinuity in CALINE2 results at the mixing cell edge. Furthermore, the assumption of a uniform concentration across the mixing cell was not supported by field measurements taken under crosswind conditions.

In CALINE3, elements are modeled using an equivalent finite line source. In this scheme, the roadway element, which is in fact an area source, is modeled as a line source of finite length centered at the element mid-point and oriented perpendicular to the wind direction. The emissions from the roadway element are distributed in a uniform manner along the equivalent finite line source whose length is determined by the element geometry and roadway-wind angle. Thus, elements are modeled using a single computational scheme which is one dimension closer to reality than the CALINE2 virtual point/box model method. Discontinuities are eliminated, and the geometry of roadway emissions are handled in a more realistic way.

8.2 Equivalent Finite Line Source Formulation

CALINE3 divides individual highway links into a series of elements from which incremental concentrations are computed and then summed to form a total concentration estimate for a particular receptor location (see Fig. 28). The receptor distance is measured along a perpendicular from the receptor to the highway centerline. The first element is formed at this point as a square with sides equal to the highway width. The lengths of subsequent elements are described by the following formula:

$$EL = W*BASE^{(NE-1)} \tag{8-2}$$

Where,

EL = Element Length

W = Highway Width

NE = Element Number

BASE = Element Growth Factor

$PHI<20°$, BASE=1.1

$20° \leq PHI<50°$, BASE=1.5

$50° \leq PHI<70°$, BASE=2.0

$70° \leq PHI$, BASE=4.0

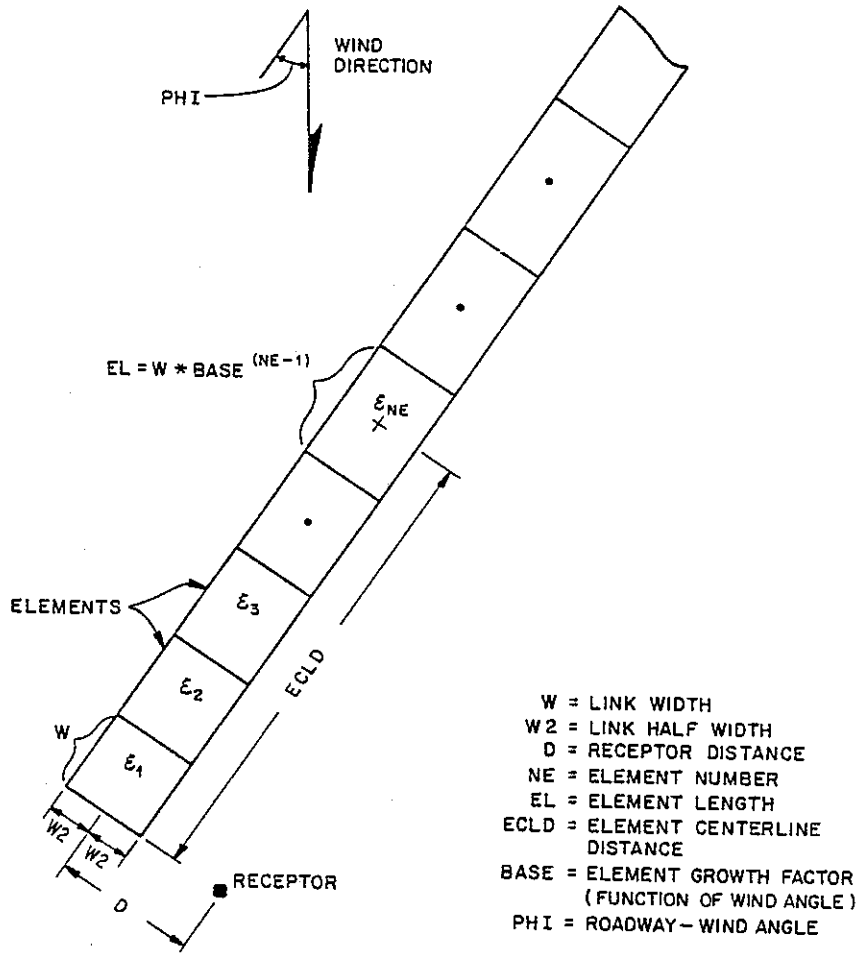

ELEMENT SERIES USED BY CALINE3

FIGURE 28

Thus, as element resolution becomes less important with distance from the receptor, elements become larger to permit efficiency in computation. The choice of the element growth factor as a function of roadway-wind angle (PHI) range represents a good compromise between accuracy and computational efficiency. Finer initial element resolution is unwarranted because the vertical dispersion curves used by CALINE3 have been calibrated for the link half-width (W2) distance from the element centerpoint.

Each Element is modeled as an "equivalent" finite line source (EFLS) positioned normal to the wind direction and centered at the element midpoint (see Fig. 29). A local x-y coordinate system aligned with the wind direction and originating at the element midpoint is defined for each element. The emissions occurring within an element are assumed to be released along the EFLS representing the element. The emissions are then assumed to disperse in a Gaussian manner downwind from the element. The length and orientation of the EFLS are functions of the element size and the angle (PHI, ϕ) between the average wind direction and highway alignment (see Fig. 30). Values of PHI=0 or PHI=90 degrees are altered within the program an insignificant amount to avoid division by zero during the EFLS trigonometric computations.

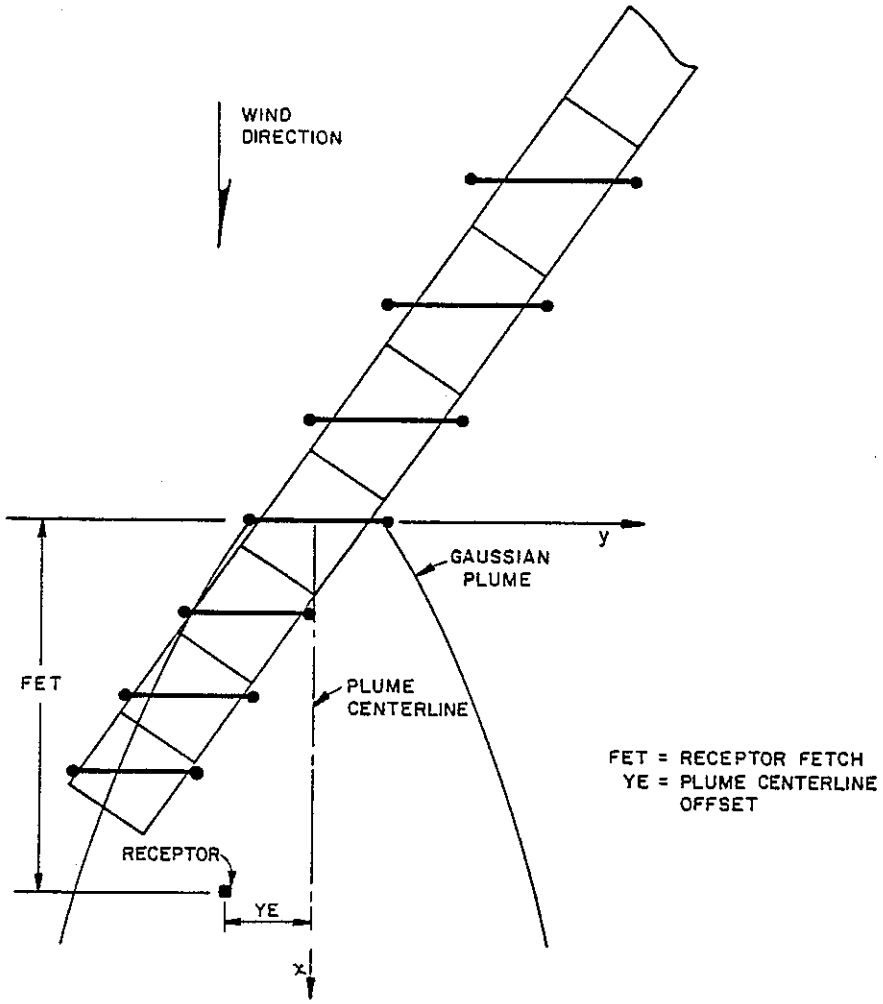

ELEMENT SERIES REPRESENTED BY
SERIES OF EQUIVALENT FINITE LINE SOURCES

FIGURE 29

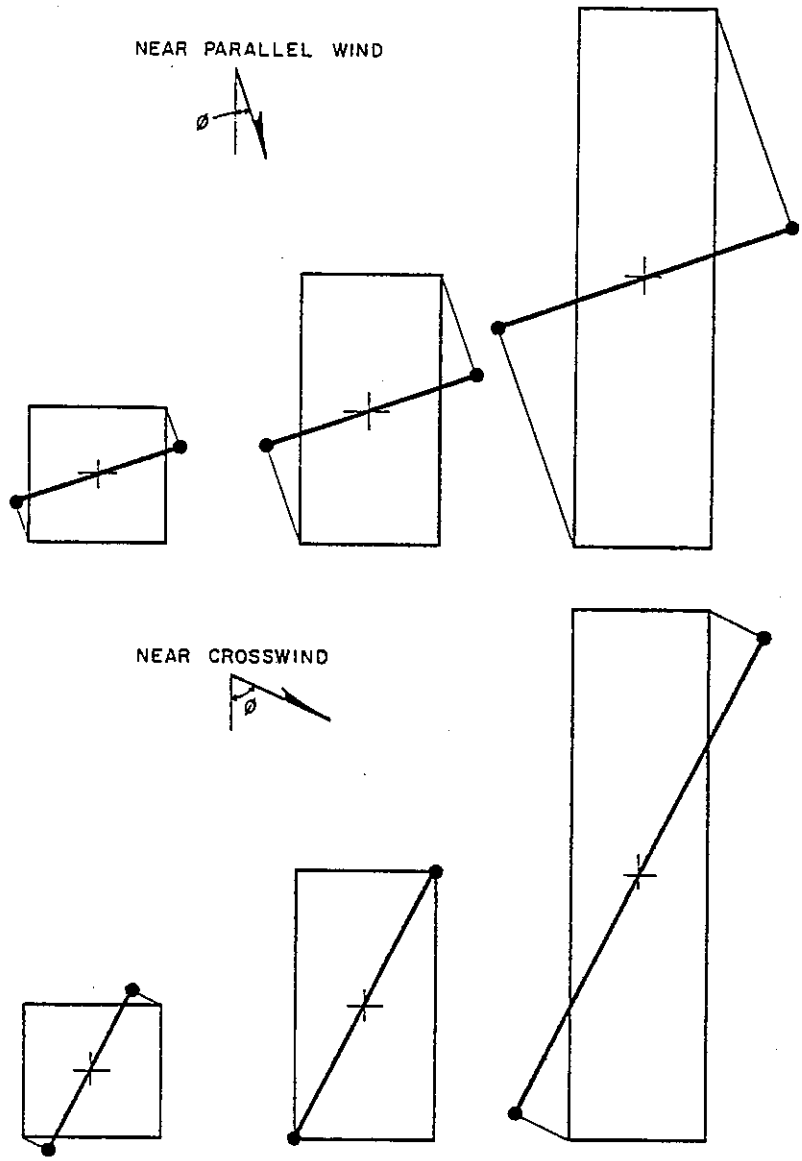

EQUIVALENT FINITE LINE SOURCE REPRESENTATION FOR VARIOUS ELEMENT SIZES AND WIND ANGLES

FIGURE 30

In order to distribute emissions in an equitable manner, each element is divided into five discrete sub-elements represented by corresponding segments of the EFLS (see Figs. 31 & 32). The use of five sub-elements yields reasonable continuity to the discrete element approximation used by the model while not excessively increasing the computational time. The source strength for the segmented EFLS is modeled as a step function whose value depends on the sub-element emissions. The emission rate/unit area is assumed to be uniform throughout the element for the purposes of computing this step function. The size and location of the sub-elements are a function of element size and wind angle (see Fig. 33).

Downwind concentrations from the element are modeled using the crosswind finite line source (FLS) Gaussian formulation. Consider the receptor concentration attributable to an FLS segment of length dy shown in Figure 34:

$$dC = \frac{q\,dy}{2\pi u \sigma_y \sigma_z}\left[\exp\left(\frac{-y^2}{2\sigma_y^2}\right)\right]\left\{\exp\left[\frac{-(z-H)^2}{2\sigma_z^2}\right] + \exp\left[\frac{-(z+H)^2}{2\sigma_z^2}\right]\right\} \tag{8-3}$$

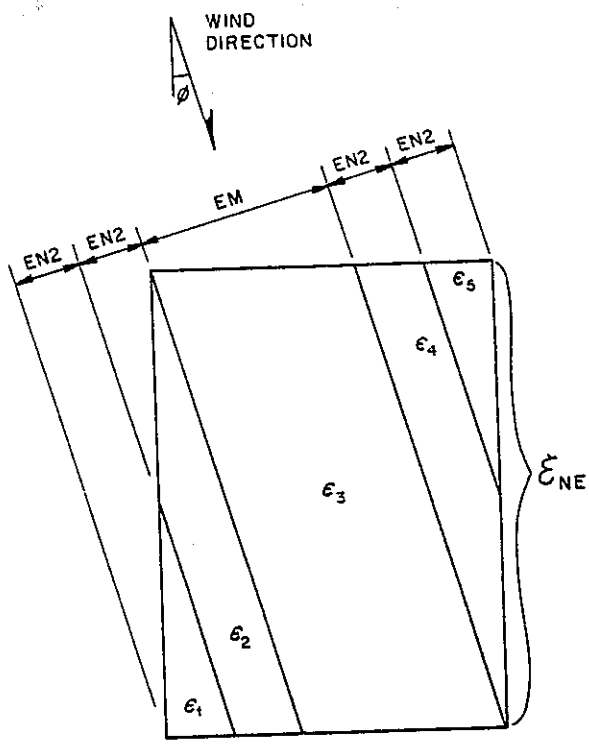

$\epsilon_1 \rightarrow \epsilon_5$ = SUB-ELEMENTS
EM, EN2 = SUB-ELEMENT WIDTHS

CALINE3 SUB-ELEMENTS

FIGURE 31

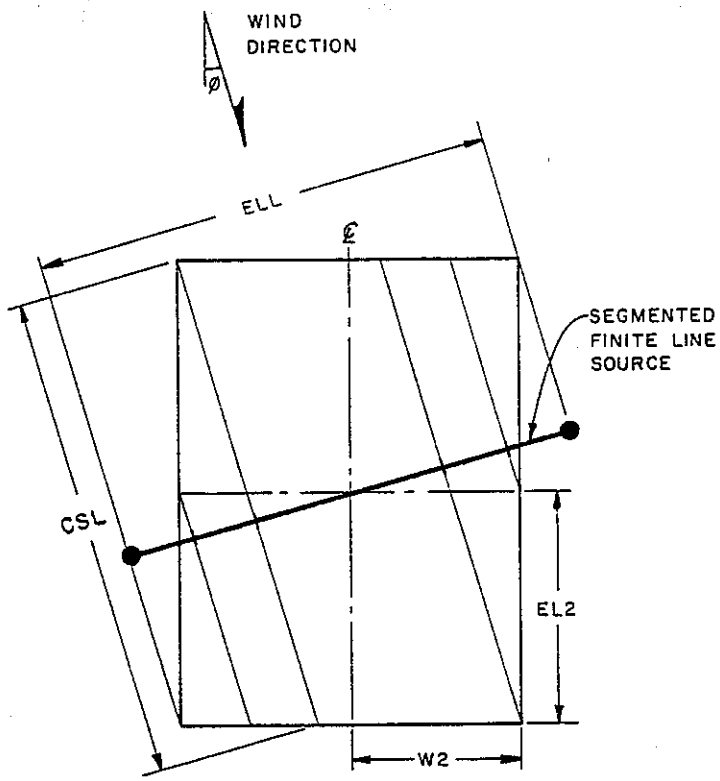

ELL = EQUIVALENT LINE LENGTH
CSL = CENTRAL SUB-ELEMENT LENGTH

CALINE3 FINITE LINE SOURCE
ELEMENT REPRESENTATION

FIGURE 32

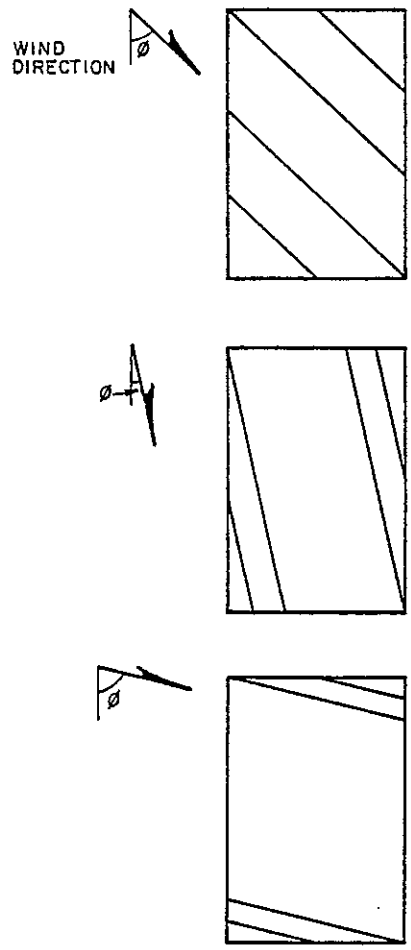

SUB-ELEMENT CONSTRUCTION FOR VARIOUS WIND ANGLES

FIGURE 33

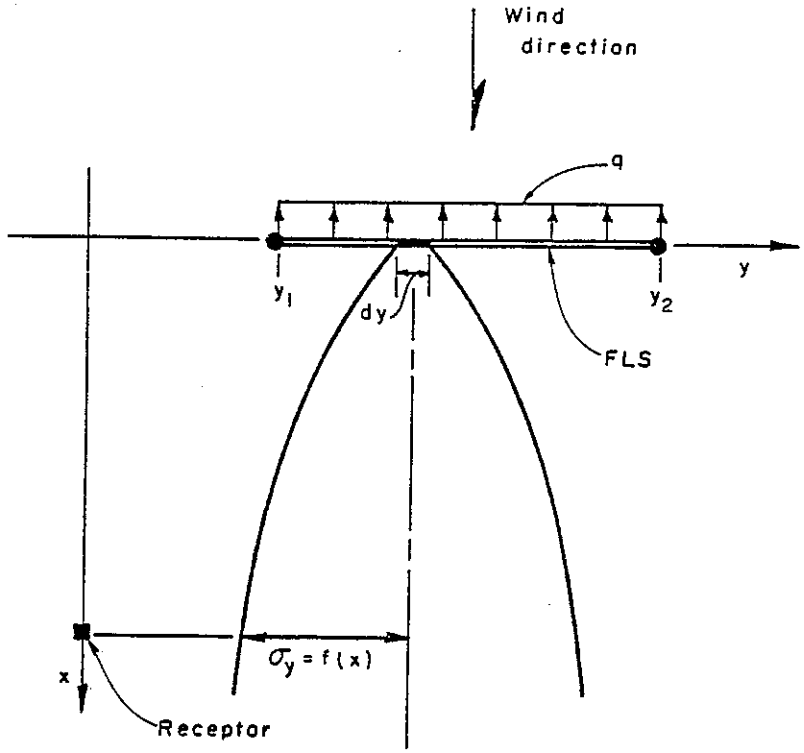

q = UNIFORM LINE SOURCE STRENGTH

σ_y = HORIZONTAL DISPERSION PARAMETER

GENERALIZED FINITE LINE SOURCE (FLS)

FIGURE 34

where, dC = Incremental Concentration

q = Lineal Source Strength

u = Wind Speed

H = Source Height

σ_y, σ_z = Horizontal and Vertical Dispersion Parameters

Since σ_z is constant with respect to y, let:

$$A = \exp\left[\frac{-(z-H)^2}{2\sigma_z^2}\right] + \exp\left[\frac{-(z+H)^2}{2\sigma_z^2}\right] \tag{8-4}$$

Integrating over the FLS length yields:

$$C = \frac{Aq}{2\pi u \sigma_y \sigma_z} \int_{y_1}^{y_2} \exp\left(\frac{-y^2}{2\sigma_y^2}\right) dy \tag{8-5}$$

Note that σ_y and σ_z are functions of x, not y.
Substituting $p=y/\sigma_y$ and $dp=dy/\sigma_y$:

$$C = \frac{Aq}{2\pi u \sigma_y \sigma_z} \int_{y_1/\sigma_y}^{y_2/\sigma_y} \exp\left(\frac{-p^2}{2}\right) \sigma_y \, dp \tag{8-6}$$

Backsubstituting for A and removing σ_y from the integral leaves:

$$C = \frac{q}{2\pi\sigma_z u}\left\{\exp\left[\frac{-(z-H)^2}{2\sigma_z^2}\right] + \exp\left[\frac{-(z+H)^2}{2\sigma_z^2}\right]\right\}\int_{y_1/\sigma_y}^{y_2/\sigma_y} \exp\left(\frac{-p^2}{2}\right) dp \tag{8-7}$$

This can be rewritten as:

$$C = \frac{q}{\sqrt{2\pi}\sigma_z u}\left\{\exp\left[\frac{-(z-H)^2}{2\sigma_z^2}\right] + \exp\left[\frac{-(z+H)^2}{2\sigma_z^2}\right]\right\} \cdot PD \tag{8-8}$$

Where,

$$PD = \frac{1}{\sqrt{2\pi}}\int_{y_1/\sigma_y}^{y_2/\sigma_y} \exp\left(\frac{-p^2}{2}\right) dp = \text{Normal Probability Density Function} \tag{8-9}$$

CALINE3 computes receptor concentrations by approximating the crosswind FLS equation in the following manner (see Fig. 35):

(8-10)

$$C = \frac{1}{\sqrt{2\pi}\,U} * \sum_{i=1}^{n} \left\{ \frac{1}{SGZ_i} * \sum_{k=-CNT}^{CNT} \left[\exp\left(\frac{-(Z-H+2*k*L)^2}{2*SGZ_i^{\,2}} \right) + \exp\left(\frac{-(Z+H+2*k*L)^2}{2*SGZ_i^{\,2}} \right) \right] * \sum_{j=1}^{5} (WT_j * QE_i * PD_{ij}) \right\}$$

Where,

n = Total number of elements

CNT = Number of multiple reflections required for convergence

U = Wind speed

L = Mixing height (MIXH in coding)

SGZ_i = σ_z as f(x) for ith element

QE_i = Central sub-element lineal source strength for ith element

WT_j = Source strength weighting factor for jth sub-element (WT_1 = 0.25, WT_2 = 0.75, ...)

$$PD_{ij} = \frac{1}{\sqrt{2\pi}} \int_{\frac{Y_j}{SGY_i}}^{\frac{Y_{j+1}}{SGY_i}} \exp\left(\frac{-p^2}{2}\right) dp$$

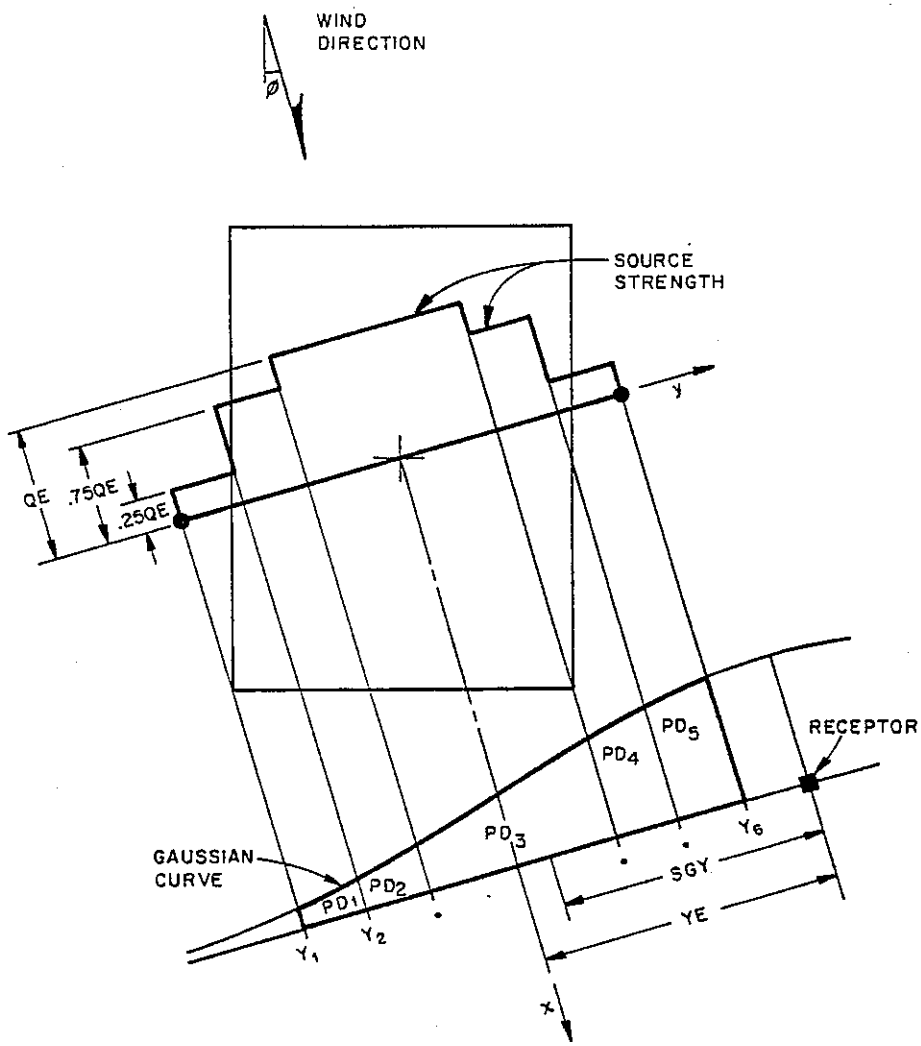

QE = EQUIVALENT LINE SOURCE STRENGTH
PD = PROBABILITY DENSITY
SGY = HORIZONTAL DISPERSION PARAMETER
YE = PLUME CENTERLINE OFFSET

CALINE3 INTEGRATED FINITE LINE SOURCE AND SUB-ELEMENT MODEL

FIGURE 35

Y_j, Y_{j+1} = Offset distances for jth sub-element

$SGY_i = \sigma_y$ as f(x) for ith element

PD_{ij} is calculated by use of a fifth order polynomial approximation (Abramowitz, 1968). Note the addition of multiple reflection terms represented by non-zero k indices to account for restricted mixing height (L).

The source strength weighting factor (WT_j) adjusts the central sub-element lineal source strength measured with respect to the y-axis (QE) to the mean lineal source strength for each peripheral sub-element. Because of the uniform width of the peripheral sub-elements (EN2) and the assumption of uniform emissions over the element, q=0 @ $y=Y_1$, q=QE/2 @ $y=Y_2$, q=QE @ $y=Y_3$, etc.

Therefore,

$$WT_1*QE = WT_5*QE = (QE/2+0)/2 = 0.25\ QE \qquad (8\text{-}11)$$

$$WT_2*QE = WT_4*QE = (QE+QE/2)/2 = 0.75\ QE \qquad (8\text{-}12)$$

The element summation of the FLS equation is actually initiated twice for each highway link specified by the user (see Fig. 36). The computation takes place first in the upwind direction, ending when the element limits go beyond the

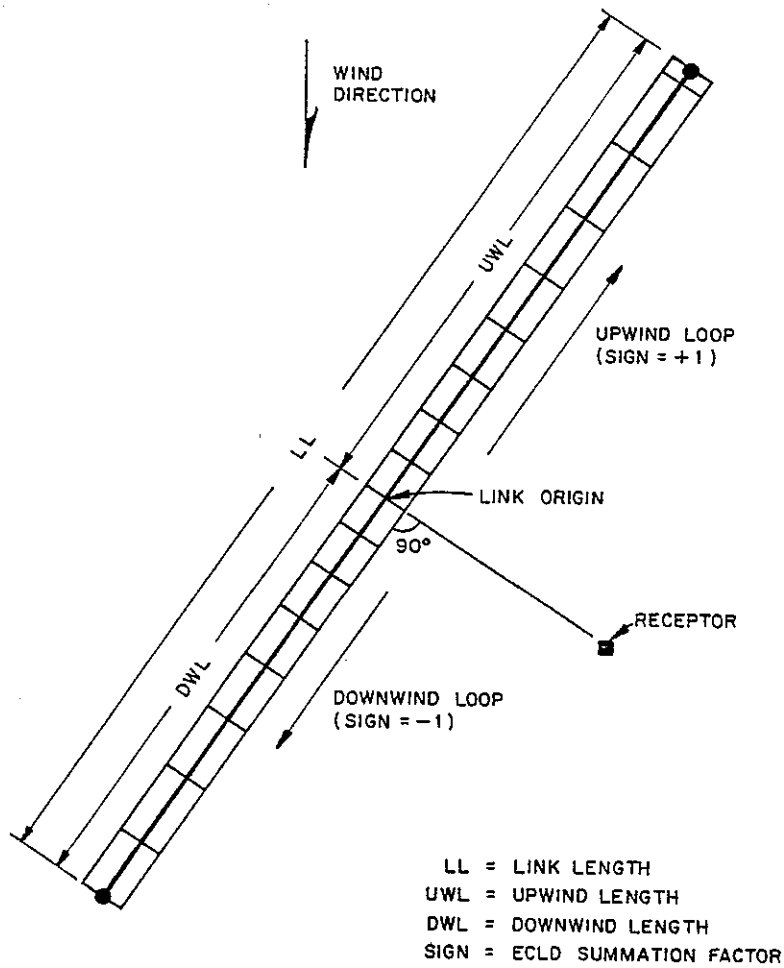

CALINE3 LINK – ELEMENT REPRESENTATION

FIGURE 36

upwind length (UWL) for the link. The length of the last element is modified to conform with the link endpoint.

The program then proceeds in the downwind direction until the downwind length (DWL) is exceeded. As soon as a negative value of fetch (FET) is encountered, the program automatically concludes the downwind loop computations. If a receptor is located within an element or downwind from part of an element, only the upwind portion of the element is used to determine the source strength.

8.3 Mixing Zone Model

CALINE3 treats the region directly over the highway as a zone of uniform emissions and turbulence. This is designated as the mixing zone, and is defined as the region over the traveled way (traffic lanes - not including shoulders) plus three meters on either side (see Fig. 37). The additional width accounts for the initial horizontal dispersion imparted to pollutants by the vehicle wake effect (Dabberdt, 1975).

Within the mixing zone, the mechanical turbulence created by moving vehicles and the thermal turbulence created by hot vehicle exhaust is assumed to predominate near the

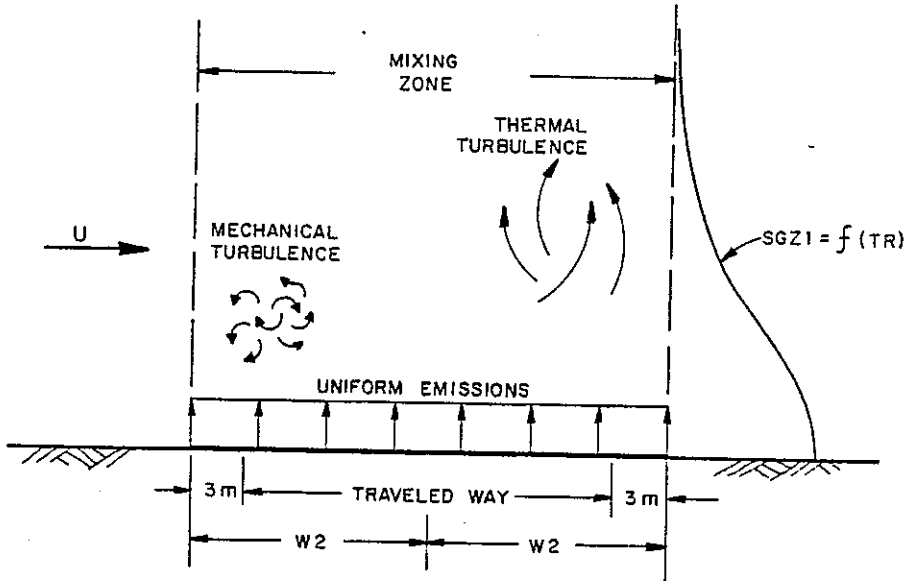

SGZ1 = INITIAL VERTICAL DISPERSION PARAMETER
TR = MIXING ZONE RESIDENCE TIME

CALINE3 MIXING ZONE

FIGURE 37

ground. The findings presented in Sections 5 and 6 indicate that this is a valid assumption for all but the most unstable atmospheric conditions. Since traffic emissions are released near the ground level and model accuracy is most important for neutral and stable atmospheric conditions, it is reasonable to model initial vertical dispersion (SGZ1) as a function of the turbulence within the mixing zone. Analysis of the data base indicates that SGZ1 is insensitive to changes in traffic volume and speed within the ranges of 4,000 to 8,000 vehicles/hr and 30 to 60 mph (Benson and Squires, 1979). This may be due in part to the offsetting effects of traffic speed and volume. Higher volumes increase thermal turbulence but reduce traffic speed, thus reducing mechanical turbulence. For the range of traffic conditions cited, mixing zone turbulence may be considered a constant. However, pollutant residence time within the mixing zone, as dictated by the wind speed, significantly affects the amount of vertical mixing that takes place within the zone. As shown in Section 6, a distinct linear relationship between SGZ1 and residence time exists.

CALINE3 arbitrarily defines mixing zone residence time as:

$$TR = W2/U \qquad (8\text{-}13)$$

Where, W2 = Highway half-width

U = Wind speed

This definition is independent of wind angle and element size. It essentially provides a way of making the EFLS model compatible with the actual two-dimensional emissions release within an element. For oblique winds and larger elements, the plume is assumed to be sufficiently dispersed after traveling a distance of W2 such that the mixing zone turbulence no longer predominates.

The equation used by CALINE3 to relate SGZ1 to TR is:

$$\underset{(m)}{SGZ1} = 1.8 + 0.11 * \underset{(secs.)}{TR} \qquad (8\text{-}14)$$

Equation 8-14 was derived from an earlier analysis of the GM data base exclusive of easterly crosswind cases. Consideration of these additional cases leads to the slightly different version of Equation 8-14 shown in Figure 25. The differences are well within the 95% confidence limits for both the intercept and slope, and therefore do not justify a change in the established model.

SGZ1 is adjusted in the model for averaging times other than 30 minutes (used in the GM study) by the following power law:

$$SGZ1_{ATIM} = SGZ1_{30} * (ATIM/30)^{0.2} \quad . \qquad (8\text{-}15)$$

Where, ATIM = Averaging time (minutes)

The value of SGZ1 is considered by CALINE3 to be independent of surface roughness and atmospheric stability class. The user should note that SGZ1 accounts for all the enhanced dispersion over and immediately downwind of the roadway. Thus, the stability class used to run the model should be representative of the upwind or ambient stability without any additional modifications for traffic turbulence.

8.4 Vertical Dispersion Curves

The vertical dispersion curves used by CALINE3 are formed by using the value of SGZ1 from the mixing zone model, and the value of σ_z at 10 kilometers (SZ10) as defined by Pasquill (1974) and Smith (1972). In effect, the power curve approximation suggested by Pasquill is elevated near the highway by the intense mixing zone turbulence (see Fig. 38). The significance of this added turbulence to

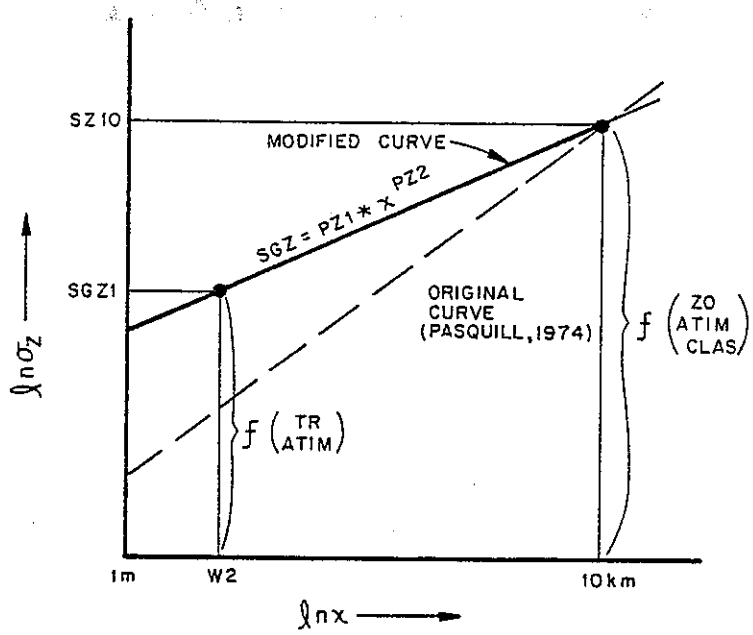

ZO = AERODYNAMIC ROUGHNESS
ATIM = AVERAGING TIME
CLAS = STABILITY CLASS
TR = MIXING ZONE RESIDENCE TIME
x = PLUME CENTERLINE AXIS
σ_Z = VERTICAL DISPERSION PARAMETER

MODIFIED VERTICAL DISPERSION CURVE – CALINE3

FIGURE 38

plume growth lessens with increased distance from the source. The 10 kilometer length is chosen to provide continuity between CALINE3 and the original 5 mile length assumed by CALINE2. It is not meant to imply that measurable effects of vehicle induced turbulence exist 10 kilometers downwind from the roadway, but that the original power curve approximation to the true Pasquill-Smith curve, which is actually concave to the ℓnx axis, becomes increasingly inaccurate beyond 10 kilometers and is only an approximation with a maximum error of 10% for distances less than 10 kilometers. Sensitivity analyses reveal that contributions from elements greater than 10 kilometers from the receptor are insignificant even under the most stable atmospheric conditions.

An alternate method proposed by Calder (1973, see Equation 3-11) for modifying the Pasquill power curve to match the initial roadside dispersion parameter was also examined. This method had the advantage of asymptotically approaching the Pasquill curve rather than intersecting it, thus providing a smooth transition from the modified to conventional form of the curve.

To compare the two methods, residual root mean squares were calculated for individual runs of the GM and SRI data bases

as follows,

$$RMS1 = \left[\frac{\sum_{i=2}^{n} ({}_1\hat{\sigma}_{z_i} - \sigma_{z_i})^2}{n} \right]^{1/2} \qquad (8\text{-}16)$$

$$RMS2 = \left[\frac{\sum_{i=2}^{n} ({}_2\hat{\sigma}_{z_i} - \sigma_{z_i})^2}{n} \right]^{1/2} \qquad (8\text{-}17)$$

where, σ_{z_i} = observed vertical dispersion parameter based on ground level results,

${}_1\sigma_{z_i} = PZ1 * x^{PZ2}$

${}_2\sigma_{z_i} = a(x+c)^b$

PZ1 and PZ2 were calculated by setting SGZ1 equal to the σ_z measured closest to the roadway (σ_{z_i}), and c was determined by assuming the Pasquill values for a and b, and solving for c given σ_{z_1} measured at distance x.

The results of this analysis are shown in Figures 39 and 40 as the difference between RMS1 and RMS2 plotted against the inverse Obukhov Length. The predominance of negative

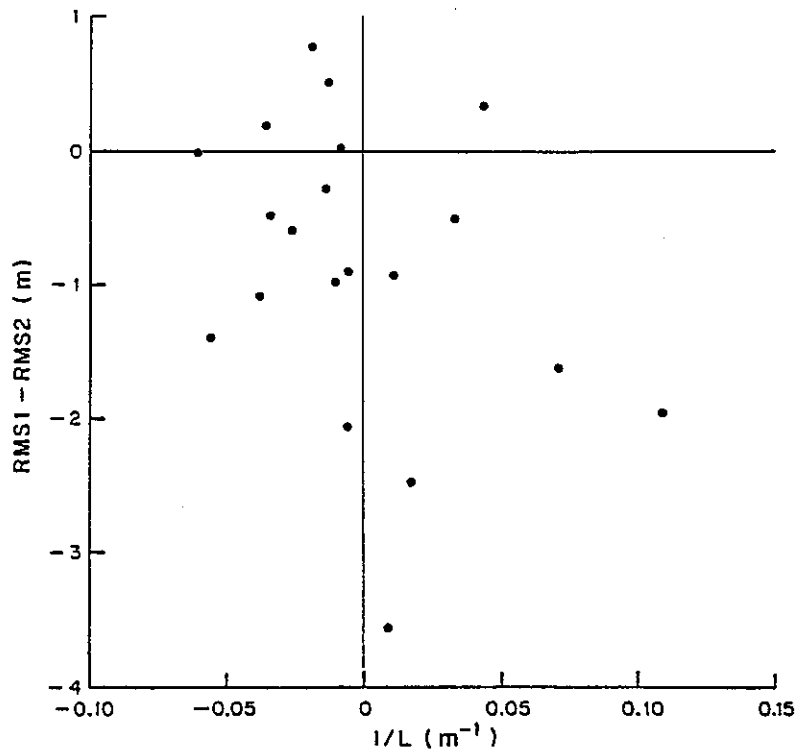

DIFFERENCE BETWEEN RESIDUAL ROOT MEAN SQUARES
USING CALINE3 (RMS1) AND CALDER (RMS2) METHODOLOGIES
VERSUS STABILITY
GM DATA, GROUND LEVEL VALUES

FIGURE 39

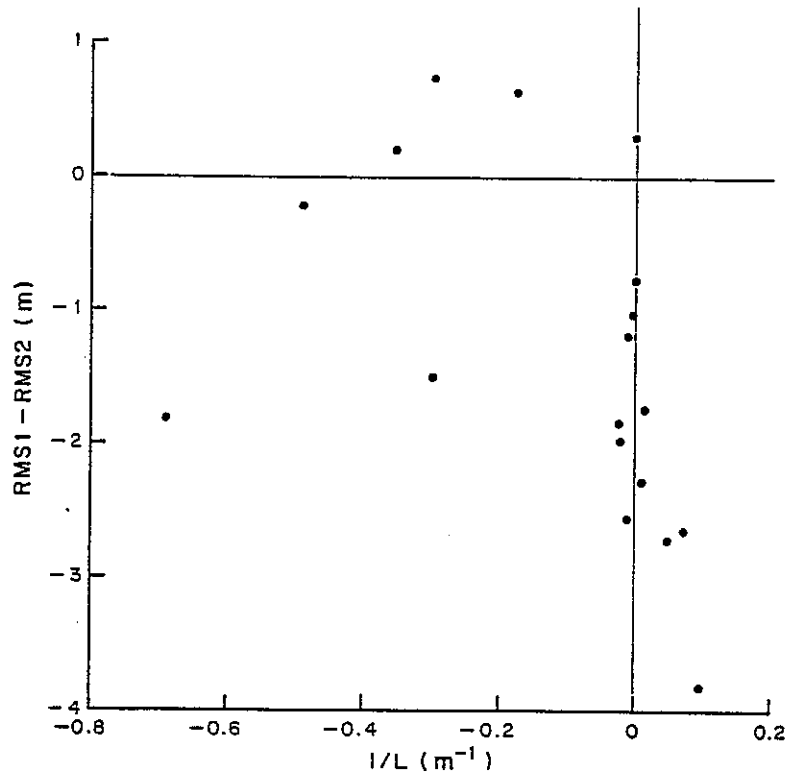

DIFFERENCE BETWEEN RESIDUAL ROOT MEAN SQUARES
USING CALINE3 (RMS1) AND CALDER (RMS2) METHODOLOGIES
VERSUS STABILITY
SRI DATA, GROUND LEVEL VALUES

FIGURE 40

results, especially for neutral to stable conditions, indicates that a better degree of fit to observed results is attained by the intersecting power curve than by Calder's method. In fact, residual plots reveal that the Calder curve has a tendency to return to the original Pasquill curve much faster than the measured data.

The rates of plume growth for the two types of curves are,

$$\frac{d_1\sigma_z}{dx} = PZ1*PZ2*x^{(PZ2-1)} \qquad (8\text{-}18)$$

$$\frac{d_2\sigma_z}{dx} = ab(x + c)^{b-1} \qquad (8\text{-}19)$$

Because Equation 8-19 is so strongly dependent on the original Pasquill values for a and b, it cannot account for the lingering effects of vehicle induced turbulence downwind of the roadway. For this reason, the Calder methodology, when applied using Pasquill values for a and b determined from upwind stability measurements, severely underpredicts mid-distance values for σ_z.

For a given set of meteorological conditions, surface roughness (ZO) and averaging time (ATIM), CALINE3 uses the same vertical dispersion curve for each element within a highway link. This is possible since SGZ1 is always defined as occurring at a distance W2 downwind from the element centerpoint. SZ10 is adjusted for ZO and ATIM by the following power law factors:

$$SZ10_{ATIM,ZO} = SZ10*(ATIM/3)^{0.2}*(ZO/10)^{0.07} \qquad (8\text{-}20)$$

Where, ATIM = Averaging time (minutes)

ZO = Surface roughness (cm)

Table 23 contains recommended values of ZO for representative land use types (Myrup and Ranzieri, 1976).

The vertical dispersion of CO predicted by the model can be confined to a shallow mixed layer by means of the conventional Gaussian multiple reflection formulation (Turner, 1970). This capability was included in the model to allow for analysis of low traffic flow situations occurring during extended nocturnal low level inversions. Surprisingly high 8 hour CO averages have been measured under such conditions (Remberg et. al., 1979).

TABLE 23

Surface Roughness for Various Land Uses

Type of Surface	Z0 (cm)
Smooth mud flats	0.001
Tarmac (pavement)	0.002
Dry lake bed	0.003
Smooth desert	0.03
Grass (5-6 cm)	0.75
(4 cm)	0.14
Alfalfa (15.2 cm)	2.72
Grass (60-70 cm)	11.4
Wheat (60 cm)	22
Corn (220 cm)	74
Citrus orchard	198
Fir forest	283
City land-use	
Single family residential	108
Apartment residential	370
Office	175
Central Business District	321
Park	127

It is recommended for these cases that reliable, site specific field measurements be made. The following mixing height model proposed by Benkley and Schulman (1979) can then be used:

$$MIXH = \frac{0.185*U*k}{\ln(Z/Z0)*f} \qquad (8\text{-}21)$$

Where, U = Wind speed (m/s)

Z = Height U measured at (m)

Z0 = Surface roughness (m)

k = von Karman constant (0.35)

f = Coriolis parameter

= $1.45 \times 10^{-4} \cos\Theta$ (radians/sec)

Θ = 90° - site latitude

For nocturnal conditions with low mixing heights, wind speeds are likely to be less than 1 m/s. Extremely sensitive wind speed and direction instrumentation would be required for reliable results at such low wind speeds. In order to use CALINE3 for these conditions, measurements of the horizontal wind angle standard deviation will be needed. The model can then be modified to calculate horizontal dispersion parameters based on the methodology developed by Pasquill (1976) or Draxler (1976). The user is cautioned

that the model has not been verified for wind speeds below 1 m/s, and that assumptions of negligible along-wind dispersion and steady state conditions are open to question at such low wind speeds.

Mixing height computations must be made for each element-receptor combination, and thus add appreciably to program run time. As has been shown by sensitivity analyses, the mixing height must be extremely low to generate any significant response from the model. Therefore, it is recommended that the user bypass the mixing height computations for all but special nocturnal simulations. This is done by assigning a value of 1000 meters or greater to MIXH.

8.5 Horizontal Dispersion Curves

The horizontal dispersion curves used by CALINE3 are identical to those used by Turner (1970) except for averaging time and surface roughness power law adjustments similar to those made for the vertical dispersion curves (see Fig. 41). The model makes no corrections to the initial horizontal dispersion near the roadway. The only roadway related alterations to the horizontal dispersion curves occur indirectly by defining the highway width as the

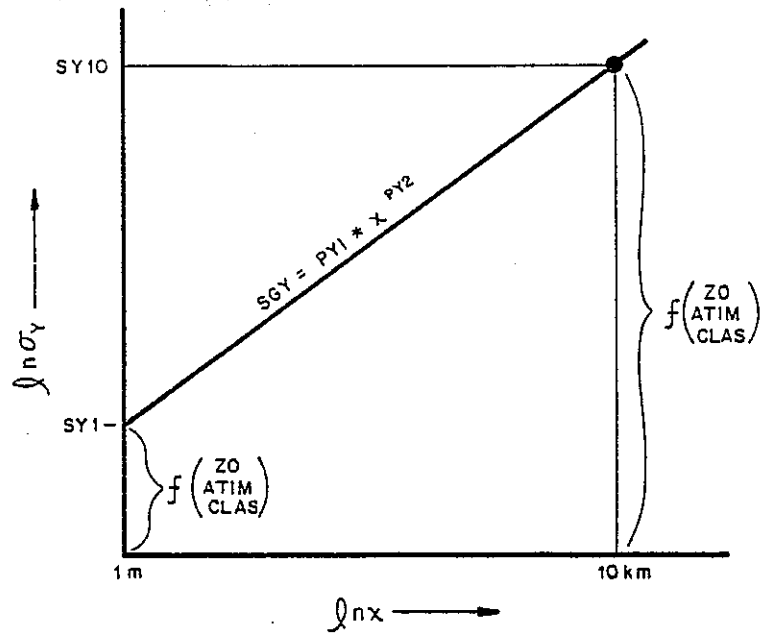

ZO = AERODYNAMIC ROUGHNESS
ATIM = AVERAGING TIME
CLAS = STABILITY CLASS
x = PLUME CENTERLINE AXIS
σ_Y = HORIZONTAL DISPERSION PARAMETER
PY1 = exp (SY1)

HORIZONTAL DISPERSION CURVE – CALINE3

FIGURE 41

width of the traveled way plus 3 meters on each side, and assuming uniform emissions throughout the element.

If field measurements of the horizontal wind angle standard deviation are available, site specific horizontal dispersion curves can be generated using the methodology developed by Pasquill (1976) or Draxler (1976). CALINE3 can then be easily reprogrammed to incorporate the modified curves. This approach is recommended whenever manpower and funding are available for site monitoring.

8.6 Site Geometry

CALINE3 permits the specification of up to 20 links and 20 receptors within an X-Y plane (not to be confused with the local x-y coordinate system associated with each element). A link is defined as a straight segment of roadway having a constant width, height, traffic volume, and vehicle emission factor. The location of the link is specified by its end point coordinates (see Fig. 42). The location of a receptor is specified in terms of X, Y, Z coordinates. Thus, CALINE3 can be used to model multiple sources and receptors, curved alignments, or roadway segments with varying emission factors. The wind angle (BRG) is given in terms of an azimuth bearing (0 to 360°). If the Y-axis is

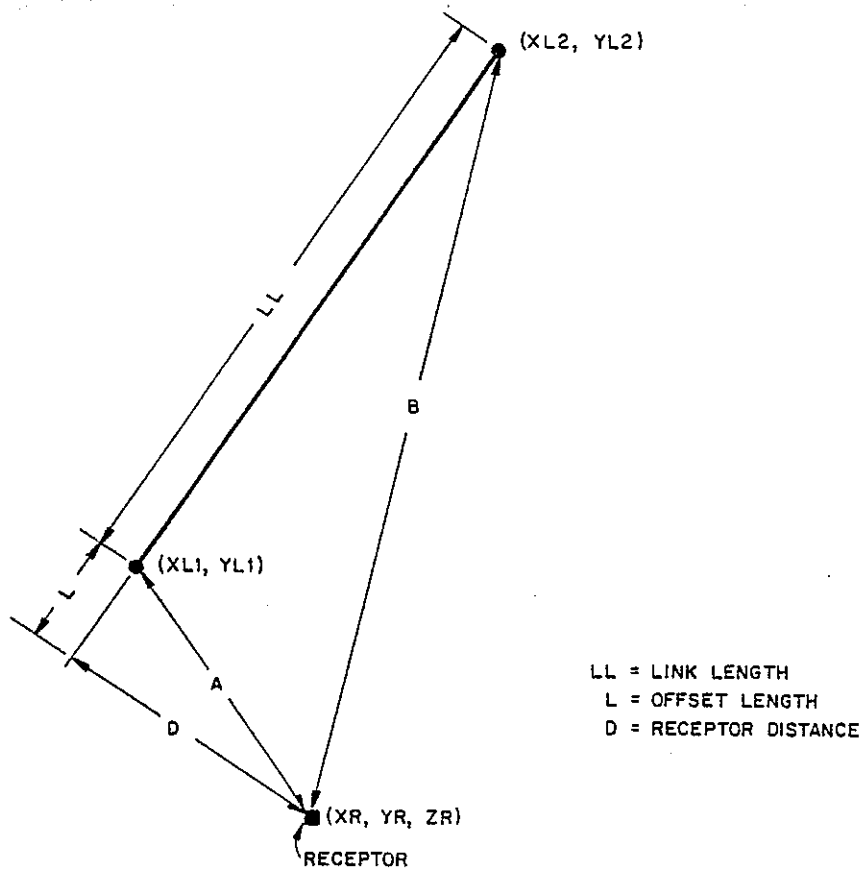

CALINE3 LINK GEOMETRY

FIGURE 42

aligned with due north, then wind angle inputs to the model will follow accepted meteorological convention (i.e. 90° equivalent to a wind directly from the east).

The program automatically sums the contributions from each link to each receptor. After this has been completed for all receptors, an ambient or background value (AMB) assigned by the user is added. Surface roughness is assumed to be reasonably uniform throughout the study area. The meteorological variables of atmospheric stability, wind speed, and wind direction are also taken as constant over the study area. The user should keep this assumption of horizontal homogeneity in mind when assigning link lengths. Assigning a 10 kilometer link over a region with a terrain induced wind shift after the first 2 kilometers should be avoided. A 2 kilometer link would be more appropriate.

The elements for each link are constructed as a function of receptor location as described in Section 8.2 (see Fig. 43). This scheme assures that the finest element resolution within a link will occur at the point closest to the receptor. An imaginary displacement of the receptor in the direction of the wind is used by CALINE3 to determine whether the receptor is upwind or downwind from the link (see Fig. 44).

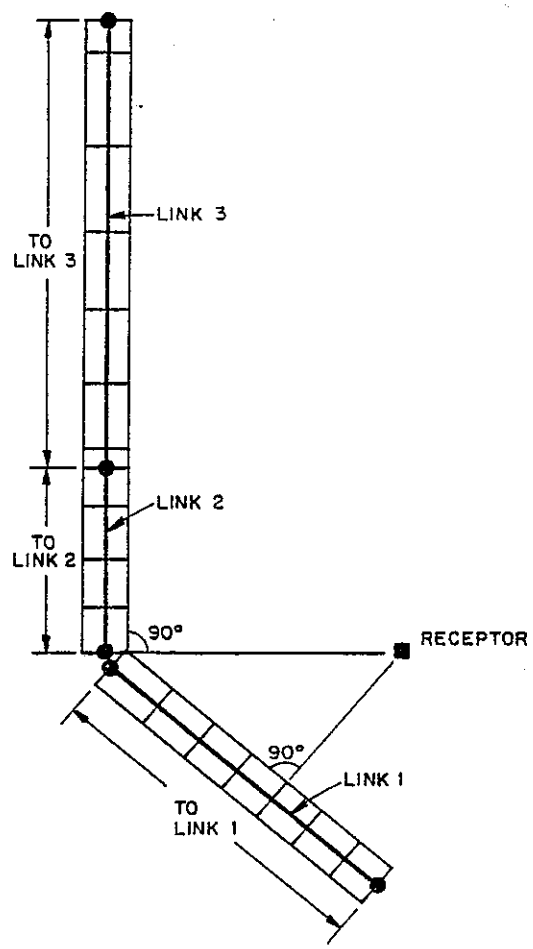

CALINE3 LINK-ELEMENT ASSIGNMENT

FIGURE 43

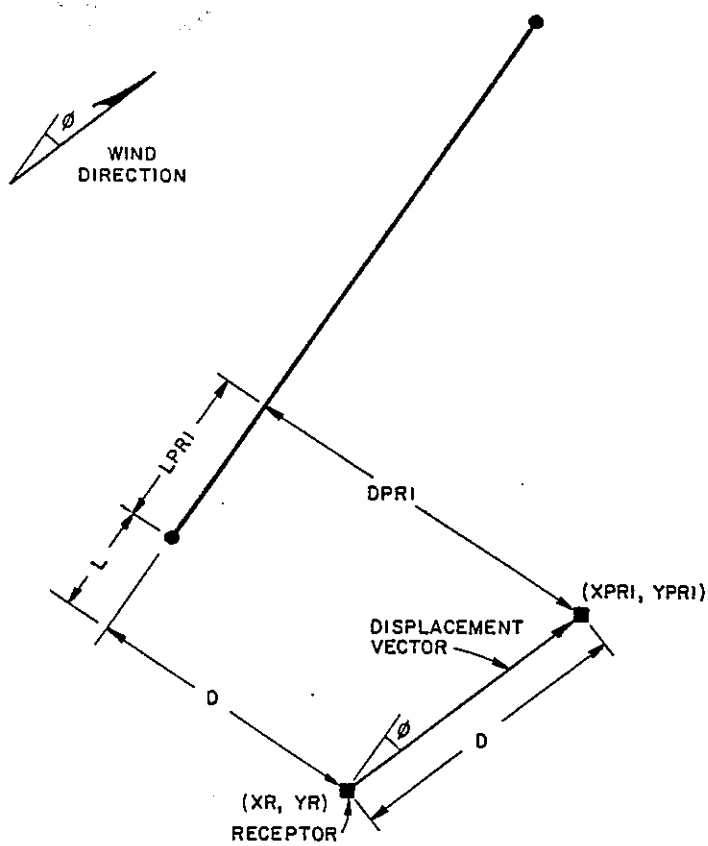

IF DPRI < D THEN D = −D

IF LPRI < L THEN $\begin{cases} UWL = -DWL \\ DWL = -UWL \end{cases}$

IMAGINARY DISPLACEMENT SCHEME USED BY CALINE3

FIGURE 44

For each highway link specified, CALINE3 requires an input for highway width (W) and height (H). The width is defined as the width of the traveled way (traffic lanes only) plus 3 meters on each side. This 3 meter allowance accounts for the wake-induced horizontal plume dispersion behind a moving vehicle. The height is defined as the vertical distance above or below the local ground level or datum. CALINE3 should not be used in areas where the terrain in the vicinity of the highway is uneven enough to cause major spatial variability in the meteorology. Also, the model should not be used for links with values of H greater than 10 meters or less than -10 meters.

Elevated highway sections may be of either the fill or bridge type. For a bridge, air flows above and below the source in a relatively undisturbed manner. This sort of uniform flow with respect to height is an assumption of the Gaussian formulation. For bridge sections, H is specified as the height of the roadway above the surrounding terrain. For fill sections, however, the model automatically sets H to zero. This assumes that the air flow streamlines follow the terrain in an undisturbed manner. Given a 2:1 fill slope (effectively made more gradual as the air flow strikes the highway at shallower horizontal wind angles) and stable atmospheric conditions (suppressing

turbulence induced by surface irregularities), this is a reasonable assumption to make (Gloyne, 1964).

For depressed sections greater than 1.5 meters deep, CALINE3 increases the residence time within the mixing zone by the following empirically derived factor,

$$DSTR = 0.72 * ABS(H)^{0.83} \qquad (8\text{-}22)$$

This formulation was derived by determining the ratio of the average best fit values for σ_z obtained for the median towers of the LA1 depressed section site and the fill section LA3 site, and using Equation 8-14 to compute the corresponding ratio in residence times. A smooth power curve was then fit to this point (H = 7.3 meters, DSTR = 3.7) and a value of DSTR = 1 at H = -1.5 meters (a rough measure of the average vehicle height scale).

Application of the depressed section residence time factor, DSTR, leads to a higher initial vertical dispersion parameter (SGZ1) at the edge of the highway. The increased residence time, characterized in the model as a lower average wind speed, yields extremely high concentrations within the mixing zone. The wind speed is linearly adjusted back to the ambient value at a distance of 3*H downwind from the

edge of the mixing zone. By this point the effect of the higher value for SGZ1 dominates, yielding lower concentrations than an equivalent at-grade section.

For depressed sections, the model is patterned after the behavior observed at the Los Angeles depressed section site studied by Caltrans. Compared to equivalent at-grade and elevated sites, higher initial vertical dispersion was occurring simultaneously with higher mixing zone concentrations. It was concluded that channeling and eddying effects were effectively decreasing the rate of pollutant transport out of the depressed section mixing zone. Lower concentrations downwind of the highway were attributed to the more extensive vertical mixing occurring within the mixing zone. Consequently, the model yields higher values for concentrations within or close to the mixing zone, and somewhat lower values than would be obtained for an at-grade section for downwind receptors. Except for these adjustments, CALINE3 treats depressed sections computationally the same as at-grade sections.

It has been suggested that the model could be used for evaluating parking lot impacts. If the user wishes to run the model to simulate dispersion from a parking lot, it is recommended that SGZ1 be kept constant at 1 meter, and that

the mixing zone width not be increased by 3 meters on each side as in the normal free flow situation. This is because the slow moving vehicles within a parking lot will impart much less initial dispersion to their exhaust gases.

8.7 Deposition and Settling Velocity

Deposition velocity (VD) is a measure of the rate at which a pollutant can be adsorbed or assimilated by a surface. It involves a molecular, not turbulent, diffusive process through the laminar sublayer covering the surface. Settling velocity (VS) is the rate at which a particle falls with respect to its immediate surroundings. It is an actual physical velocity of the particle in the downward direction.

CALINE3 contains a method by which predicted concentrations may be adjusted for pollutant deposition and settling. This procedure, developed by Ermak (1977), is fully compatible with the Gaussian formulation of CALINE3. It allows the model to include such factors as the settling rate of lead particulates near roadways (Little and Wiffen, 1978) or dust transport from unpaved roads. A recent review paper by McMahon and Denison (1979) on deposition parameters provides an excellent reference.

Most studies have indicated that CO deposition is negligible. In this case, both deposition and settling velocity adjustments can be easily bypassed in the model by assigning values of 0 to VD and VS.

REFERENCES

Abramowitz, M. (1968), Handbook of Mathematical Functions, National Bureau of Standards, Washington, D.C.

Barad, M. L. and Haugen, D. A. (1959), A Preliminary Evaluation of Sutton's Hypothesis for Diffusion From a Continuous Point Source, Journal of Meteorology, Vol. 16, 12.

Beaton, J. L., Ranzieri, A. J., Shirley, E. C. and Skog, J. B. (1972), Mathematical Approach to Estimating Highway Impact on Air Quality, Vol. IV, Federal Highway Administration, FHWA-RD-72-36, Washington, D.C.

Bemis, G. R., Ranzieri, A. J., Benson, P. E., Peter, R. R., Pinkerman, K. O. and Squires, B. T. (1977), Air Pollution and Roadway Location, Design and Operation - Project Overview, California Department of Transportation, FHWA/CA/TL-7080-77-25, Sacramento, California.

Benkley, C. W. and Schulman, L. L. (1979), Estimating Hourly Mixing Depths From Historical Meteorological Data, Journal Applied Meteorology, Vol. 18, 772.

Benson, P. E. (1978), Validation of the Line Source Air Pollutant Model, CALINE2, Unpublished Termination Report, California Department of Transportation, Sacramento, California.

Benson, P. E. (1979), CALINE3 - A Versatile Dispersion Model for Predicting Air Pollutant Levels Near Highways and Arterial Streets, California Department of Transportation, FHWA/CA/TL-79/23, Sacramento, California.

Benson, P. E. and Squires, B. T. (1979), Validation of the CALINE2 Model Using Other Data Bases, California Department of Transportation, FHWA/CA/TL-79-09, Sacramento, California.

Bowne, N. E. (1974), Diffusion Rates, APCA Journal, Vol. 24, 832.

Bullin, A. B., Green, N. J. and Polasek, J. C. (1980), Determination of Vehicle Emission Rates From Roadways by Mass Balance Techniques, Environmental Science & Technology, Vol. 14, 700.

Businger, J. A., Wyngaard, J. C., Izumi, Y. and Bradley, E. F. (1971), Flux-Profile Relationships in the Atmospheric Surface Layer, Journal of Atmospheric Science, Vol. 28, 181.

Cadle, S. H., Chock, D. P., Monson, P. R. and Heuss, J. M. (1977), General Motors Sulfate Dispersion Experiment: Experimental Procedures and Results, APCA Journal, Vol. 27, 33.

Calder, K. L. (1973), On Estimating Air Pollution Concentrations From a Highway in an Oblique Wind, Atmospheric Environment, Vol. 7, 863.

Chimonas, G. (1980), Reynolds Stress Deflections of the Bivane Anemometer, Journal Applied Meteorology, Vol. 19, 329.

Chock, D. P. (1977), General Motors Sulfate Dispersion Experiment - An Overview of the Wind, Temperature, and Concentration Fields, Atmospheric Environment, Vol. 11, 553.

Cramer, H. E. (1957), A Practical Method for Estimating the Dispersal of Atmospheric Contaminants, Proc. 1st Nat'l Conf. App. Met., American Meteorological Society, Hartford, C-33.

Dabberdt, W. F. (1968), Wind Disturbance by a Vertical Cylinder in the Atmospheric Surface Layer, Journal Applied Meteorology, Vol. 7.

Dabberdt, W. F. (1975), Studies of Air Quality On and Near Highways, Second Interim Report, Contract DOT-FH-11 8125, Federal Highway Administration, Washington, D.C.

DeTar, D. F. (1979), A New Model for Estimating Concentrations of Substances Emitted From a Line Source, APCA Journal, Vol. 29, 138.

Draper, N. R. and Smith, H. (1966), Applied Regression Analysis, John Wiley & Sons, New York, 266.

Draxler, R. R. (1976), Determination of Atmospheric Diffusion Parameters, Atmospheric Environment, Vol. 10, 99.

Drivas, P. J. and Shair, F. H. (1974), Dispersion of an Instantaneous Cross-wind Line Source of Tracer Released From an Urban Highway, Atmospheric Environment, Vol. 8, 475.

Ermak, D. L. (1977), An Analytical Model for Air Pollutant Transport and Deposition From a Point Source, Atmospheric Environment, Vol. 11, 231.

Eskridge, R. E. and Hunt, J. C. R. (1979), Highway Modeling. Part I: Prediction of Velocity and Turbulence Fields in the Wake of Vehicles, Journal Applied Meteorology, Vol. 18, 387.

Eskridge, R. E., Binkowski, F. S., Hunt, J. C. R., Clark, T. L. and Demerjian, K. L. (1979), Highway Modeling. Part II: Advection and Diffusion of SF_6 Tracer Gas, Journal Applied Meteorology, Vol. 18, 401.

Fay, J. A. and Eng, K. D. (1975), Wake-Induced Dispersion of Automobile Exhaust Pollutants, Proceedings 68th Annual Meeting of the Air Pollution Control Association, Boston.

Geomet (1971), Validation and Sensitivity Analysis of the Gaussian Plume Multiple-Source Urban Diffusion Model, Final Report, Contract CPA 70-94, Environmental Protection Agency, Research Triangle Park, North Carolina.

Gifford, F. A. (1961), Use of Routine Meteorological Observations for Estimating Atmospheric Dispersion, Nuclear Safety, Vol. 2, No. 4, 47.

Gifford, F. A. (1975), Atmospheric Dispersion Models for Environmental Pollution Applications, Lectures on Air Pollution and Environmental Impact Analyses, American Meteorological Society, Boston, 35.

Gloyne, R. W. (1964), Some Characteristics on the Natural Wind and Their Modification by Natural and Artificial Obstructions, Proceedings, 3rd International Congress of Biometeorology, Pergamon Press, 7.

Golder, D. (1972), Relations Among Stability Parameters in the Surface Layer, Boundary-Layer Meteorology, Vol. 3, 47.

Hanna, S. R., Briggs, G. A., Deardorff, J., Egan, B. A., Gifford, F. A., Pasquill, F. (1977), AMS Workshop on Stability Classification Schemes and Sigma Curves - Summary of Recommendations, Bulletin American Meteorological Society, Vol. 58, 1305.

Hay, J. S. and Pasquill, F. (1959), Diffusion From a Continuous Source in Relation to the Spectrum and Scale of Turbulence, Frenkiel, F. N. and Sheppard, P. A. (eds.), Atmospheric Diffusion and Air Pollution, Advances in Geophysics, Vol. 6, Academic Press, 345.

Islitzer, N. F. and Slade, D. H. (1968), Diffusion and Transport Experiments, Meteorology and Atomic Energy, Report TID-24190, U.S. Atomic Energy Commission, 117.

Johnson, W. B. (1974) Field Study of Near-Roadway Diffusion Using a Fluorescent Dye Tracer, Symposium on Atmospheric Diffusion and Air Pollution, American Meteorological Society, Boston, 261.

Kaimal, J. C., Cramer, H. E., Record, F. A., Tillmal, J. E., Businger, J. A. and Miyake, M. (1964), Comparison of Bivane and Sonic Techniques for Measuring the Vertical Wind Component, Royal Meteorological Soc. Quarterly Journal, Vol. 90, 467.

Lane, D. D. and Stukel, J. J. (1976), Dispersion of Pollutants in Automobile Wakes, Journal of the Environmental Engineering Division, June, 571.

Little, P. and Wiffen, R. D. (1978), Emission and Deposition of Lead From Motor Exhausts, Atmospheric Environment, Vol. 12, 1331.

Luna, R. E. and Church, H. W. (1972), A Comparison of Turbulence Intensity and Stability Ratio Measurements to Pasquill Stability Classes, Journal Applied Meteorology, Vol. 11, 663.

McCormick, R. A. and Xintaras, C. (1962), Variations of Carbon Monoxide Concentrations as Related to Sampling Interval, Traffic and Meteorological Factors, Journal Applied Meteorology, Vol. 1, 237.

McMahon, T. A. and Denison, P. J. (1979), Empirical Atmospheric Deposition Parameters - A Survey, Atmospheric Environment, Vol. 13, 571.

Monin, A. S. and Obukhov, A. M. (1954), Basic Laws of Turbulent Mixing in the Ground Layer of the Atmosphere, Geophys. Inst., Acad. Sci. U.S.S.R., Vol. 24, No. 151, 163.

Monin, A. S. (1959), Smoke Propagation in the Surface Layer of the Atmosphere, Frenkiel, F. N. and Sheppard, P. A. (eds.), Atmospheric Diffusion and Air Pollution, Advances in Geophysics, Vol. 6, Academic Press, 331.

Munn, R. E. (1966), Descriptive Micrometeorology, Academic Press, New York, 77.

Myrup, L. O. and Ranzieri, A. J. (1976), A Consistent Scheme for Estimating Diffusivities to be Used in Air Quality Models, California Department of Transportation, FHWA/CA/TL-7169-76-32, Sacramento, California, 14.

Noll, K. E., Miller, T. L. and Claggett, M. (1978), A Comparison of Three Highway Line Source Dispersion Models, Atmospheric Environment, Vol. 12, 1323.

Panofsky, H. A. (1961), Scale Analysis of Atmospheric Turbulence at 2 Meters, Royal Meteorological Society Quarterly Journal, Vol. 88, 57.

Pasquill, F. (1961), The Estimation of the Dispersion of Windborne Material, Meteorological Magazine, Vol. 90, 33.

Pasquill, F. (1974), Atmospheric Diffusion, Ellis Horwood Ltd., Chichester and John Wiley & Sons, New York.

Pasquill, F. (1976), Atmospheric Dispersion Parameters in Gaussian Plume Modeling, Part 2, Environmental Protection Agency, EPA-600/4-76-030b, Research Triangle Park, North Carolina.

Pasquill, F. (1978), Atmospheric Dispersion Parameters in Plume Modeling, Environmental Protection Agency, EPA-600/4-78-021, Research Triangle Park, North Carolina.

Peter, R. R., Pinkerman, K. O. and Shirley, E. C. (1977), Variables Affecting Air Quality Instrument Operation, California Department of Transportation, FHWA/CAL/TL-7080-77-15, Sacramento, California.

Prandtl, L. (1934), The Mechanics of Viscous Fluids, Durand, W. F. (ed.), Aerodynamic Theory, Vol. III.

Rao, S. T., Chen, M., Keenan, M. T., Gopal, S., Peddada, R., Wotzak, G. and Kolak, N. (1978), Dispersion of Pollutants Near Highways - Experimental Design and Data Acquisition Procedures, Environmental Protection Agency, EPA-600/4-78-037, Research Triangle Park, North Carolina.

Rao, S. T. and Keenan, M. T. (1980), Suggestions for Improvement of the EPA-HIWAY Model, APCA Journal, Vol. 30, 247.

Rao, S. T., Sedefian, L. and Czapski, U. H. (1979), Characteristics of Turbulence and Dispersion of Pollutants Near Major Highways, Journal Applied Meteorology, Vol. 18, 283.

Remsberg, E. E., Buglia, J. J. and Woodbury, G. E. (1979), The Nocturnal Inversion and Its Effect on the Dispersion of Carbon Monoxide at Ground Level in Hampton, Virginia, Atmospheric Environment, Vol. 13, 443.

Reynolds, A. J. (1974), Turbulent Flows in Engineering, John Wiley & Sons, London.

Reynolds, O. (1895), On the Dynamical Theory of Incompressible Viscous Fluids and the Determination of the Criterion, Philosophical Transactions of the Royal Soc. (London), Series A, Vol. 186, 123.

Robertson, J. M. (1963), A Turbulence Primer, University of Illinois Bulletin, Vol. 60.

Smith, F. B. (1972), A Scheme for Estimating the Vertical Dispersion of a Plume From a Source Near Ground Level, Air Pollution-Modeling, No. 14, CCMS, NATO, Brussels.

Surgeon General (1962), Motor Vehicles, Air Pollution and Health, House Document 87-489, U.S. Public Health Service, Washington, D.C.

Sutton, O. G. (1932), A Theory of Eddy Diffusion in the Atmosphere, Proc. Royal Soc. (London), Series A, Vol. 135, 143.

Taylor, G. I. (1921), Diffusion By Continuous Movements, Proc. London Math. Soc., Series 2, Vol. 20, 196.

Tennekes, H. and Lumley, J. L. (1972), A First Course in Turbulence, MIT Press, Cambridge, 42-44.

Townsend, A. A. (1976), The Structure of Turbulent Shear Flow, Cambridge University Press.

Turner, D. B. (1964), A Diffusion Model for an Urban Area, Journal Applied Meteorology, Vol. 3, 83.

Turner, D. B. (1970), Workbook of Atmospheric Dispersion Estimates, Environmental Protection Agency, Research Triangle Park, North Carolina.

Ward, C. E., Ranzieri, A. J. and Shirley, E. C. (1976), CALINE2 - An Improved Microscale Model for the Diffusion of Air Pollutants From a Line Source, California Department of Transportation, CA-DOT-TL-7218-1-76-23, Sacramento, California.

Wilkins, E. T. (1956), Some Measurements of Carbon Monoxide in the Air of London, Royal Soc. Promotion Health Journal, Vol. 76, 677.

Winter, W. A. and Farrockhrooz, M. (1976), Mini-computer Software - Data Acquisition and Process Control System for Air Pollution Monitoring, California Department of Transportation, CA/DOT/TL-7080-3-76-39, Sacramento, California.

Zimmerman, J. R. and Thompson, R. S. (1974), HIWAY: A Highway Air Pollution Model, Environmental Protection Agency, Research Triangle Park, North Carolina.

Caltrans

CALIFORNIA DEPARTMENT OF TRANSPORTATION

TRANSPORTATION LABORATORY

FOUNDED IN 1912